THE EFFECTS OF ENGINEERED SILICA NANOPARTICLES ON THE CELLULAR BEHAVIOURS OF HUMAN HEPATOCELLULAR CARCINOMA CELL LINES

A Thesis Submitted to
the Graduate School of Engineering and Sciences of
İzmir Institute of Technology
in Partial Fulfillment of the Requirements for the Degree of

DOCTOR OF PHILOSOPHY

in Bioengineering

by
Özge TÜNCEL ÇERİK

July 2018
İZMİR

We approve the thesis of **Özge TÜNCEL ÇERİK**

Examining Committee Members:

Prof. Dr. Serdar ÖZÇELİK
Department of Chemistry, İzmir Institute of Technology

Prof. Dr. Ş. Esra ERDAL BAĞRIYANIK
Department of Medical Biology, Dokuz Eylül University

Prof. Dr. Bilge KARAÇALI
Department of Electrical and Electronics Engineering, İzmir Institute of Technology

Doç. Dr. Dilek ODACI DEMİRKOL
Department of Biochemistry, Ege University

Prof. Dr. Ali ÇAĞIR
Department of Chemistry, İzmir Institute of Technology

05 July 2018

Prof. Dr. Serdar ÖZÇELİK
Supervisor, Department of Chemistry
İzmir Institute of Technology

Prof. Dr. S. Neşe ATABEY
Co-advisor, Department of Medical
Biology, Dokuz Eylül University

Assoc. Prof. Dr. Engin ÖZÇİVİCİ
Head of the Department of Biotechnology
and Bioengineering

Prof. Dr. Aysun SOFUOĞLU
Dean of the Graduate School of
Engineering and Sciences

ACKNOWLEDGMENTS

Firstly, I would like to express my deep and sincere gratitude to my advisor Prof. Dr. Serdar ÖZÇELİK for his suggestions, guidance, encouragement and support throughout my Ph.D. study.

I would like to thank Prof. Dr. S. Neşe ATABEY for her guidance, understanding, motivation and excellent support. I would like to thank my committee, Prof. Dr. Ali ÇAĞIR, Prof. Dr. Bilge KARAÇALI, Prof. Dr. Ş. Esra ERDAL BAĞRIYANIK, Doç. Dr. Dilek ODACI DEMİRKOL for their encouragement, insightful comments, and questions.

I would like to thank all the staff and facility managers at İYTE MAM and BİYOMER for their help and suggestions.

I would like to thank my friends and lab mates İpek ERDOĞAN, Melek ÜÇÜNCÜ, Seçil SEVİM ÜNLÜTÜRK, Eylem KURULGAN DEMİRCİ, Murat DELMAN, Erkan KAHRAMAN, Özlem ECE for their sincere help and their good friendship. I also wish to express my thanks to all my other friends working in Nanobiolab and IYTE Chemistry Department.

Finally, I would like to thank my family for both financial and moral supports They showed in every stage of my life. .

I want to express special thanks to my family for their love, encouragement, patience and support during my education.

ABSTRACT

THE EFFECTS OF ENGINEERED SILICA NANOPARTICLES ON THE CELLULAR BEHAVIOURS OF HUMAN HEPATOCELLULAR CARCINOMA CELL LINE

Physicochemical properties of the silica nanoparticles have vital roles in determining the physiological behaviours of the cells. Applications of nanoparticle treatments have some outcomes as a response of the cells in living systems as mitochondrial disruption, oxidative stress, reactive oxidative species (ROS) generation, altered cell cycle regulation and DNA damage.

In this study 10 and 100 nm sized SiNPs were prepared and physicochemically characterized in the second part. Well characterized silica nanoparticles were used to assess the cytotoxicity and genotoxicity of the hepatocellular carcinoma cell lines as HuH-7 and SK-HEP-1 and lymphocytes. The cell cycle analysis was performed for engineered SiNPs to elucidate the DNA damage in the third part. In the fourth part mitochondrial responses of the cells were determined by real time confocal microscopy at single cell level. An image analysis method for evaluating the cellular responses by mitochondrial staining was developed. DCF stained cells were analyzed in order to assess the production of ROS in the cells. Localization of the SiNPs were determined by lysosomal and mitochondrial staining. Pearson correlation coefficients of the images were used for evaluating the colocalization of organelles with SiNPs. Lastly, diffusion coefficients of the SiNPs in the cells were determined by quantitative confocal microscopy.

The SiNPs were found as non-toxic up to 200 μg/ml for 5 days. The SiNPs did not induce the formation of micronuclei in lymphocytes. The SiNPs were not cause an arrest in cell cycle progression. Mitochondrial potentials were not changed after SiNP exposure as well. They were mostly internalized at 30 minutes in both cell line in lysosomal parts without increasing ROS in the cells. It can be concluded that the SiNPs can be safely used for targeted delivery of organic compounds, biological molecules or drugs in medicine, and may be utilized as a probe system in biological studies.

ÖZET

BIYOMÜHENDISLIK ÜRÜNÜ SILIKA NANOPARÇACIKLARIN HEPATOSELÜLER KARSINOM HÜCRE DIZILERININ BIYOLOJIK DAVRANIŞLARINA ETKILERI

Nanotaneciklerin hücre kültürü ortamlarındaki davranışlarının üzerinde fizikokimyasal karakterlerinin etkisi oldukça büyüktür. Nanoparçacıkların hücre kültürü uygulamaları mitokondriyel bozunma, oksidatif stres, reaktif oksijen türlerinin oluşumu gibi sonuçlara sebep olabilmektedir. Bu çalışmada mühendislik ürünü silika nanotanecikler sentezlenmiş ve fizikokimyasal karakterizasyonları yapılmıştır. Bu aşamaya ait sonuçlar ilk kısımda sunulmuştur. Silika taneciklerin karaciğer kanser hücreleri üzerindeki sitotoksik ve genotoksik etkileri HuH-7, SK-HEP-1 ve lenfosit hücreleri üzerinde çalışılmıştır. Hücre döngüsü analizleri ile birlikte bu sonuçlar 3. bölümde anlatılmıştır. Mitokondri cevabı gerçek zamanlı konfokal mikroskobi ile belirlenmiş ve hücre cevabının değerlendirilmesi için bir görüntü analizi önerilmiştir. Hücrede oluşan reaktif oksijen türleri DCF boyası ile boyanan hücrelerde belirlenmiş ve görüntü analizi ile birlikte 4. bölümde sunulmuştur. Lizozomal ve mitokondriyel boyamalarla hücre içindeki silika taneciklerin yeri kolokalizasyon katsayıları belirlenerek incelenmiştir. Son bölümde de silika taneciklerin hücre içindeki difüzyon katsayıları kantitatif konfokal mikroskobi ile belirlenmiştir.

Silika nanotaneciklerin 200 μg/ml'ye kadar 5 gün boyunca toksik olmadığı belirlenmiştir. Lenfositlerde mikronükleus oluşumunu tetiklemediği ve hücre döngüsünü etkilemedikleri belirlenmiştir. Hücrelerin mitokondri potansiyeli de silika muamelesiyle değişmemektetir. ROS üretimini tetiklemeden lizozomal bölgelerde 30. dakikada hücre içine girmeye başladıkları gözlemlenmiştir. Bu taneciklerin organik bileşiklerin, biyolojik moleküllerin veya ilaçların hedeflendirilmiş iletiminde tıp uygulamalarında kullanılabileceği ve belki de prob sistemlerinde kullanılabileceği sonucuna varılmıştır.

TABLE OF CONTENTS

LIST OF FIGURES

Figure **Page**

LIST OF TABLES

Table **Page**

CHAPTER 1

INTRODUCTION

Silica (silicon dioxide) nanoparticles, SiNPs, are good candidate materials for biological and medical applications due to their unique properties such as large surface area, controllable particle size and good biocompatibility (Wang et al. 2015), its ease of production and relatively low cost of production (Chang et al. 2007). In this thesis work, it was firstly aimed to synthesize SiNPs in order to tune the particle size and to alter their surfaces instead of using commercially available silica nanoparticles. The synthesis chemistry of silica nanoparticles were studied and a size control mechanism have been developed in our laboratory previously (Durgun, Ocakoglu, and Ozcelik 2011).

Experimental and possible pathophysiological outcomes (responses) of cells to nanomaterials could be protein, DNA or membrane injury, mitochondrial perturbation, apoptosis, possible organ dysfunction, losing of enzyme activity, proliferation and cell cycle arrest (Nel et al. 2006). Cytotoxicity and genotoxicity of SiNPs have been assessed in various studies (Nel et al. 2006) (Napierska et al. 2010) by using viability tests such as MTT (3-(4,5-Dimethyl-2-thiazolyl)-2,5-diphenyl-2H-tetrazolium bromide) based assays, SRB (sulforhodamine B) and genotoxicity tests as micronucleus and Comet assay.

The aims of this thesis are:

- to synthesize 10 and 100 nm sized non-fluorescent and 100 nm sized fluorescent (FITC-conjugated) silica nanoparticles. Results were represented in Chapter 2.
- to characterize the SiNPs by using physicochemical and elemental analysis methods. Results were represented in Chapter 2.
- to assess the possible cytotoxic effects of silica nanoparticles on hepatocellular carcinoma cell lines. Results were represented in Chapter 3.
- to assess the genotoxic effects of silica nanoparticles on lymphocytes. Results were represented in Chapter 3.
- to visualize the silica nanoparticles in the cells with lysosome and mitochondria staining by confocal microscopy. Results were represented in Chapter 4.

- to quantify the changes in mitochondrial potentials after silica nanoparticle treatments by image analysis. Results were represented in Chapter 4.
- to determine the diffusion coefficients of silica nanoparticles by particle tracking studies. Results were represented in Chapter 5.

Overview of effects of silica nanoparticles on cellular physiology;

Nanoparticles are defined as three orthogonal dimensions in the nanoscale by International Organization for Standardization (ISO) (ISO/TC 229 2017). Silver nanoparticles, iron nanoparticles, titanium dioxide, aluminium oxide, cerium oxide, zinc oxide, gold nanoparticles and silicon dioxide, also known as silica, are considered as engineered nanomaterials (Heather Herd et al. 2013). Silica based nanoparticles (SiNPs) have advantages as ease of synthesis and relatively inert chemical composition (Yu, Malugin, and Ghandehari 2011) which makes silica as a promising candidate material for medical and biological applications such as non-viral vector for gene and drug delivery (Julia et al. 2013). However, it is crucial to understand mechanisms underlying any biological responses to SiNPs before using them *in vitro* and *in vivo* applications.

The search results for literature were indexed by Stober silica nanoparticles indicated that the silica nanoparticles have been widely used in material science, physics, engineering, polymer sciences and chemistry area according to Web of Science database. The data for the graph for the literature search recorded from Web of Science database in Figure 1.1.

Similarly "silica nanoparticles" were searched in US National Library of Medicine National Institutes of Health (NCBI-pubmed). The results were sorted by year of publications. The survey included years of publications between 1989 and 2018. The literature search indicated that publications were increased by year up to 2015 in National Library of Medicine.

Stöber silica nanoparticles were recorded at mostly used databases in high ranks. The search data were graphed in Figure 1.2 of which the csv file was available at NCBI Pubmed web-site (as of June 6, 2018).

The literature was searched for "toxicity" and "silica nanoparticles" and indexed by cell type, nanoparticle amount, incubation time, size and viability values. The viability percentages were collected from experiments from each studies regarding to cell line. The values were extrapolated unless the viabilities were recorded in numbers.

All data were transferred into Excel and graphed.

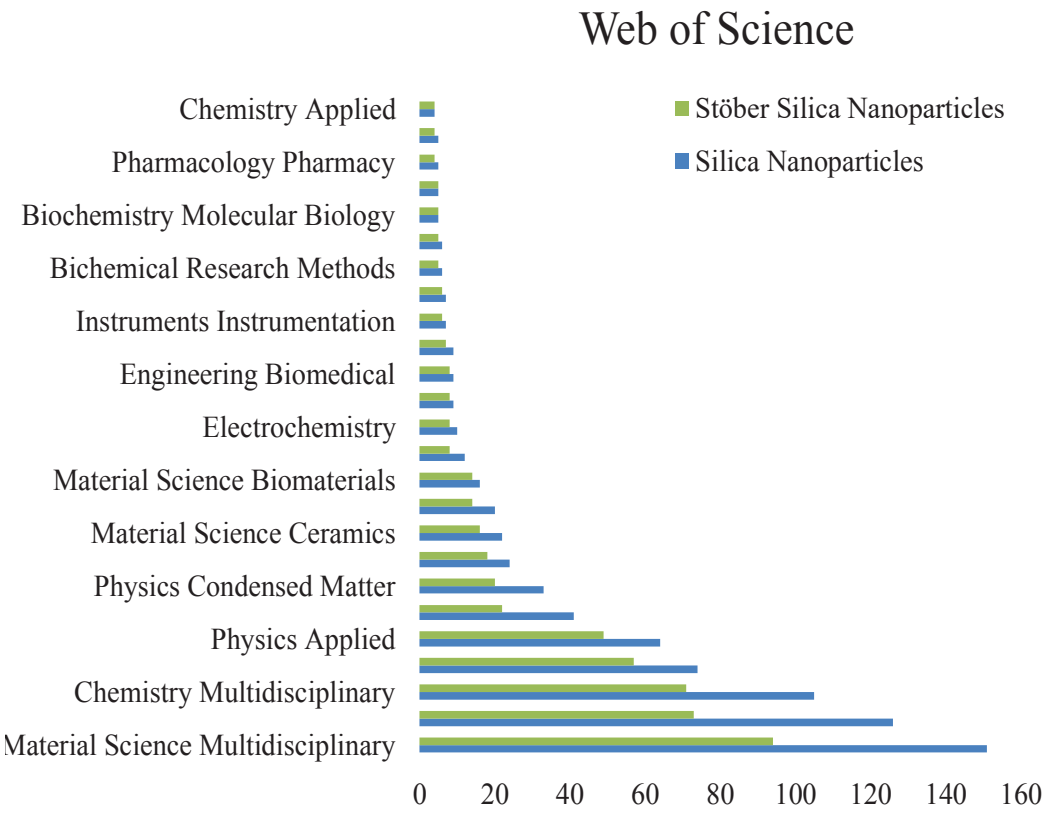

Figure 1.1. The distribution of SiNPs based papers on Web of Science based search for Stöber SiNPs and SiNPs.

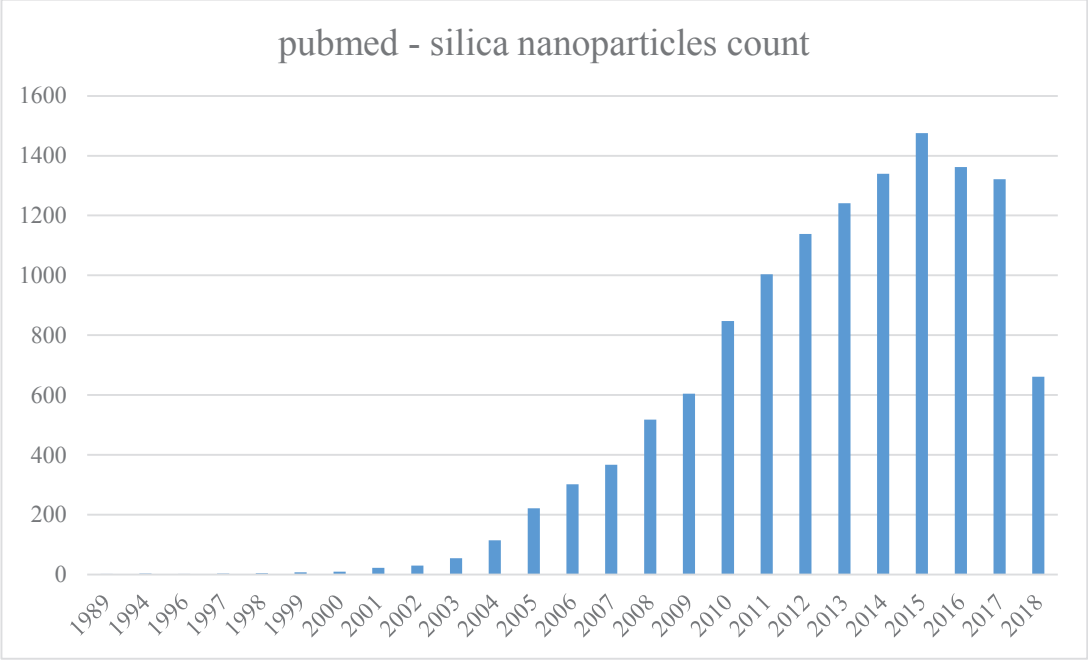

Figure 1.2. The search results from Pubmed for silica nanoparticles.

Fourteen cell types such as primary epithelial cells, Balb/3T3, MC3T3-E1, HT29, MRC-5, HUVECs, HaCat, HCEC, LBC-3, LN-18, EAHY926, HEK293 notably A549 and RAW 264.7 cells were exposed to SiNPs. The maximum amount of SiNP used was 640 µg/ml among the 56 cytotoxicity cases. The cellular response substantially differed depending upon by cell type and size of nanoparticles. The viability against amount and size respectively were graphed in Figure 1.3 and Figure 1.4. The cell types were coded with colours in both graphs.

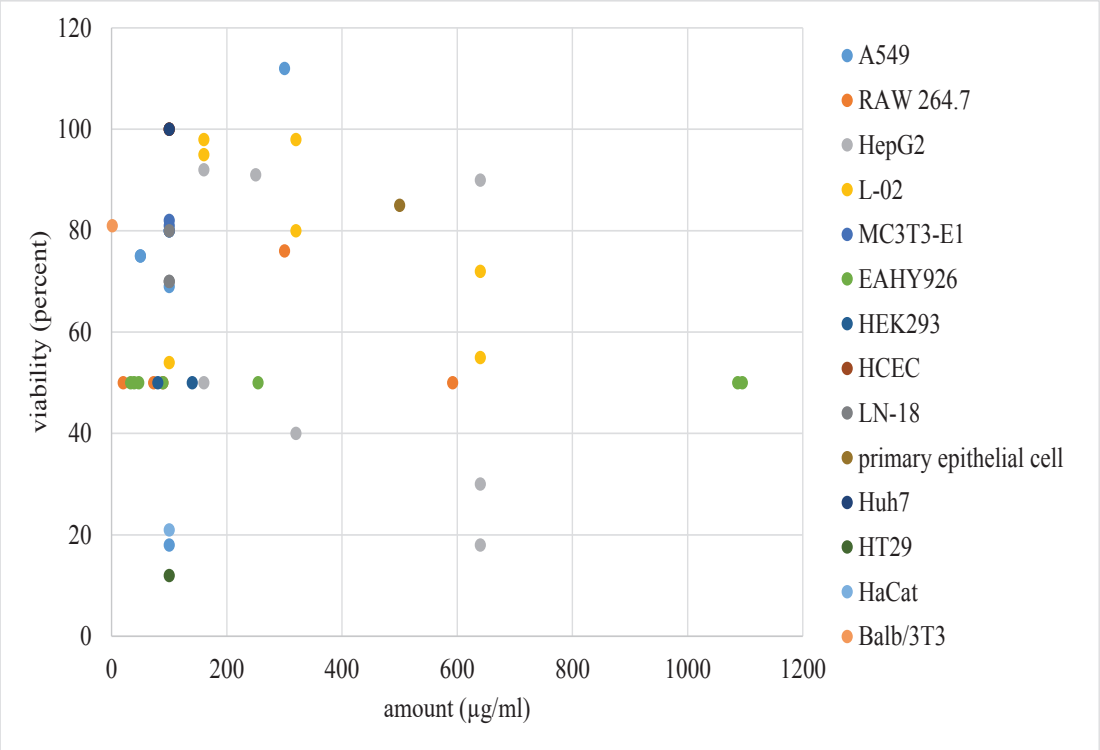

Figure 1.3. The data from the cytotoxicity experiments plotted by viability (%) vs amount.

Cytotoxicity of non-porous or amorphous silica nanoparticles were tested mostly for the concentration below 200 µg/ml with a size range of 5-335 nm. The viability responses of the cells treated with SiNPs were varied based on particle size and incubation time. HepG2, as a hepatocellular carcinoma cell line, was tested below and above 200 µg/ml SiNP concentration.

Viability percentages from different studies were graphed by size or amount in Figure 1.5 and 1.6. The graphs were divided in mainly two and represented by dashed red (toxic) and green (biosafe) rectangular areas. The number of cases in the biosafe regions is respectively 7, 4 and 2 for the amount of 1-200 µg/ml, 200-400 µg/ml and 400-700

µg/ml. The number of cases having viability below the 80 percent is 21 for different sized SiNPs for the amount between 1-200 µg/ml.

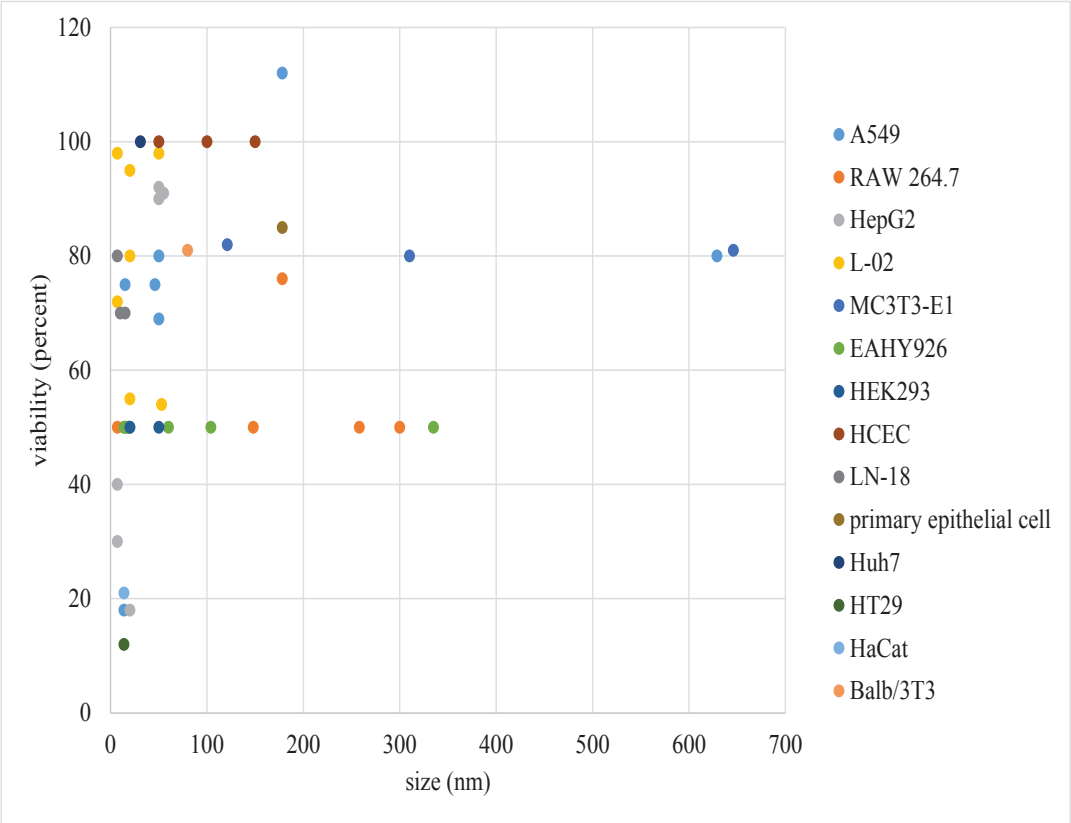

Figure 1.4. The data from the cytotoxicity experiments plotted by viability (%) vs size of Stöber SiNPs

It was deduced from the size graphs that 18 cases (out of 56) of silica nanoparticles were found in the the biosafe (green) area. 23 cases were found in the toxic (red) area. The viability of the cells >=80 were observed for 21 groups of SiNPs that the cells were treated. The viability of the cells for 12 groups were between 50% and 80%.

The 15 of SiNPs were labeled in unsafe and only 5 of them were labeled in biologically safe subgroup up to nearly 25-nm sized SiNPs. It was thought that mostly the silica nanoparticles were not safe when they were produced smaller than 25 nm size range.

The viability of the cells were above 70% after 25-75 nm sized SiNP incubation for 9 groups except for 5 groups. 8 groups of SiNPs that larger than 75-nm were distributed in safe area up to 400 nm diameter however 6 groups of SiNPs were seemed to be toxic for the cells.

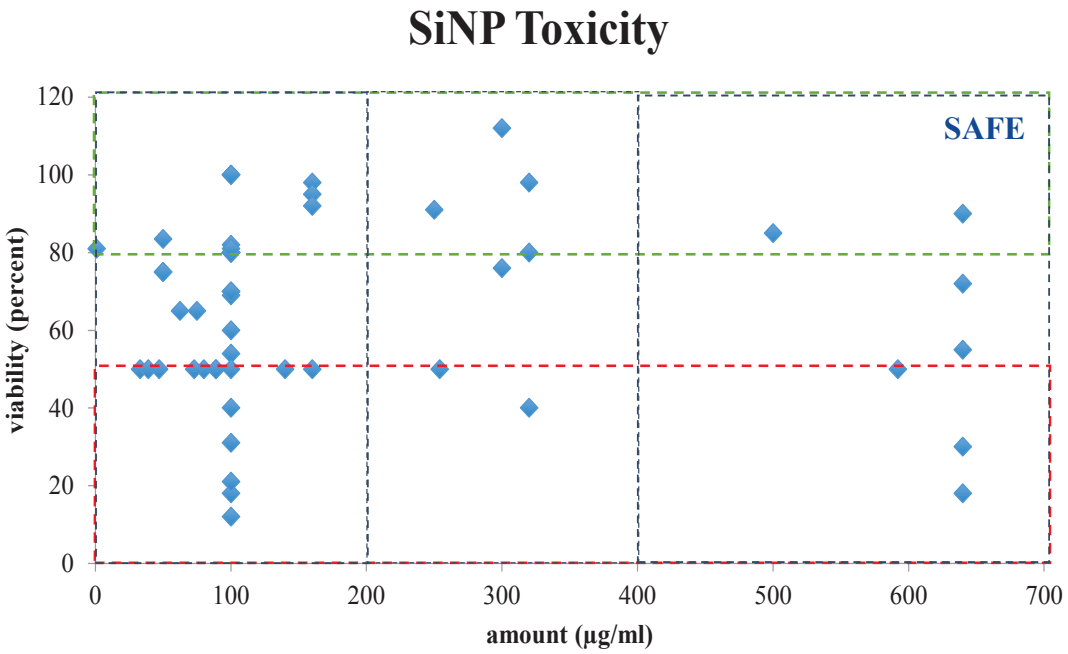

Figure 1.5. The viability data vs amount of SiNPs

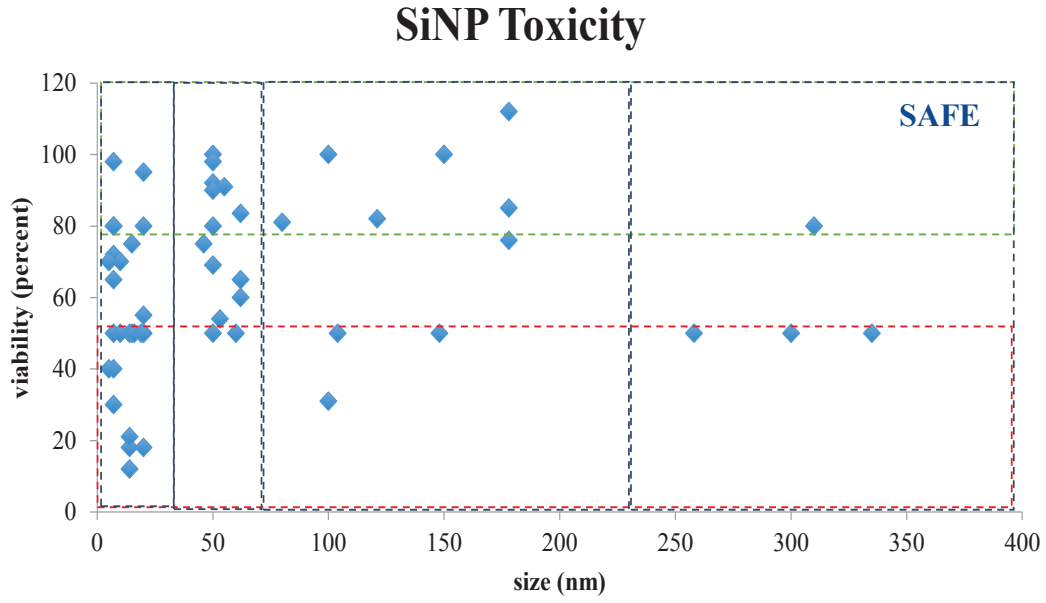

Figure 1.6. The viability data vs the sizes of SiNPs.

HepG2, L-02, RAW 264.7, MRC-5, LBC-3 and LN-18 cells were exposed to SiNPs with size of 7-nm and concentrations up to 640 µg/ml. The most sensitive cells

were RAW 264.7 macrophages for 24 hours of incubation at 20 µg/ml. HepG2 cells were ranked second for concentration of 320 µg/ml up to 48 hours and size of 7-nm. RAW 264.7 mouse macrophage cells seemed to be more sensitive than other cell types exposed to 7-300 nm sized SiNPs. Though the macrophage cells are used to evaluate the effective bioactivity of the product, the cellular responses cannot be differentiated by the particle size in the literature. Supportingly, Merly et al. suggested that the responses of RAW 264.7 cells can be misleading to determine overall bioactive potential of the substances (Merly and Smith 2017). A549 cells were exposed to SiNPs with the size range of 14-629 nm up to 72 hours. Mu et al. showed that viability of A549 cells was 18 percent of control after 14-nm SiNPs treatment at nanoparticle concentrations ≥ 1 µg/ml. The sizes of SiNPs were enlargered up to 500 nm in the cell culture medium in 24 hours. However 15-nm SiNPs were not caused toxicity for A549 cells and viability was reported around 75 percent of control cells for in another study (Guarnieri et al. 2014). Additionally the viability of the cells was reported mostly for 24 hours of incubation time. Long-term incubations were performed for 3 cases up to 72 hours. 18 and 4 groups out of 37 and 16 cases were seemed to be cytotoxic after 24, 48 and 72 hours respectively (Figure 1.7).

The details of the studies were tabulated in Table 1.1. The cell type, nanoparticle amount, incubation time, size of the SiNPs, viability percents of the cells, nanoparticle characteristics and assay types to evaluate toxicity were summarized.

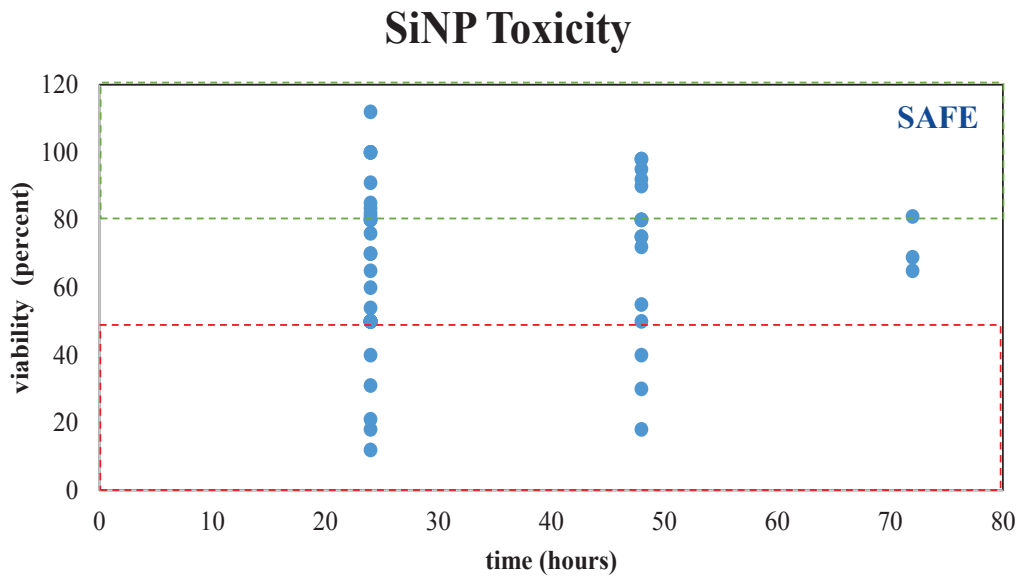

Figure 1.7. The viability data vs the time of exposure.

Genotoxicity of SiNPs were studied for Balb/3T3 cells exposed to amount of 100 μg/ml with the particle sizes of 16, 39, 100, 187, 333-nm. Exposure of Balb/3T3 cells with SiNPs did not induce micronuclei formation for 24 hours of treatment (Park et al. 2011). Comet assay for 30, 80, 400-nm amorphous silica nanoparticles represented no genotoxicity at either 4 or 40 μg/ml of doses on 3T3-L1 fibroblasts cells for 24 hours. On the other hand significant DNA damage was reported at 10 μg/ml of 14-nm SiNPs on A549 cells for 24 hours (Guarnieri et al. 2014). All of those cells have chromosomal instability and are not recommended by OECD (Organisation for Economic Co-operation and Development).

The findings are in conflicts and diversed for cytotoxic and genotoxic effects of silica nanoparticles. A potential explanation for the conflict should be related to how nanoparticles are dispersed in cells cultures and/or treated. There is no guidance on how to prepare nanoparticles for *in vitro* toxicity studies that may influence cytotoxicity and genotoxicity responses of cells (Park et al. 2011). Also, suspension of nanoparticles, dispersibility and effective amount in the commercially available media such as DMEM and RPMI (Roswell Park Memorial Institute) for cell cultivation may affect the cell viability (Napierska et al. 2009). Incompatible data may be resulted from general lack of standard procedures, as well as insufficient characterization of nanomaterials in biological systems. Besides, the control of assays and assay conditions has equal importance with physico-chemical properties of the SiNPs (Napierska et al. 2010). It is highlighted that the particles tend to be aggregated or agglomerated in culture medium to form assemblies of NPs. They have indicated that the sizes of amorphous silica nanoparticles higher in cell culture media which results in reduced cell viability (Xie et al. 2014). Moreover, when nanoparticles are injected intravenously their surface is rapidly covered with a layer of blood proteins called protein corona (Napierska et al. 2009), (Julia et al. 2013). Undesirable protein adsorption on the surface of nanoparticles may cause reduction of blood circulation times.

For successful clinical trials or treatments, SiNPs should be designed being non-toxic effectively targeted and having good bioclerance profiles. However, some studies critisized physicochemical behaviour of SiNPs, as well as their cytotoxic and genotoxic patterns (Mu, Hondow, Krzeminski, et al. 2012).

Generally nanoparticle clearance can be processed by renal, hepatobiliary system or via the mononuclear phagocyte system. The nanoparticles that cannot be cleared by renal system will be processed by liver. Hepatocytes are programmed to eliminate the

foreign particulates by endocytosis via enzymatic breakdown or excretion into the bile. Supportingly dosimetry results of clinically applied 7-nm sized multimodal SiNPs indicated that they were mostly accumulated in kidneys, liver and spleen both in mouse and human melanoma models (Xu et al. 2014).

It has been reported that there are great variety of nanoparticles studied for toxicity led to a vast amount of publications with conflicting data. In order to identify the real causes of these variabilities, 5 labs were conducted in Europe in 2017. They have used well-defined experimental parameters and well-characterized NPs. The participants analyzed the *in vitro* biocompatibility of silica and polymer NPs on human hepatocellular carcinoma cell lines (HepG2 cells). They have realized that the small variations in nanoparticle preparation, cell culture conditions and the type of culture slide influenced the nanoparticle stability and the evaluation of cell assays (Landgraf et al. 2017).

In this thesis, we physicochemically characterized 10 nm and 100 nm sized SiNPs as the model system before using them in both hepatocellular carcinoma cell lines and lymphocytes. We have found that 10 nm and 100 nm sized SiNPs do not affect cytotoxicity up to 200 μg/mL concentration in biologically different models as an epithelial like and mesenchymal like cell line which are respectively HuH-7 and SK-HEP-1. It has been reported that HuH-7 cell line is well differentiated, low motile and less invasive cell line where as SK-HEP-1 cells are poorly differentiated, highly invasive and highly motile characteristics (Eun et al. 2014, Yuzugullu et al. 2009a).

Our micronucleus tests results indicated that SiNPs have no genotoxic effect up to 20 μg/mL concentration for 72 hours on lymphocytes derived from healthy volunteers compatible with OECD (Organisation for Economic Co-operation and Development) guideline.

Additionally single cell based quantitative analysis of microscopic images showed that SiNPs tend to accumulate in lysosomes rather than nucleus or mitochondria. Mitochondria potential of the cells were altered after silica nanoparticle treatments regardless of nanoparticle size. The amount of reactive oxygen species of the cells were not significantly changed after 10 or 100 nm sized silica nanoparticle treatment.

We have represented a method for evaluation of the cellular response of the cells to silica nanoparticles at single cell and organelle level. Image processing of mitochondrial stainings and visualization of reactive oxygen species into the cells are powerful methods in terms of obtaining the data from real-time scanning of cellular responses of the cells.

Table 1.1. Literature summary for SiNP toxicity.

Cell Line	amount (ug/ml)	Time (hours)	Size (nm)	Viability (percent)	NP characteristics	References
A549	100	48	50	80	TMR and RuBipy - conjugated	(Jin et al. 2007)
A549	100	72	50	69		
A549	50	48	15	75	crystalline silica (Min-U-Sil 5)	(Lin et al. 2006)
A549	50	48	46	75		
A549	100	48	629	80		
RAW 264.7	300	24	178	76	spherical SiNPs	(Herd et al. 2013)
A549	300	24	178	112		
primary epithelial cell	500	24	178	85		
RAW 264.7	73	24	148	50	non-porous SiNP	(Yu, Malugin, and Ghandehari 2011)
RAW 264.7	89	24	258	50	mesoporous SiNP	
A549	100	24	14	18	amorphous silica nanoparticles	(Mu, Hondow, Krzemiński, et al. 2012)
HT29	100	24	14	12		
HaCat	100	24	14	21		
Balb/3T3	1	72	80	81	amorphous silica nanoparticles	(Uboldi et al. 2012)
MC3T3-E1	100	24	121	82	amorphous silica nanoparticles	(Xu et al. 2014)
MC3T3-E1	100	24	310	80		
MC3T3-E1	100	24	646	81		
EAHY926	33	24	14	50	amorphous silica nanoparticles	(Napierska et al. 2009)
EAHY926	39	24	15	50		
EAHY926	47	24	16	50		
EAHY926	89	24	19	50		
EAHY926	254	24	60	50		
EAHY926	1095	24	104	50		
EAHY926	1087	24	335	50		
RAW 264.7	20	24	7	50	amorphous silica nanoparticles	(Waters et al. 2009)
RAW 264.7	592	24	300	50		
HEK293	80	24	20	50	Laboratory for Ultrafine Materials, non-functionalized	(Wang et al. 2009)
HEK293	140	24	50	50		
HCEC	100	24	50	100	non-functionalized	(Park et al. 2016)
HCEC	100	24	100	100		
HCEC	100	24	150	100		
LBC-3	100	24	7	80	amorphous	(Kretowski et al. 2017)
LBC-3	100	24	10	40	porous	
LBC-3	100	24	15	50	porous	
LN-18	100	24	7	80	amorphous	
LN-18	100	24	10	70	porous	
LN-18	100	24	15	70	porous	
HuH-7	100	24	31	100	-OH functionalized	(Lunova et al. 2017)

CHAPTER 2

SILICA NANOPARTICLE SYNTHESIS

The aim of the Chapter 2 of this thesis is to synthesize both non-fluorescent and fluorescent (fluorescein isothiocyanate -conjugated) silica nanoparticles as a model to assess physiological responses of hepatocellular cells depending on the particle size.

We preferred to synthesize the silica nanoparticles instead of purchasing from any manufacturer to have chemical flexibility and precise control on physicochemical properties. The size of the particles were tuned and optimized in our laboratory previously (Durgun, Ocakoglu, and Ozcelik 2011). It has been discovered that initial amount of ethanol is the major factor regulating the particle size.

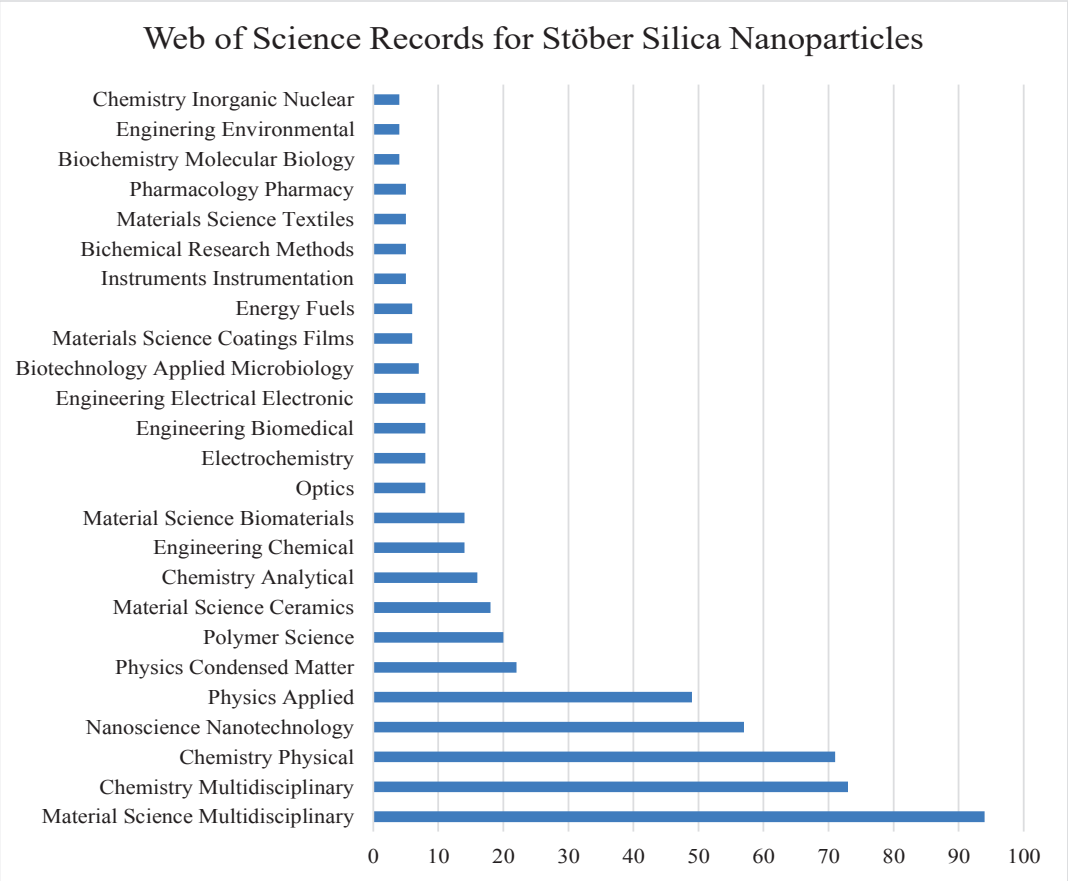

Figure 2.1. The Stöber silica nanoparticle search records data from Web of Science database.

From now on most of the studies were published in Material Science, Chemistry, Physical Chemistry and Nanotechnology and Nanoscience fields between 2011 and 2018. Our study can be rated in Biomedical Engineering, Materials Science, Nanoscience-Nanotechnology and Physical Chemistry areas. The number of articles were recorded from the search from Web of Science database and the data were graphed in Figure 2.1. Same criteria were used in Pubmed research area for silica nanoparticles that applied in biological studies. 41 publications were recorded for silica nanoparticles that were applied on hepatocellular carcinoma as a model. There are no search recordings for Stöber silica nanoparticles and hepatocellular carcinoma in Pubmed (up to now). The results showed that silica nanoparticles mostly modified or functionalized by variable chemical groups for cell culture applications (Figure 2.2). The silica nanoparticles were produced as mesoporous nanoparticles to cargo the drug molecules or microRNAs in hepatocellular carcinoma cells. (Chen et al. 2016), (Xie et al. 2014), (Yu, Qian, et al. 2015), (Wu et al. 2015, Zhang et al. 2015) (Chang et al. 2015). In Figure 2.3 the blue bars represented the size of the for differently modified silica nanparticles.in the literature (Figure 2.3).

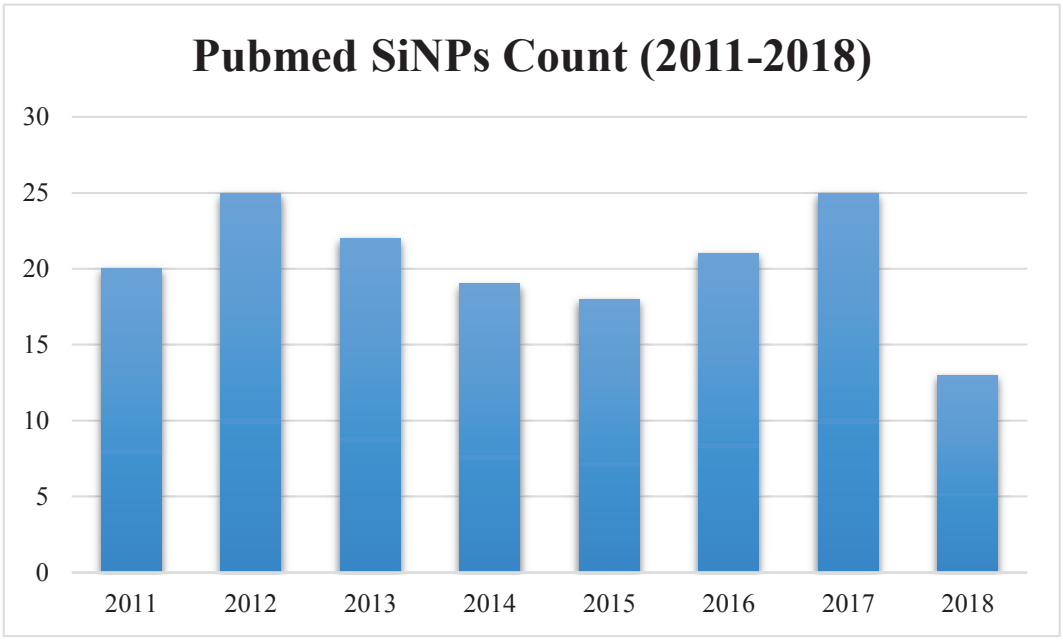

Figure 2.2. Silica nanoparticle search recordings from Pubmed database.

The mostly used HCC cell line was detected as HepG2 cell line among the 41 different publications in Pubmed. All cytotoxicity data from those studies have been summarized and represented in Chapter 3.

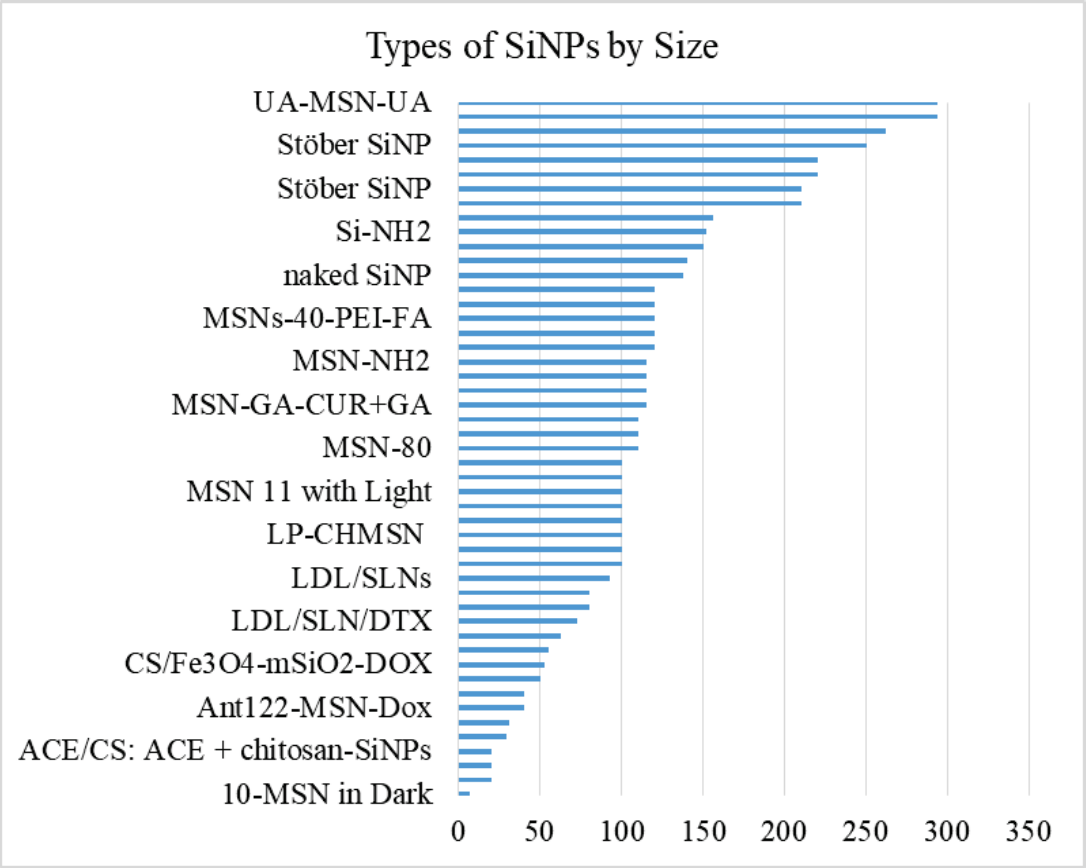

Figure 2.3. The type of SiNPs that were used for hepatocarcinoma cell lines.

10 and 100 nm sized Stöber silica nanoparticles were used in this study on HuH-7 and SK-HEP-1 cell lines as hepatocellular carcinoma cell lines.

2.1. The Synthesis and Physicochemical Characterization of Silica Nanoparticles

2.1.1. Materials

For the synthesis of silica nanoparticles tetraethylorthosilicate (TEOS) (Sigma), ethanol (EtOH) (Merck), ammonia solution (NH_4OH) (Merck), fluoresceinisothiocyanate (FITC)(Sigma),carboxyethylsilanetriol,sodiumsalt, (3-mercaptopropyl)trimethoxysilane,

2-[Methoxy(polyethyleneoxy)propyl]trimethoxysilane were used. The chemicals were used after immediately delivered in our laboratory.

2.1.2. Instruments and Equipments

Synthesis and physicochemical characterization of silica nanoparticles;

The reactor for silica nanoparticle synthesis was purchased from Radley's (The Carousel Parallel Synthesis System). Size and zeta potentials of the nanoparticle suspensions were measured by Dynamic Light Scattering method (DLS) Malvern Zetasizer NanoZS in IZTECH-Chemistry Department. The size and zeta potential measurements were measured by disposable size and capillary cell cuvettes which were purchased from Malvern. The measurements for size and zeta potentials of the SiNPs were repeated three times in a single run. Particles dispersed in a liquid have Brownian motion (free diffusion). The Brownian motion of particles or molecules in suspension causes laser light to be scattered at different intensities. Analysis of these intensity yields the velocity of the Brownian motion and hence the particle size using the Stokes-Einstein relationship (Patravale, Dandekar, and Jain 2012).

Morphology, size and uniformity of the particles were determined by Scanning Electron Microscopy (SEM, Phillips (FEI) XL30- SFEG) and energy dispersive x-ray spectroscopy (EDS) (SEM, Phillips (FEI) XL30 - SFEG in IZTECH- Center for Materials Research and/or Zeiss Sigma 500 in IBG-Izmir. Elemental composition analysis were performed in order to identify the amount of silica and oxygen atoms for 10SiNPs and 100SiNPs. SEM microscopy is composed of backscattered electron images in the display. EDS allow us to use of the X-ray spectrum emitted by a solid powdered sample bombarded with a focused beam of electrons to obtain a localized chemical analysis One can determine the atomic number elements and their distribution in the specimen by compositional contrast (Shindo and Oikawa 2002).

Additionally Fourier transform infrared spectroscopy (FTIR) was used for elemental analysis. FTIR analysis have been performed in Chemistry Department (IZTECH) by using Perkin Elmer and Nicolet 550 spectroscopy units. FTIR Spectroscopy relies on the fact that the most molecules absorb light in the infra-red region of the electromagnetic spectrum. This absorption corresponds specifically to the bonds present

in the molecule. The frequency range are measured as wave numbers typically over the range 4000 – 600 cm^{-1}. The absorption spectrum from the bond natural vibration frequencies indicates the presence of various chemical bonds and functional groups present in the sample. FTIR was used for identification of molecular groups and compounds due to the range of functional groups, side chains and cross-links involved, which have vibrational frequencies in the infra-red range (Faix 1992).

Spectroscopy measurements were performed by using Varian Cary 50 UV-VIS and Varian Cary fluorescence spectrophotometers.

XRD (X-Ray Diffraction) (Philips X'Pert Pro) analysis were performed in CMR-IZTECH (Central for Materials Research-IZTECH). Powder form of particles were used for elemental analyses. XRD spectroscopy is used for phase identification of a crystalline material and can provide information on unit cell dimensions (Alexander and Klug 1948).

ICP-AES analysis were performed by Varian Liberty Series II in IZTECH-Chemical Engineering Department. ICP-AES analysis was performed in Chemical Engineering Department by using Varian Liberty Series II).

2.1.3. Synthesis of Non-Fluorescent Silica Nanoparticles

Silica nanoparticles were synthesized by using the Stöber method (Stöber, Fink, and Bohn 1968) based on hydrolysis and condensation of tetraethylorthosilicate (TEOS) as a silica source. Briefly, ethanol (EtOH) was mixed with ammonia solution (NH_4OH) and stirred for five minutes. TEOS was added under N_2 and they were all stirred for 24 hours at room temperature followingly. An additional, 245 µl (1.1 mmoles) of TEOS was added into the solution which makes silica nanoparticles more soluble by giving more hydroxyl terminals at the surface modification step (Durgun, Ocakoglu, and Ozcelik 2011) The reaction steps were illustrated in Figure 2.4. The Carousel Parallel Synthesis System with round bottom flasks were used to synthesize both types of nanoparticles

The Carousel System has 6 parallel synthesis parts which allowed to synthesize silica nanoparticles in different sizes at the same time. We have used this system in order to optimize synthesis conditions. The chemicals and experimental set-up for both 10 and 100 nm sized silica nanoparticles were summarized in Table 2.1 The amounts of the

chemicals were determined according to previously optimized procedure in our laboratory (Durgun, Ocakoglu, and Ozcelik 2011)

Briefly TEOS and EtOH concentrations were kept constant however the size was controlled by changing ammonia amount in the reaction. The ammonia concentration was changed 0.25-0.91M in range.

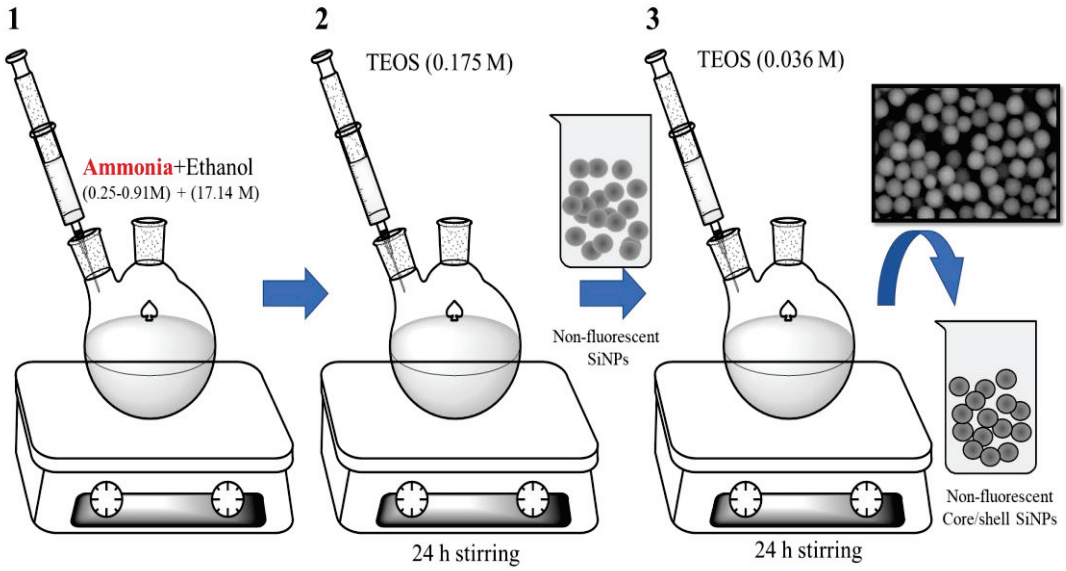

Figure 2.4. Reaction steps of the synthesis of non-fluorescent SiNPs.

Table 2.1. The optimized amounts of the chemicals for the synthesis of 10 and 100 nm sized SiNPs

Type of SiNP	NH_4OH (ml)	TEOS (ml)	EtOH (ml)
100SiNP	1.85	1.2	30
10SiNP	0.5	1.2	30

2.1.4. Synthesis of Fluorescent Silica Nanoparticles

FITC-conjugated (fluorescein isothiocyanate) silica nanoparticles were synthesized in order to determine the sub-cellular localization of SiNPs in the cell. In a typical

synthesis, APTES (0.385 mmol) and FITC (0.0135 mmol) were dissolved in 1.0 ml of absolute ethanol in the dark and under nitrogen atmosphere conditions with stirring for 24 hours at room temperature. Structures of APTES, FITC and conjugate was sketched in Figure 2.5. The stock solution of APTES-FITC conjugate was kept in the dark to prevent photobleaching. APTES-FITC conjugate, ammonia, ethanol and TEOS were mixed for 24 hours. At the last step additional 245 µl TEOS was added for the post-coating of SiNPs as explained in surface coating part. The FITC-conjugated silica particles were washed four times with ethanol to remove unconjugated dyes and other reagents. The purified samples were then dried under nitrogen for physicochemical characterization. The schematic synthesis diagram for the fluorescent nanoparticle was sketched in Figure 2.6.

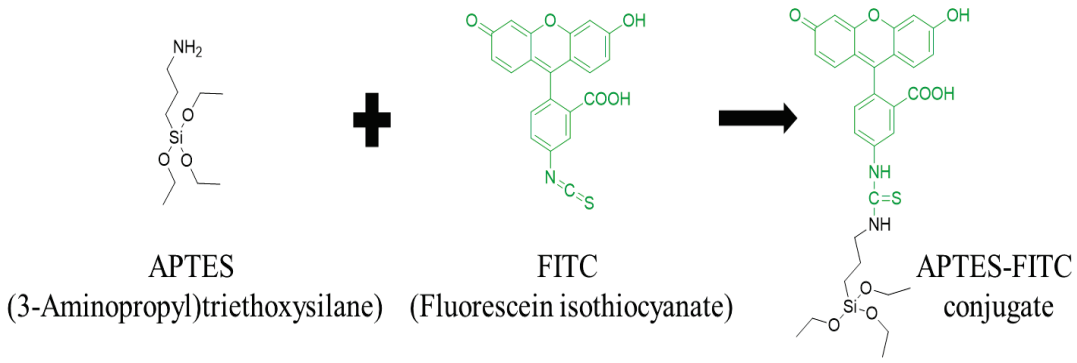

Figure 2.5. Structures of APTES, FITC and APTES-FITC conjugate.

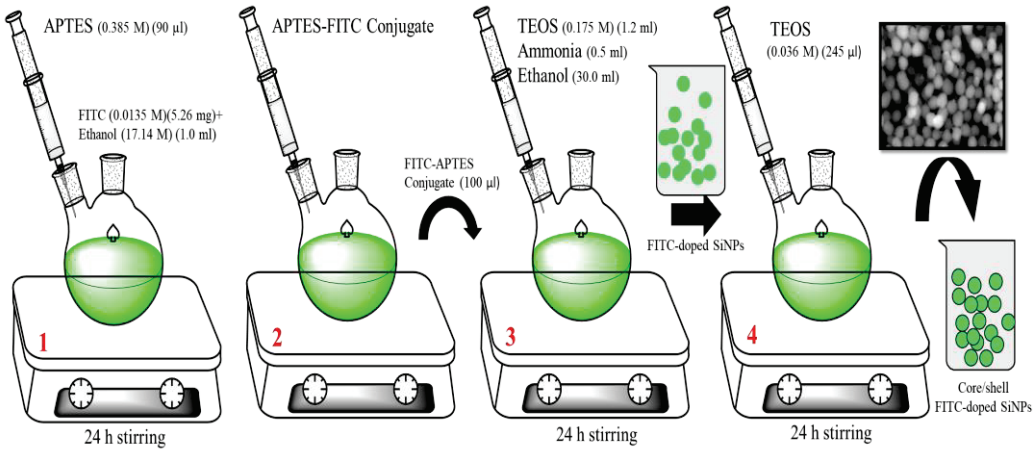

Figure 2.6. The diagram for FITC-conjugated SiNPs synthesis

2.2. Dispersing of Synthesized Silica Nanoparticles

10 nm and 100 nm sized and dried silica nanoparticles were chosen for dissolving in different solvents as ethanol, cell culture medium DMEM (Dulbecco's Modified Eagle Medium). After synthesis step of the nanoparticles the 100SiNP solution was centrifuged at 6000 RPM for 10 minutes in order to remove unreacted reagents.

Resulting pellet was washed and resuspended in pure ethanol. This step was repeated at least 5 times until there is no turbidity seen in reaction tube. 10SiNPs were precipitated by Optima Max XP ultracentrifugation (Beckman Coulter) with MLA-55 rotor. The solutions were centrifuged by quick-seal polyallomer tubes at 50.000 RPM for 18 hours.

After the centrifugations the pellet was laid down side wall of the 50.0 ml reaction tube for overnight. Silica nanoparticles were suspended in buffers up to 1.0 mg/ml concentration. The solutions was then vigorously vortexed (IKA model) and sonicated in waterbath sonicator (Elma Ultrasonic S). The conditions were 25^0C, 30 minutes and sweep mode for waterbath, max. speed for vortex.

2.3. Results and Discussion

2.3.1. Characterization of Silica Nanoparticle Synthesis

2.3.1.1. Dynamic Light Scattering (DLS) Measurements

Silica nanoparticles with two different sizes of SiNPs (10 and 100nm) were prepared by using a modified Stöber method. The size of nanoparticles was tuned by adjusting amount of ammonia between 0.25M and 0.91M. The histograms for size distributions were demonstrated in Figure 2.7 (A and B).

The DLS measurements were performed immediately after the synthesis ("EtOH") to confirm the size of the nanoparticles. The size distributions of 10SiNPs and 100SiNPs in EtOH indicated narrow bandwidths: the particle sizes were respectively 10±3 nm and 99 ± 22 nm for 10SiNPs and 100SiNPs in diameter.

Powdered form of SiNPs (purified) were re-suspended in DMEM+FBS. DLS measurements were repeated. The size of nanoparticles was greater in diameters in cell culture media as expected. 10SiNPs and 100SiNPs had 28±7 nm and 103±39 nm in diameters in DMEM+FBS solution due to biological contents of the media.

The hydrodynamic size of the FITC-conjugated silica nanoparticles were measured as 81±24 nm and 91±25 nm in ethanol and DMEM respectively. The sizes of 10SiNPs and 100SiNPs were represented as black and red lines respectively

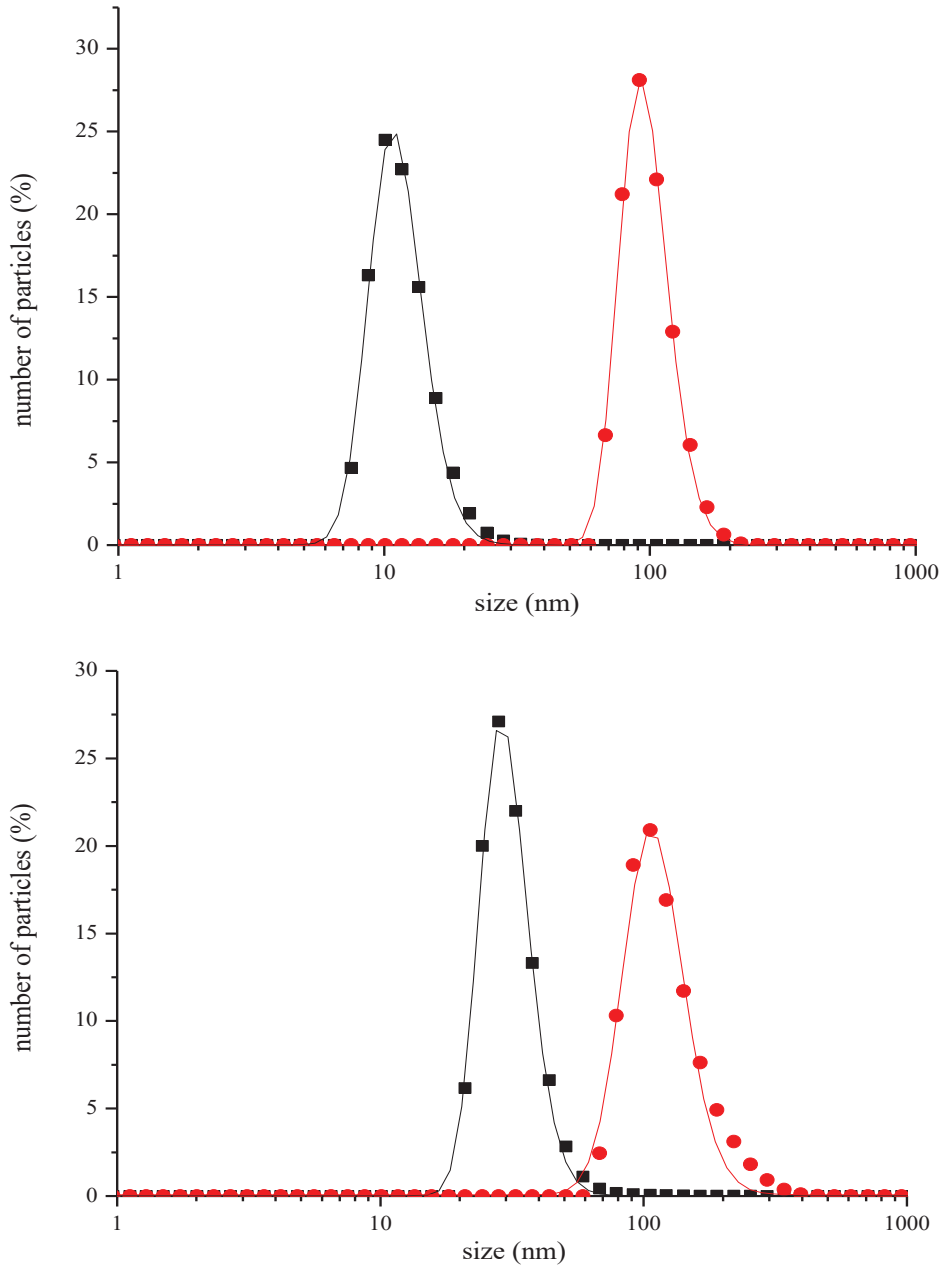

Figure 2.7. The sizes of 10SiNP and 100SiNP nanoparticles in EtOH and DMEM

The size distribution graphs in EtOH were plotted at the above and the size distributions of SiNPs in DMEM were plotted at the below. Size, zeta potential and diffusion coefficient graphs were fitted by using Extreme fitting algorithm in Origin Software.

The presence of protein shell, as anticipated, on nanoparticles could be detected by zeta potential readings. The average zeta potential values of 10SiNPs and 100SiNPs were -13 and -35 mV in EtOH respectively. The measurements were repeated at three runs. One of the three measurements was used for representing the distributions.

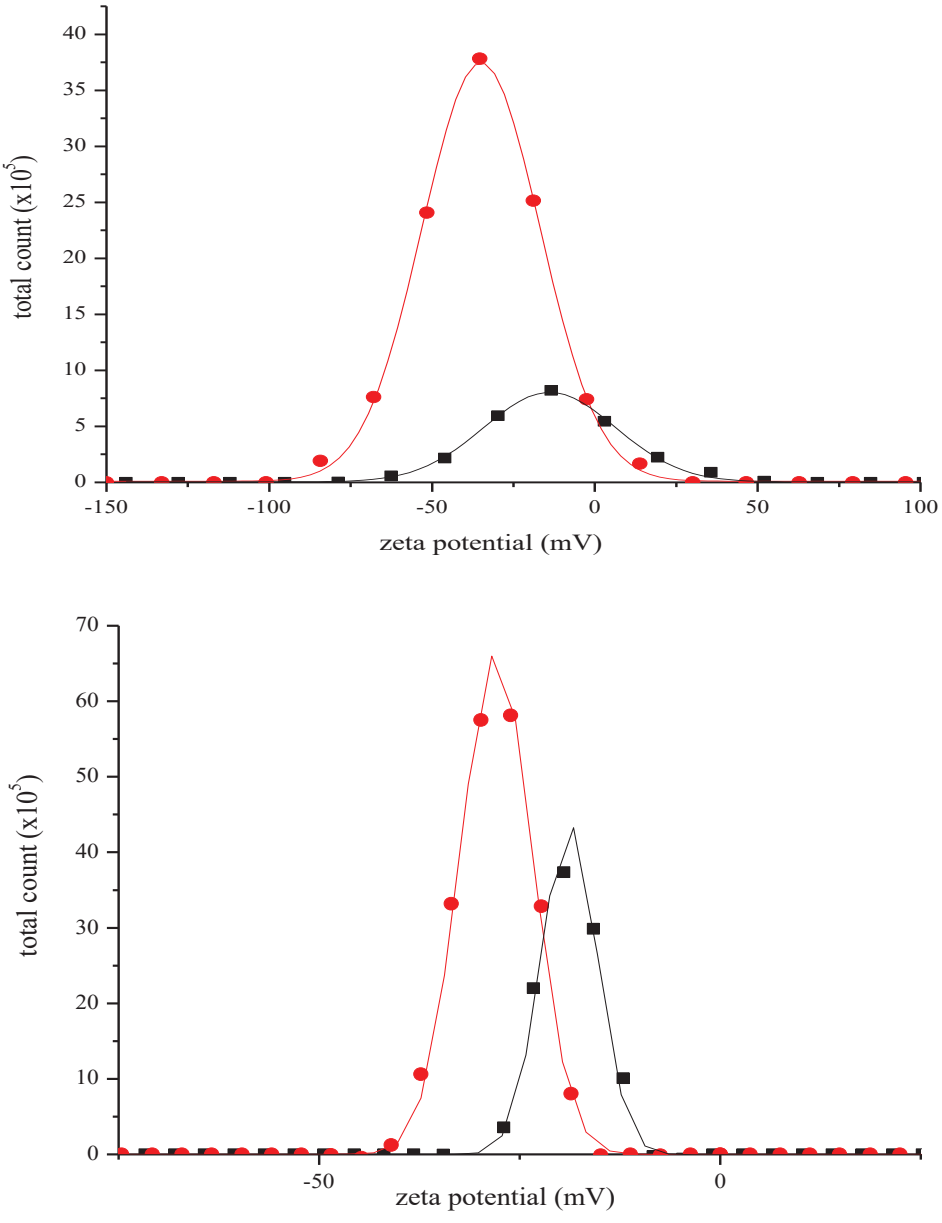

Figure 2.8. Zeta potential graph of silica nanoparticles in EtOH and DMEM

Despite the SiNPs registering different zeta potential reading in EtOH, the zeta potentials in the culture medium were found to be in a similar range; -19 to -28 mV. Adsorption of proteins on the silica surfaces may be facilitated by the electrostatic interactions or van der Waals forces between proteins in serum (FBS) and the surfaces. The zeta potential distributions were displayed and fitted as in C and D (Figure 2.8).

The zeta potentials of 10SiNPs and 100SiNPs were represented as black and red lines respectively. The zeta potential graphs in EtOH were plotted at the above and the size distributions of SiNPs in DMEM were plotted at the below.

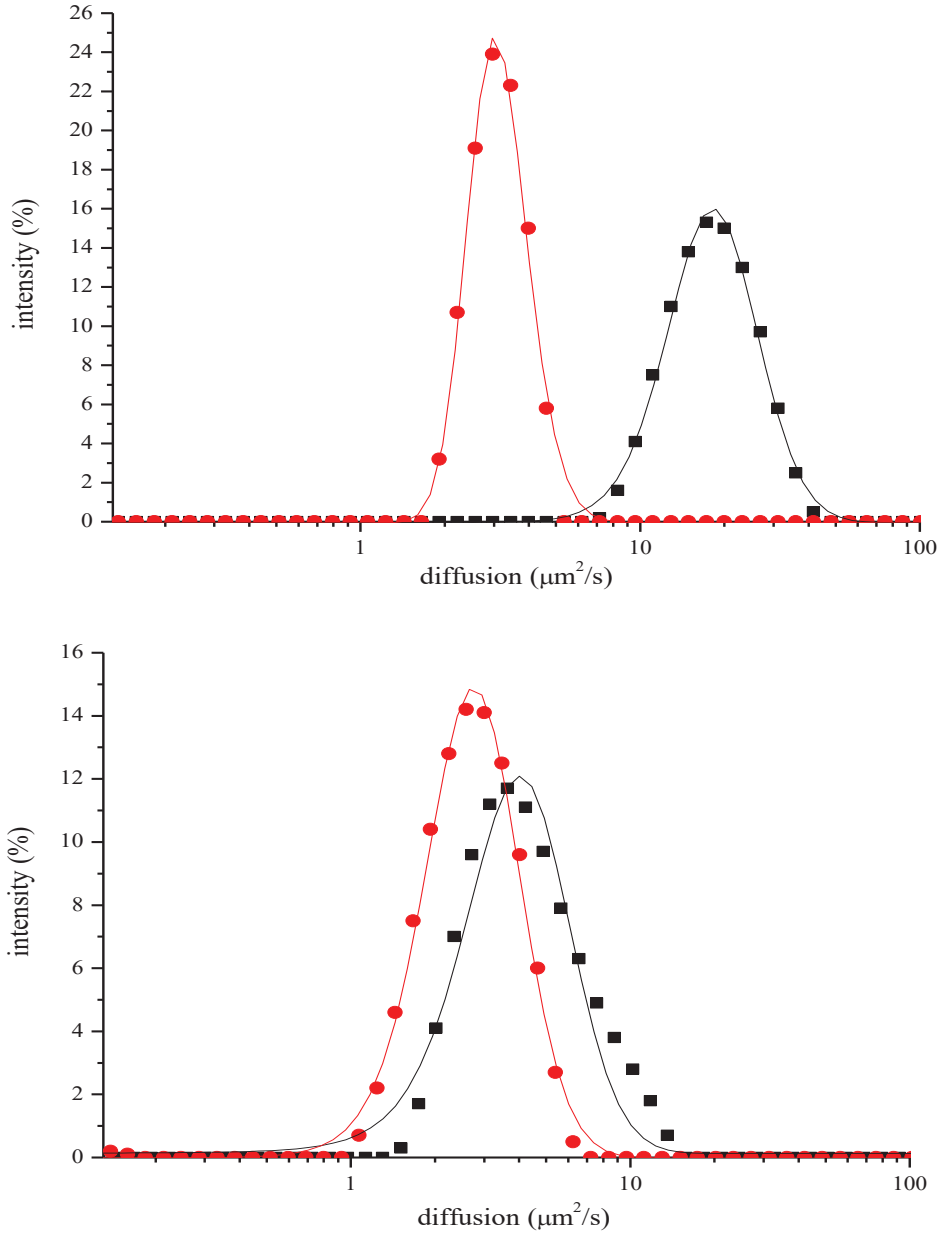

Figure 2.9. Diffusion coefficient distributions were provided in EtOH and DMEM

The size of particles was inversely proportional to diffusion coefficients due to the Stokes-Einstein equation. The diffusion coefficients of 10SiNPs and 100SiNPs were graphed in E and F (Figure 2.9) and found to be 19.0 and 3.0 $\mu m^2/s$ respectively. 10SiNPs in EtOH have higher diffusion coefficients than 100 SiNPs, however, 10SiNPs tend to be agglomerated in aqueous media after purification steps. This resulted an apparent decrease in the diffusion coefficient of 10SiNPs in DMEM+FBS as approx. 4 $\mu m^2/s$.

Diffusions of 100SiNPs in EtOH and DMEM + FBS almost identical (3 $\mu m^2/s$) pointing that the change in size due to the medium is limited.

The diffusions of 10SiNPs and 100SiNPs were represented as black and red lines respectively. The diffusion graphs in EtOH were plotted at the above and the size distributions of SiNPs in DMEM were plotted at the below.

2.3.1.2. TEM and SEM Imaging of SiNPs

TEM images of silica nanoparticles were captured at 25 kV. The samples were prepared by dropwise addition of nanoparticle solutions on formvar grids. Uniformed and spherical shaped nanoparticle structure of 100SiNPs has been shown in representative images in 26K magnifications (Figure 2.10).

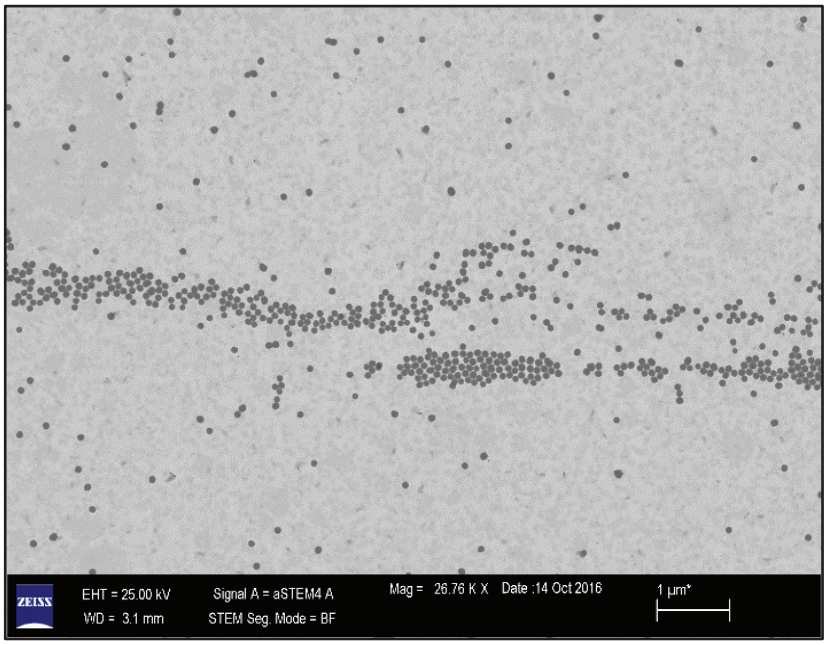

Figure 2.10 TEM images of non-fluorescent silica nanoparticles.

The structural composition of the powdered form of 100SiNPs was analysed by Scanning Electron Microscopy (SEM) with Energy Dispersive X-Ray Spectroscopy (EDS). The silicium and oxygen signals on EDS graph confirming that 100SiNP powder was composed of silicium (47%) and oxygen (53%) atoms (Table 2.2 and Figure 2.10). Representative 100SiNP SEM images have shown the monodisperse size distribution of powdered nanoparticles in 25.000 and 50.000X magnifications (Figure 2.11).

Table 2.2. The composition of SiNP in terms of weight and atomic percentages in powder.

Element	Wt % of Elements in SiNPs	Atomic % of Elements in SiNPs
Si	47	33
O	53	67
Total:	100	100

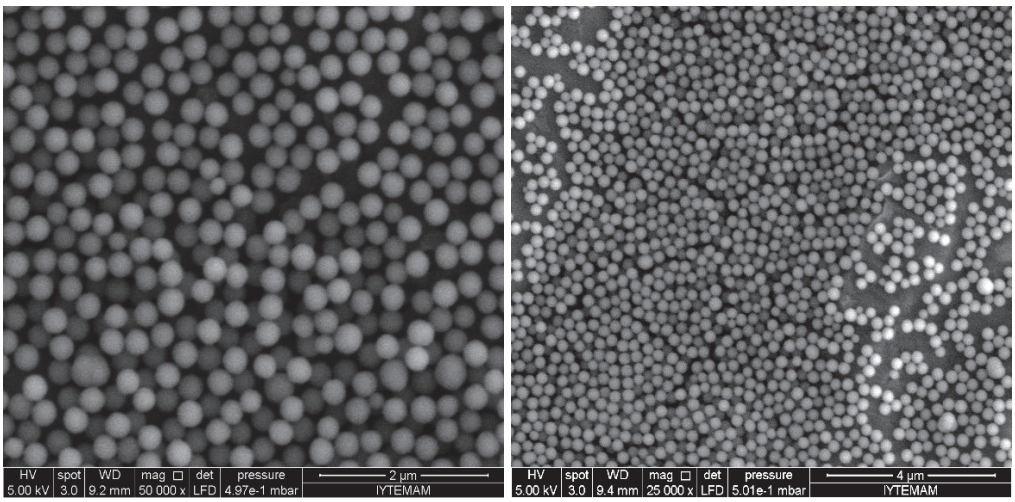

Figure 2.11. SEM images of non-fluorescent 100SiNPs at different magnifications.

2.3.1.3. FTIR Spectroscopy

The ammonia-catalyzed reactions of TEOS in EtOH (the Stöber synthesis) were used for the preparation of silica nanoparticles in the size range of 10 to 100 nm. FTIR spectroscopy confirmed that synthesized 10SiNP and 100SiNP nanoparticles have the

same frequencies in the spectra given in the Figure 2.12. FTIR spectrum of TEOS was inserted for comparison with powdered silica nanoparticles as used silicon source in the synthesis part of the study. The FTIR spectra shows that particles were composed of Si and O atoms in both 10 nm SiNP (B-blue) and 100 nm SiNP (B-red). FTIR spectrum of TEOS was provided for comparison (B-black)

FTIR results indicated that absorption bands arising from asymmetric vibration of Si-O-Si (1090 cm^{-1}), asymmetric vibration of Si-OH (950 cm^{-1}) validated the formation of silica nanoparticles. Si-O-Si and Si-OH vibrations were similar but intensities were decreased in purified nanoparticles as it was expected. The absorption band 2980 cm^{-1} (CH_3) and 2930 cm^{-1} (CH_2) in TEOS spectrum were disappeared in silica nanoparticle spectra meaning that TEOS was converted to nanoparticle in suspensions. Absorption bands of molecular water between 3300 cm^{-1} and 3500 cm^{-1} and the band at 1635 cm^{-1} assigned to O–H stretching were observed as well.

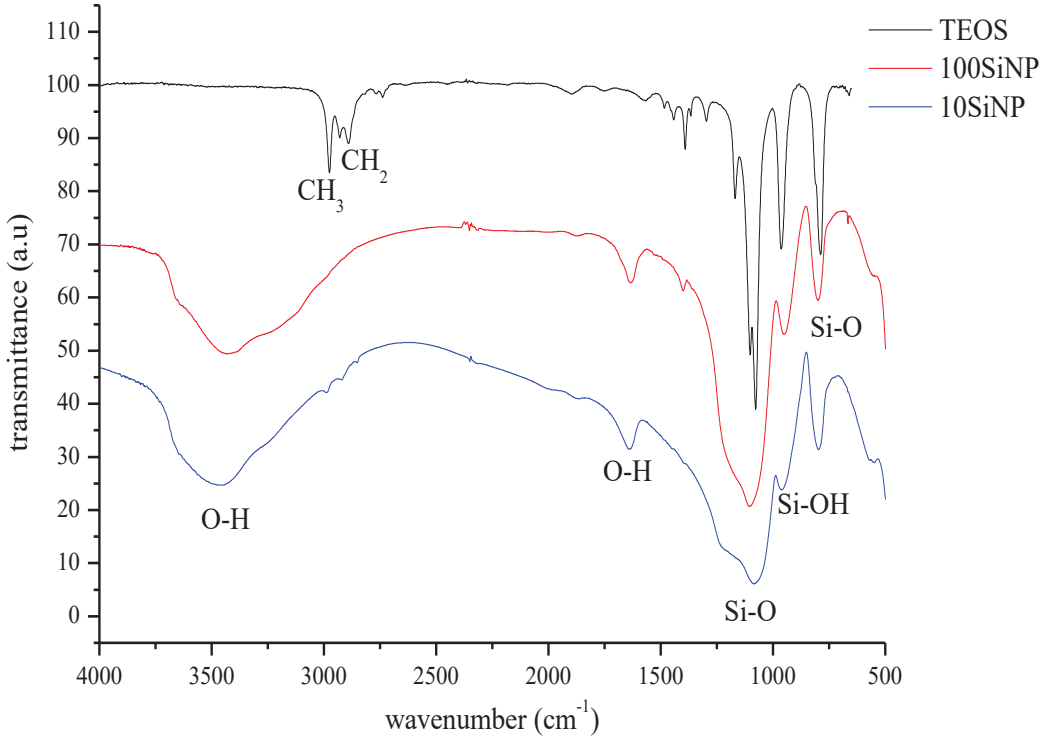

Figure 2.12. The FTIR spectra of 10SiNP, 100SiNP and TEOS.

Additionally ^{13}C and ^{29}Si NMR spectroscopy were carried out and data published by our lab in 2011 (Durgun, Ocakoglu, and Ozcelik 2011). ^{29}Si NMR measurements were performed by Bruker Avance 500WB 99 MHz NMR spectrometer. It is possible to

determine the chemical structure of substances that can be prepared from (organo)-alkoxysilanes (van Blaaderen and Vrij 1993) and to obtain information about the surface characteristics of silica particles have been formed in the coating reactions. ^{29}Si CP-MAS and ^{13}C CP-MAS NMR measurements were used to determine the fate of the ethoxy and aminopropyl groups of the (organo)-alkoxysilanes on the particle surface. The NMR spectra is revealed that the existence of $-NH_2$ groups in the particle structure, although the particles were post-coated with an additional amount of TEOS.

2.3.1.4. Determination of Si Amount in Silica Powder

2.3.1.4.1. X-Ray Diffraction Analysis

The XRD (X-Ray Diffraction) pattern of SiNPs suggests that the most compatible structure is tetrahedral α-cristobalite structure. We estimated the volume, mass and number of 10SiNP and 100SiNP nanoparticle in 2.0 mg of powder by using numerical data for the α-cristobalite lattice structure and dimensions. The XRD pattern for the α-cristobalite were given for 100SiNP in the Figure 2.13.

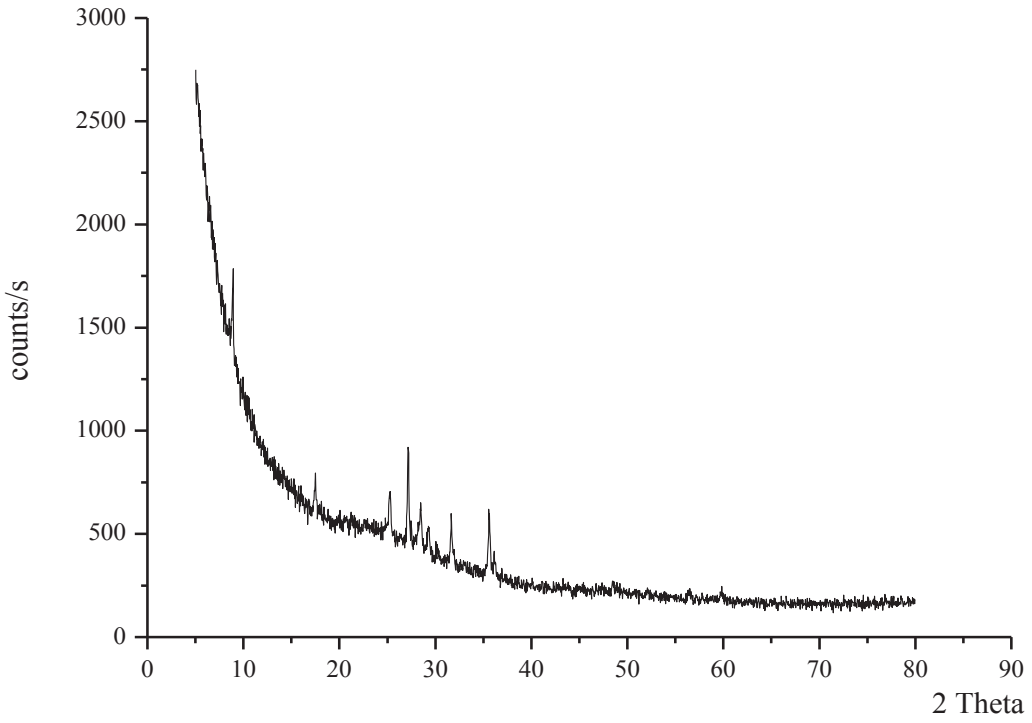

Figure 2.13. XRD pattern of 100SiNP

Representative calculation of number of 100 nm sized SiNP per milligram are below:

Lattice parameters → a = b ≠ c → a:c = 1:1.1394 (Shackelford and Doremus 2008)

Since a= 0.7898 nm, c = 0.8999 nm

Volume of the unit cell = a×b×c = 0.7898 nm×0.7898 nm×0.8999 nm = 0.56 nm^3

$$\frac{4}{3}\pi r^3 = 5.236 \times 10^5 nm^3 \quad (2.1)$$

Number of unit cells for 100 nm sized one nanoparticle;

$$\frac{5.2 \times 10^5 nm^3}{0.56\ nm^3} = 9.3 \times 10^5 \quad (2.2)$$

Since there is 8 Si atom in one unit,

$$9.3\times 10^5 \times 8 = 7.4 \times 10^6 \text{Si atoms} \quad (2.3)$$

Total number of atoms in one nanoparticle;

In terms of Si atom and for O atom → Since Si = 2 O

$$7.4\times 10^6 \text{Siatoms} \times 2 = 1.48 \times 10^7 \text{Oatoms} \quad (2.4)$$

$$\frac{7.4 \times 10^6\ \text{Si atoms}}{6.02 \times \frac{10^{23}\ \text{atoms}}{\text{mol}}} = 1.23 \times 10^{-17}\text{mol} \quad (2.5)$$

$$\frac{1.48 \times 10^7 \text{O atoms}}{6.02 \times 10^{23}\ \text{atoms/mol}} = 2.46 \times 10^{-17}\text{mol} \quad (2.6)$$

$$1.23 \times 10^{-17}\text{mol} \times 28\frac{\text{g}}{\text{mol}} = 3.4 \times 10^{-16}\text{g} \quad (2.7)$$

$$2.46 \times 10^{-17}\text{mol} \times 16\frac{\text{g}}{\text{mol}} = 3.9 \times 10^{-16}\text{g} \quad (2.8)$$

$$3.4 \times 10^{-16} + 3.9 \times 10^{-16} = 7.3 \times 10^{-16}\text{g} \quad (2.9)$$

As a result, 1.0 g nanoparticle sample includes;

$$\frac{1\text{g}}{7.3 \times 10^{-16}\text{g}} = 1.36 \times 10^{15}\text{nanoparticles} \quad (2.10)$$

1 nanoparticle includes ;

$$\frac{3.4 \times 10^{-16}\text{g}}{7.3 \times 10^{-16}\text{g}} \times 100\% = 47\%\text{Si} \tag{2.11}$$

2.4. Conclusion

The size of the Stöber silica nanoparticles were tuned by changing the ammonia concentration in the reaction. It is crucial to identify the characteristics of the SiNPs before their usage in cell culture applications. The SiNPs were fully characterized by physicochemically. It was proved that the synthesized particles were 10 and 100 nm in size in the synthesis medium but their size were increased and zeta potentials remained nearly same when they dissolved in the cellular media. Their diffusion coefficients of the 10SiNPs were decreased when they dispersed in DMEM but diffusions of the 100SiNPs remained nearly same in cell culture media.

The fluorescent intensity of FITC-conjugated SiNPs and FITC alone were recorded in DMF, ethanol and water. The peak position shifted to red because of the solvatochromatic effect as the solvent molecules interact freely with FITC molecules. However, the spectra of FITC conjugated to the particles showed no variation with the solvents. It was considered that the solvent molecules do not reach the FITC molecules conjugated to the particle; an effective protection layer against solvents has been provided by the silica network for FITC molecules. These results supported the findings that the protection provided by the silica matrix to FITC against changes in pH of the environment.

The synthesized nanoparticles have uniformed morphology. The unit cell structure of the silica powders were found to be compatible with cristobalite structure. Calculations based on unit cell dimensions and EDS measurements were demonstrated that the number of particles per milligram for 100SiNP was respectively 1.36×10^{15} in 1.0 g of powder. Additionally 1 SiNP particle contained 47% of Si which was compatible with EDS results.

CHAPTER 3

CELLULAR BEHAVIOURS OF HEPATOCELLULAR CARCINOMA CELL LINES

Depending on their type and concentration the nanoparticles may cause either cell death or side effects; both these situations can be considered together in the term "cytotoxicity". Nanoparticles offer the unique possibility to overcome cellular barriers to improve the delivery of therapeutics as nucleotides, plasmid DNA, drugs and biomacromolecules (Panariti, Miserocchi, and Rivolta 2012). The analysis of literature sources revealed that the silica nanoparticles were produced in a large size scale for biological applications. We preferred to synthesize both 10 and 100 nm sized silica nanoparticles in order to determine the cellular behaviours of the cell depending on particle size. There are literature about the fact that most of the nanoparticles are sequestered by the liver and spleen (if >6nm) or eliminated though the kidney (if<6 nm) after administration into the body. It was logical to produce the nanoparticles at the cut-off size to elucidate the physiological responses of the cells (Zhang, Poon, et al. 2016).

There are several HCC cell lines as HepG2, HuH-7, SK-HEP-1, Hep3B, Hep40, SNU398 SNU475 SNU449, SNU387, FOCUS, Mahlavu and SNU182 (Yuzugullu et al. 2009a). The literature was searched for silica nanoparticles and HCC cell lines by using Pubmed. It has been noticed in the literature that the mostly studied HCC cell line was HepG2 to assess the cellular behaviours of hepatocarcinoma cells after silica nanoparticle exposure. HepG2 is one of the well-differentiated cell line which has low motile and low invasive characteristics (Yuzugullu et al. 2009a). The silica nanoparticle literature was analyzed for HepG2 and HCC cell lines. The Table represented the detailed information for cell type, nanoparticle modification with exposure time, amount, and size of the nanoparticles for the evaluation of cytotoxicity. The graphs show the data for viability of the cells versus time, amount and the sizes of SiNPs. The data were collected for all HCC cell lines and then filtered for HepG2 cell line (Figure 3.1. and 3.2. and Table 3.1)

The safe area can be distinguished from the 3D scattered graphs for HCC cell lines. The cells can be accepted as viable above 80% after up to 200 μg/ml concentration of ~100-nm SiNPs. The exposure range was between 1 and 72 hours. It can be deduced

from the graph that cells seemed to be viable up to 72 hours but mostly the cells were incubated with nanoparticles for 24 hours. The viability graphs for HepG2 cells were represented in Figure 3.1., 3.2. and 3.3. HepG2 cells were treated with mostly 100-nm sized silica nanoparticles up to 200 µg/ml amount for 24 hours. The silica nanoparticle types were modified for binding of a lipid, polysaccharide and a microRNA sequence or unmodified mesoporous SiNPs.

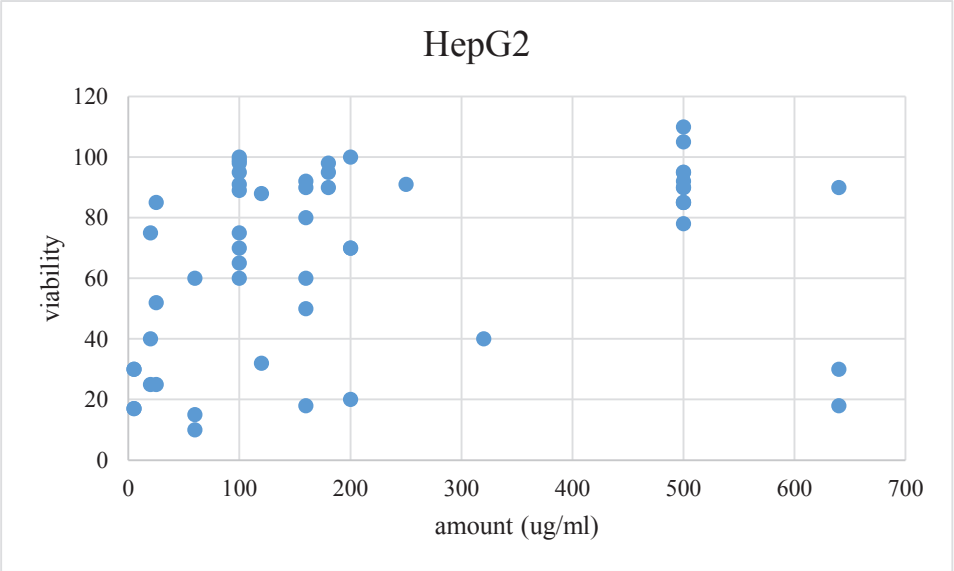

Figure 3.1. The viability vs amount graph from the literature search for HepG2.

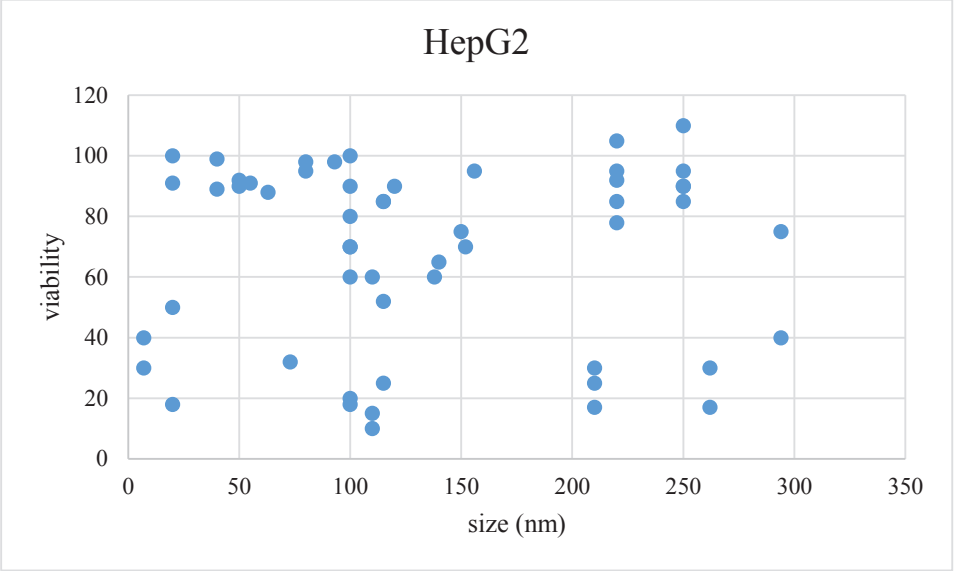

Figure 3.2. The viability vs size graph from the literature search for HepG2.

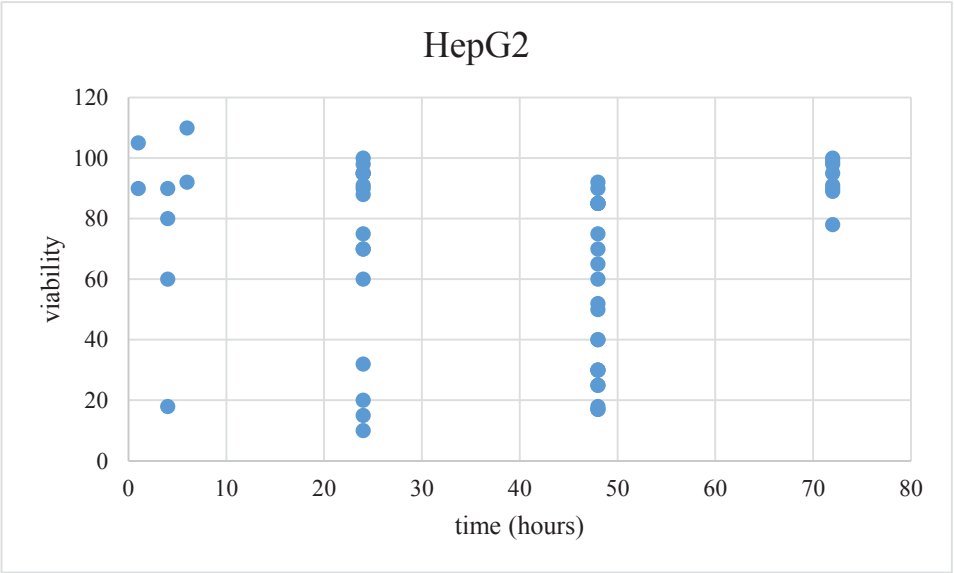

Figure 3.3. The viability vs time graph from the literature search for HepG2.

It is well-known that nanoparticles can impair cellular functions leading to promotion of oxidative stress. Nanoparticles may impair mitochondrial functions which may resulted in aborted cell cycle (Mahmoudi et al. 2011). The literature was searched for years between 2011 and 2018 about the effects of Stöber silica nanoparticles on the normal cell life cycle of the cells. The results were summarized in Table 3.1.

In 6 separated studies the cells were arrested at G0/G1 phase mostly after exposure with SiNPs that the size range was between 28 and 159 nm. The maximum nanoparticle concentration was 200 µg/ml. It seemed that apoptotic cells were only hMSC (human mesenchymal stem cells) in 10 studies that the cells were arrested at sub-G0 phase (Figure 3.4). A549 cells were arrested at G0/G1 and S phase in different studies. HUVECs seemed to be affected at mitosis phase (G2/M) however no arrest observed in another study in the literature. Even if the size of nanoparticles were recorded as nearly identical the cell cycle of the HUVECs cells were altered depending on amount of nanoparticles.

There was one study about the potential effects of the Stöber SiNPs on the cell cycle of HepG2 as a hepatocellular carcinoma cell line. This study clearly identified that the SiNP-induced adverse effects of multinucleation give a rise the urgent need to define the appropriate conditions for the safe use of SiNPs (Yu, Duan, et al. 2015).

In this study we have evaluated the toxicity of 10 and 100 nm sized SiNPs and measured the cell population at cell cycle phases up to 20 µg/ml concentration for 3 days by flow cytometry.

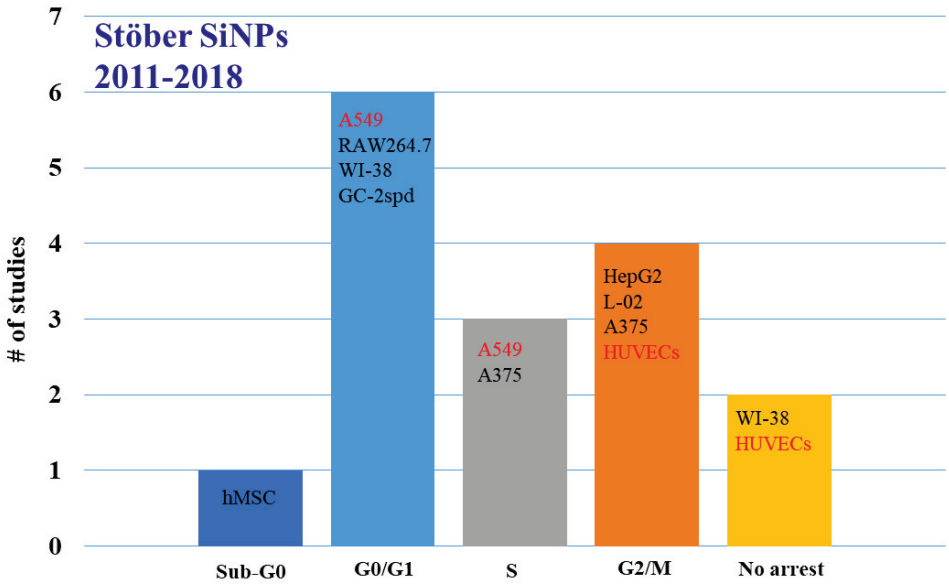

Figure 3.4. The graph from literature data for cell cycle.

Table 3.1. The effects of SiNPs on the cell cycle of the cell lines in the literature

	Cell line	NP size (nm)	NP amount (µg/ml)	Phase Arrest	References
1	HepG2	107	100	G2/M	(Yu, Duan, et al. 2015)
2	A549	28	32.5	G0/G1	(Gonzalez et al. 2014)
3	A549	59	100	G0/G1	
4	A549	139	100	S	
5	A549	174	150	S	
6	HUVECs	63	10	no arrest	(Asweto et al. 2017)
7	RAW264.7	20	125	G0/G1	(Yang et al. 2016)
8	L-02	53	200	G2/M	(Yu, Duan, et al. 2015)
9	WI-38	158	200	G0/G1	(Athinarayanan et al. 2014)
10	WI-38	158	50	no arrest	
11	A375	110	200	S	(Huang et al. 2010)
12	A375	110	200	G2/M	
13	GC-2spd	58	25	G0/G1	(Zhang, Ren, et al. 2016)
14	GC-2spd	58	50	G0/G1	
15	hMSC	45	200	sub-G0	(Periasamy et al. 2015)
16	HUVECs	62	100	G2/M	(Duan et al. 2013)

3.1. Instruments and Equipments

Cell Cultivation and Cellular Culture Studies;

The cells were cultivated in Memmert INC 108 CO2 incubator and Esco Laminar Cabinet. Hettich Rotofix 32A centrifuge and Memmert WNE7 waterbath were routinely used for maintenance of the cells.

MTT assay were read out by Varioskan Flash Spectroscopy (Thermo) after centrifugation by HETTICH ROTINA 38R in IZTECH- Izmir Institute of Technology, Biotechnology and Bioengineering Research and Application Center.

Genotoxicity was studied in IBG-Izmir in ATABEY Lab by Dr. Erkan KAHRAMAN.

Flow cytometry measurements were performed by BD FacsCanto in Izmir Institute of Technology, Biotechnology and Bioengineering Research and Application Center and BD Canto II, BD LSR Fortessa X20 in IBG-Izmir.

3.2. Cell Cultivation

We have cell culture facility in our research laboratories. Hepatocyte derived cellular carcinoma cell lines as HuH-7 and SK-HEP-1 were used in order to determine the effects of silica nanoparticles. Cells are maintained in Dulbecco's modified Eagle's medium (DMEM) containing 10% fetal bovine serum (FBS), 1% (v/v) L-Glutamine, 1% (v/v) Penicilline-Streptomisin and non-essential aminoacid solutions 1% (v/v). And the cells are incubated at 37ºC in the dark with 5% CO_2 and 95% humidification and passaged when they reached 80-85% confluency. The adherent cell lines are trypsinized and washed with 1X PBS before reculturing the detached cells. Tryphan blue staining was applied for live cell counting.

3.3. Cytotoxicity

The viability of the hepatocellular carcinoma cell lines was determined by (3-(4,5-Dimethylthiazol-2-yl)-2,5-diphenyltetrazolium bromide (MTT) assay. Test principle was

based on reduction of tetrazolium salt (MTT) into its insoluble formazan giving a purple colour by mitochondrial reductase in living cells (Yanez et al. 2004). MTT test was performed to evaluate cell's viability upon the nanoparticle treatments of the cells. HuH-7 and SK-HEP-1 cells were plated at a density of $5x10^4$ cells per well in flat bottom 96-well plates allowed to grow overnight prior to the exposure to SiNPs at different concentrations. After 24 hours, the cells were treated with 0.2, 2, 20, 200 μg/mL nanoparticles (typically 4.4×10^{16} and 8.3×10^{11} particles/mL of 10SiNP and 100SiNP) suspended in DMEM. The cells were treated with 10SiNPs and 100SiNPs and 1 mM hydrogen peroxide solution providing for a positive control in DMEM up to **120 hours**. Before adding of MTT (0.5 mg/ml) onto the wells they were washed with PBS (phosphate buffered saline) buffer. Subsequently the plates were incubated 37^0C for 4 hours. The medium containing MTT solution was replaced with DMSO and shaken 10 minutes in order to solubilize formazan crystals indicating the cells with active mitochondria. The absorbance was measured by Varioskan Spectrophotometer at both 545 nm and 720 nm to subtract background. The results were expressed as absorbance data of formazan crystals indicating amount of active mitochondria in the cells (Terry L Riss et al. 2004).

The SRB (sulphorhodamine B) assay was also used for determination of cellular density based on measuring the amount of cellular protein content. This assay differs from MTT due to measuring protein content, offering another way of assessing the cellular viability. The cells are plated on 96-well culture dishes. After incubation periods, cells were fixed with 10% trichloroacetic acid (TCA) and stained with SRB for 30 min., after that the excess dye is removed by washing repeatedly 1% acetic acid. The protein bound dye is dissolved in 10 mM Tris base solution for optical density measurement both at 510 and 565 nm using microplate reader (Orellana and Kasinski 2016).

3.4. Flow Cytometry

Flow cytometry is a technique developed in the 1940s by Shapiro. Nanoparticles could cause several effects on the cells. These effects may be arisen from interactions with cell membranes and cellular uptake, signalling pathways, ROS production to gene regulation, cell cycle dysregulation, and finally apoptosis or necrosis (Mahmoudi et al.

2011). Measuring the cell cycle changes for nanoparticle toxicity is an important index for the cellular behaviour.

The procedure for analysing the cell cycle was optimized for FACS Canto™ Flow cytometer (Becton Dickinson). The cells cultured and incubated with SiNPs for 24 hours were collected by trypsinization and washed twice with ice cold PBS. The ethanol-suspended cells were centrifuged for 5 min at 300g. The cells were permeabilized in 0.1 % TritonX-PBS solution after fixation in ice cold 75 % ethanol. DNA was stained with 0.1 mg/ml propidium iodide (PI) for 15 minutes. The cells were transferred into flow cytometer tubes and assayed with FACS Canto™ Flow cytometer (Becton Dickinson). To detect PI emission, a solid state laser at 488 nm was used for excitation, and a combination of 556/LP and 585/40 BP emission filter configuration was used for detection. Results were analyzed with FACS Diva Software v5.0.3 (Becton Dickinson) and ModFit LT 3.0 programs (Piotr Pozarowski and Darzynkiewicz 2014)

3.5. Genotoxicity Test

Genotoxicity may be resulted from low solubility of the particles and their potential to produce ROS in the cells. The nanoparticles are characterized by their small size and high atom-to-surface ratio comparing to micro sized particles. Therefore it is expected that engineered nanoparticles could potentially carry genotoxic hazard (Corvi and Madia 2017).

Ames test, erythrocyte micronucleus test, the mammalian bone marrow chromosomal aberration test, the transgenic rodent somatic and germ cell gene mutation assay, *in vivo* mammalian alkaline Comet assays mostly used for determination of genotoxic potential of the materials.

We have used cytokinesis blocked micronucleus assay in order to elucidate the toxic potential of SiNPs on lymphocytes.

First step was the isolation of lymphocytes from blood before micronuclei scoring (Corvi and Madia 2017). The frequencies of micronuclei. nuclear bund and nucleoplasmic bridge formation were assessed for non-treated, silica nanoparticle treated and Mitomycin-C treated cells. Nuclear division index (NDI) was calculated for each condition.

3.5.1 Isolation of Lymphocytes from Blood

Human peripheral blood was obtained by venipuncture from heatly male volunteer (29 age, non-smoker, not affected by radiation, and not under any medication). Fresh blood (~8ml) was collected into Vacutainer® CPTTM (Cell Preperation Tube) (BD Cat: 362761). The CPT were processed according to the manufacturer's instructions, by centrifugation at 1700 g for 20 minutes at room temperature. Cellular content was transferred to another tube and added PBS up to 15 ml. Tube was gently inverted several times and centrifuged at 300g for 15 minutes at room temperature. Lymphocyte pellet was suspended at a concentration of 106 cell / 750µl in RPMI-1640 medium supplemented with 20% FBS, 2mM L-Glutamine, 2.4 µg/ml phytohemagglutinin L, 100 units/ml penicillin and 100 µg/ml streptomycin at 37℃ in a humidified atmosphere of 5% CO_2 (W. and A. 1969).

3.5.2. CBMN Assay (Cytokinesis Blocked Micronucleus Assay)

Cytokinesis blocked micronucleus assay were performed for assessment of genotoxicity levels, as described by (Fenech 2007). Briefly, the isolated lymphocytes were incubated with the various concentrations of the SiNP (0, 0.2, 2, 20 µg/ml) at 24 hour after the start of incubation. 4.5 µg/ml Cytochalasin-B (Cyt-B) was added into cellular suspension at 44th hour and incubated until 72 hours. At the end of the incubation, the cells were harvested by centrifugation and stained with Giemsa. The cells were imaged under 1000X magnification to determine micronucleus part of the cell. Micronuclei scored in 1000 binucleated cells from each of the duplicate culture (total 2000 BN cells). Nuclear division index (NDI) was calculated according to method of Eastmund and Tucker (David and James 1989).

$$\mathrm{NDI} = (\mathrm{M1} + 2\mathrm{M2} + 3\mathrm{M3} + 4\mathrm{M4})/\mathrm{N} \qquad (3.1)$$

M1 to M4 represent number of cells with 1-4 nuclei and N is the total number of scored cells. The cell and numbers of micronucleus were statistically analysed by using One Way ANOVA and post-hoc Tukey.

3.6. Results and Discussion

3.6.1. Viability Tests

It is highlighted in the literature that cytoplasmic proteins stained within SRB assay and metabolically active mitochondria were stained by MTT. The *in vitro* cytotoxicity for hepatocellular carcinoma cell lines of HuH-7 and SK-HEP-1 were assessed by MTT and SRB assays.

The SiNP concentrations were varied from 0.2 to 200 μg/mL with incubation time up to five days (Figure 3.6). Nanoparticles were suspended and diluted from the stock solution of DMEM with FBS. As positive control, hydrogen peroxide (1 mM) was used for comparing the cell viability. DMEM absorbance was ignorable at the measurement wavelength. The viability data were expressed as percentages by comparing control and treated groups. Error bars represented the standard deviations for n=4. Differences in cell proliferation between cells were analyzed by ANOVA for repeated measurements with in GraphPad Prism®. Statistical significance indicated by the p value ($p < 0.05$). Mitochondrial activity of HuH-7 cells was not affected neither 10SiNPs nor 100SiNPs up to 120 hours. Viability of SK-HEP-1 cells remained similar with the controls at 120 hours for 10SiNPs. SK-HEP-1 cells seemed to be affected in the presence of 100SiNPs of 2, 20 and 200 μg/ml at 72 hours however the 100SiNPs did not exhibit long-term effects on SK-HEP-1 cells. Hydrogen peroxide were cytotoxic and decreased the mitochondrial activity for 1 mM concentration up to 120 hours independent of cell line, validating the assessment method of the cell viability.

Sulphorhodamine-B (SRB) test was also performed as a viability test. SRB was used in order to analyse the chemosensitivity of the cell lines (Orellana and Kasinski 2016). Moreover, SRB assay does not depend on mitochondrial enzymatic activity but on cytoplasmic protein content. We used different assays in order to identify the cells' physiological response to the SiNPs.

MTT assay results were represented in Figures after incubation of 10SiNP at the above and incubation of 100SiNP at the below.

The medium of the cells were changed with fresh media after 3 days of incubation for both MTT and SRB experiments.

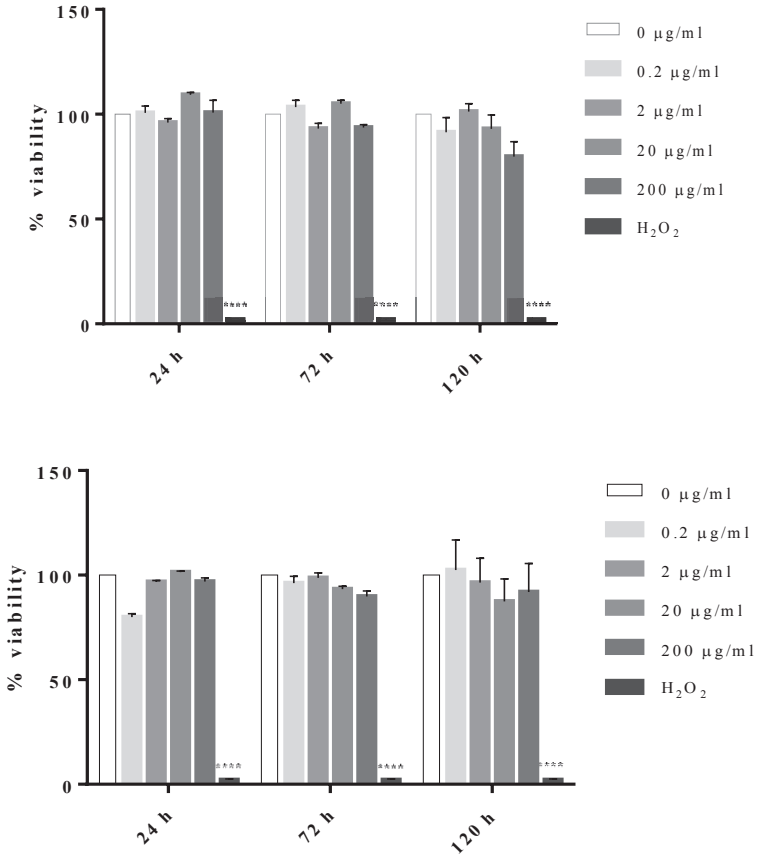

Figure 3.5. The cytotoxicity of 10SiNPs and 100SiNPs for HuH-7 cell line.

Protein content of HuH-7 cells remained after 10SiNP treatment up to 120 hours whereas they were affected by 100SiNP after 24 hours (Figure 3.7). Absorbance of the HuH-7 cells were decreased at 72 hours as comparing with absorbance of control group. 100SiNPs were decreased the absorbance of HuH-7 cells for all concentrations although there was a small increase after 0.2 µg/ml at 120 hours. 100SiNPs led to a decrease in protein absorbance of SK-HEP-1 cells at 72 hours for all concentrations. Similarly, viability of SK-HEP-1 cells remained up to 120 hours for 100SiNPs. Besides both nanoparticles did not induce the cell viability based on absorbance data for SK-HEP-1 cell lines. SRB method relies on the characteristics of SRB, which binds stoichiometrically to proteins under mild acidic conditions. The protocol can be divided into four main steps as preparation of nanoparticles, incubation of cells with nanoparticles, cell fixation and SRB staining, and absorbance measurement. Since this method does not rely on measuring metabolic activity as MTT, the method has been optimized for HuH-7 and SK-HEP-1 cell lines (Orellana and Kasinski 2016).

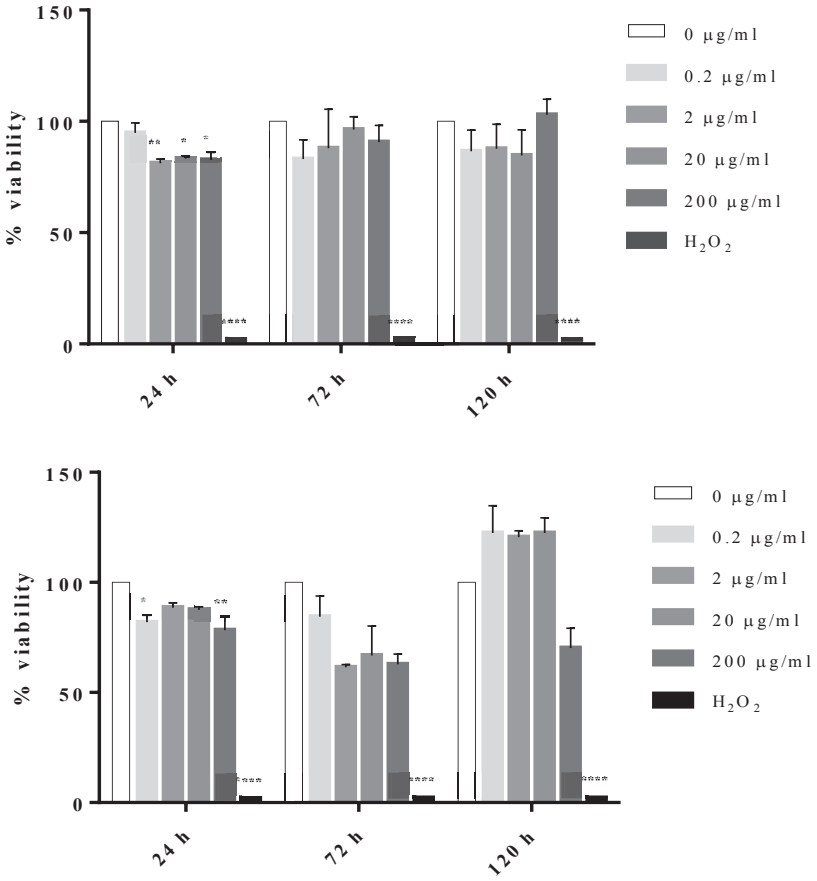

Figure 3.6. The cytotoxicity of 10SiNPs and 100SiNPs for SK-HEP-1 cell line

Nanoparticle suspensions were identical for the SRB experiments as used for MTT. The responses to 10SiNP (left) and 100SiNP (right) for both cell lines (blue: day 1, orange: day 3, grey: day 5)

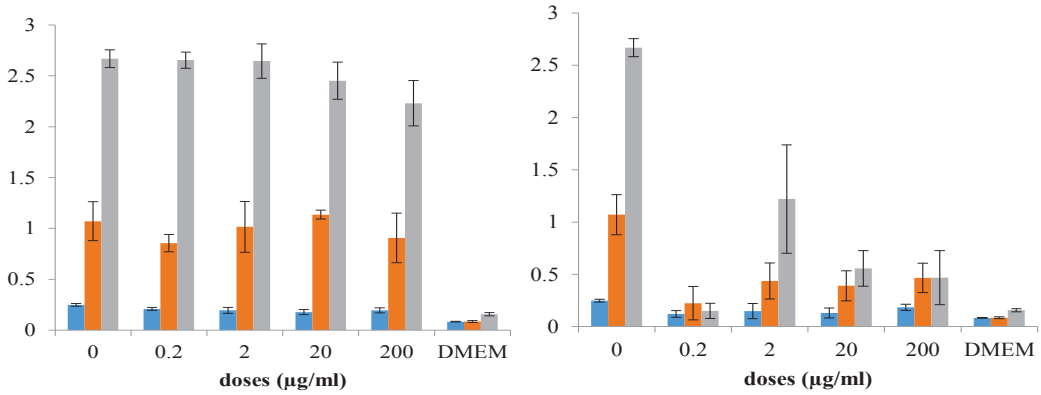

Figure 3.7. SRB assay results for the HuH-7 cell lines.

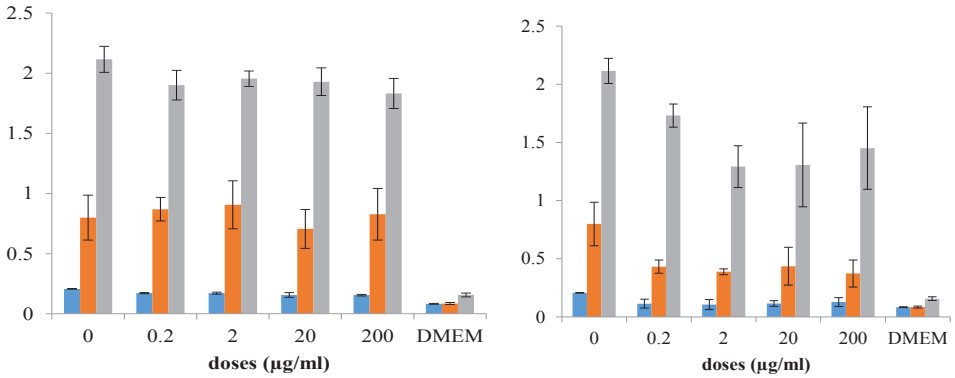

Figure 3.8. SRB assay results for the SK-HEP-1cell lines.

3.6.2. Flow Cytometry

We examined cell cycle progression of both cell lines after the treating them with 0.2, 2.0 and 20.0 µg/mL concentrations of 10SiNP and 100SiNP up to 3 days, using flow cytometry. The results were depicted in Figure 3.9 and Figure 3.10. The cell cycle graphs and the scatter plots along with the gates used for the both cell lines were shown. The graphs represented the cycle of the cells after 24, 48 and 72 hours of nanoparticle treatment. Typically, the first peak was ascribed to cells in the G0/G1 phase, while the second peak corresponds to G2/M. The S phase lies between these two peaks. The doublets or aggregates of the ethanol-fixed and PI-stained cells were dispensed in a FL2 width or height versus area scatter diagram. This gate applied to an FL2 area histogram.

G1 and G2 phases in the cell cycle of HuH-7 cells indicated similar behaviour after 24 and 48-hour treatment for 10SiNP. The HuH-7 cells which were treated with 10SiNPs displayed $p<0.05$ for G1 and G2 phase shifts during cell cycle after 24 and 48 hours for 20 µg/mL but not for 72 hours. Similary, HuH-7 cells were arrested after 48-hour treatment for 20 µg/ml of 100SiNPs (Figure 3.11).

SK-HEP-1 cells did not exhibit any significant response for 10SiNPs up to 72 hours. The cell number were nearly remained constant at 48 hours for all concentrations of 10SiNPs. 100SiNPs did not affect the cell cycle of SK-HEP-1 cells for 24 hours whereas stimulate the cells for transition between G1 and G2 after 48-hour treatment of 20 µg/mL of 100SiNPs. However cell cycle phases of SK-HEP-1 cells were not affected from 100SiNPs for 72 hours (Figure 3.12).

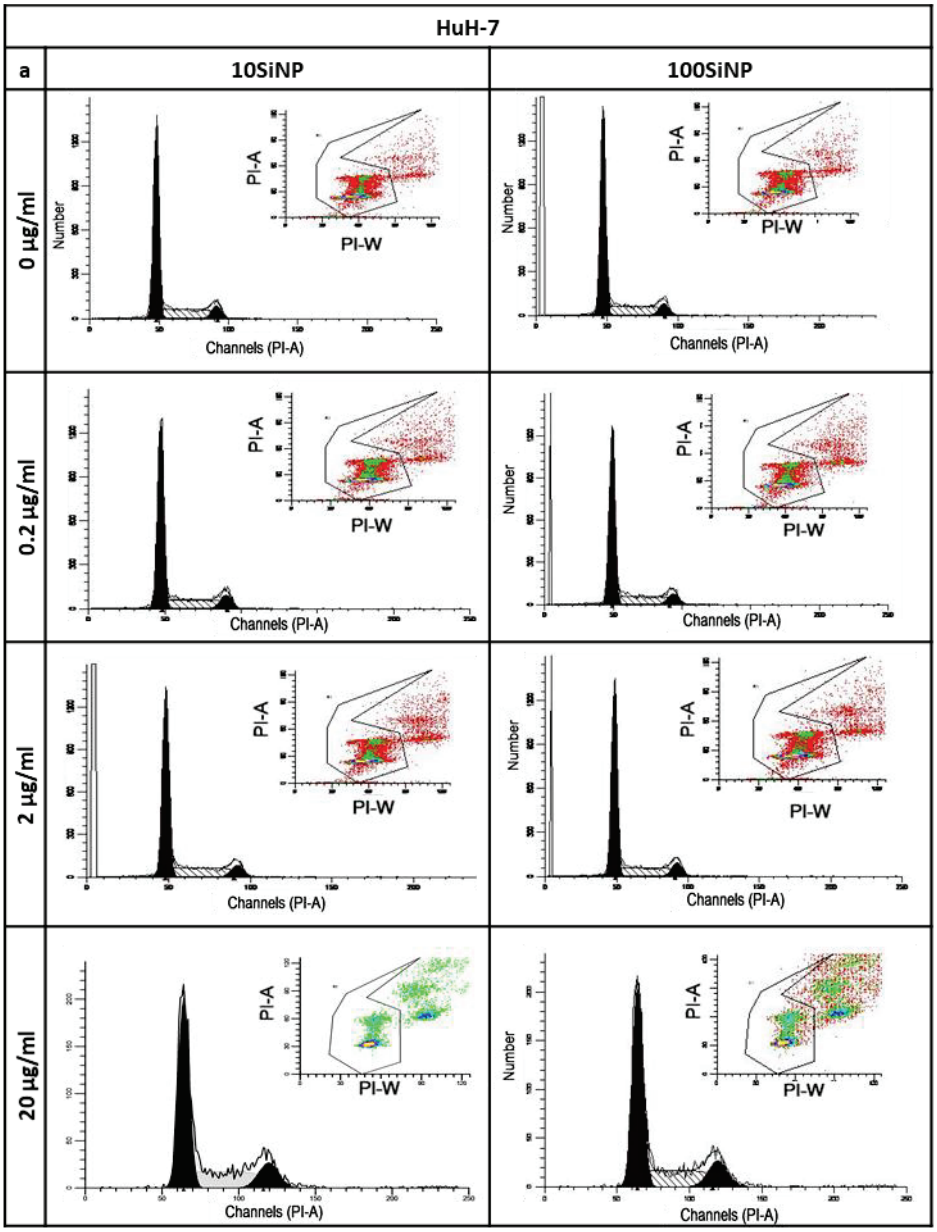

Figure 3.9. The scatter plot and histogram data for cell cycle analysis for HuH-7 cell line.

A small shift has been observed for G0/G1 phase of HuH-7 cells when the concentration of 10SiNP was increased. The S phase area of the HuH-7 cells were not altered for 10SiNP treatment. The G2/M phases were almost similar for the amount of 0.2 and 2.0 µg/ml except for 20 µg/ml. However the change for the G2/M phase were not significant on HuH-7 cells. The treatment with 100SiNP seemed to be slightly effected the cell cycle behaviour of the HuH-7 cell line for 72 hours. The small quantities of the HuH-7 cells were shifted to the S phase and the G2/M phase for the amount of 0.2 µg/ml.

But overall 100SiNP did not cause a significant transition between the phases of the cell cycles (Figure 3.10).

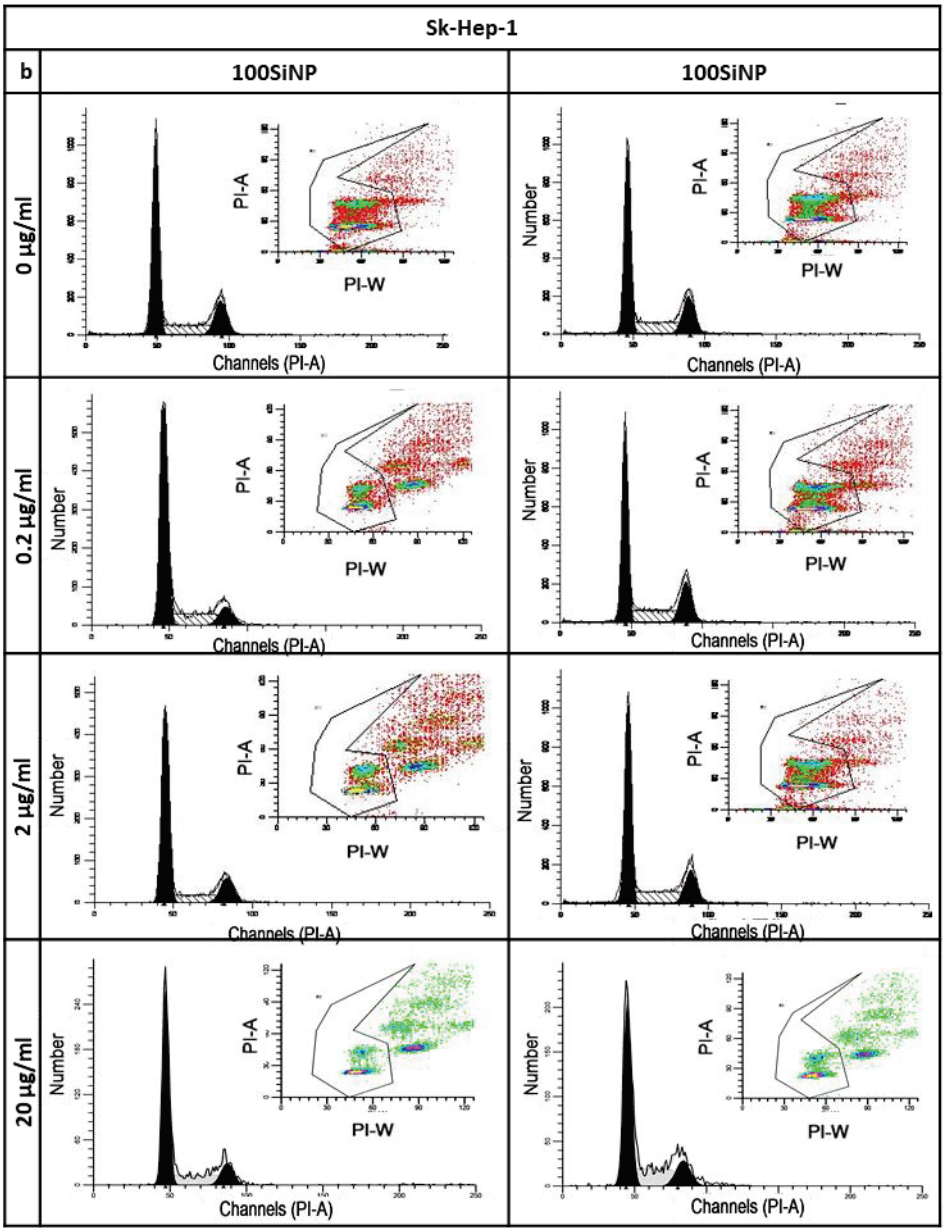

Figure 3.10. The scatter plot and histogram data for cell cycle analysis for SK-HEP-1 cell line.

The areas of the G0/G1 phases of SK-HEP-1 cell remained unchanged although there was a shift for 20 µg/ml concentration of 10SiNP Cell cycle profiles of SK-HEP-1 cells indicated that G0/G1, S and G2/M phases did not altered for 100SiNP similar to 10SiNP (Figure 3.11). SK-HEP-1 cells did not exhibit any significant response for 10SiNPs up to 72 hours. cell cycle phases of SK-HEP-1 cells were not affected from

100SiNPs for 72 hours (Figure 3.11). The data were summarized in graphs for indicating the changes in cell cycle phase distribution for 72 hours for both cells.

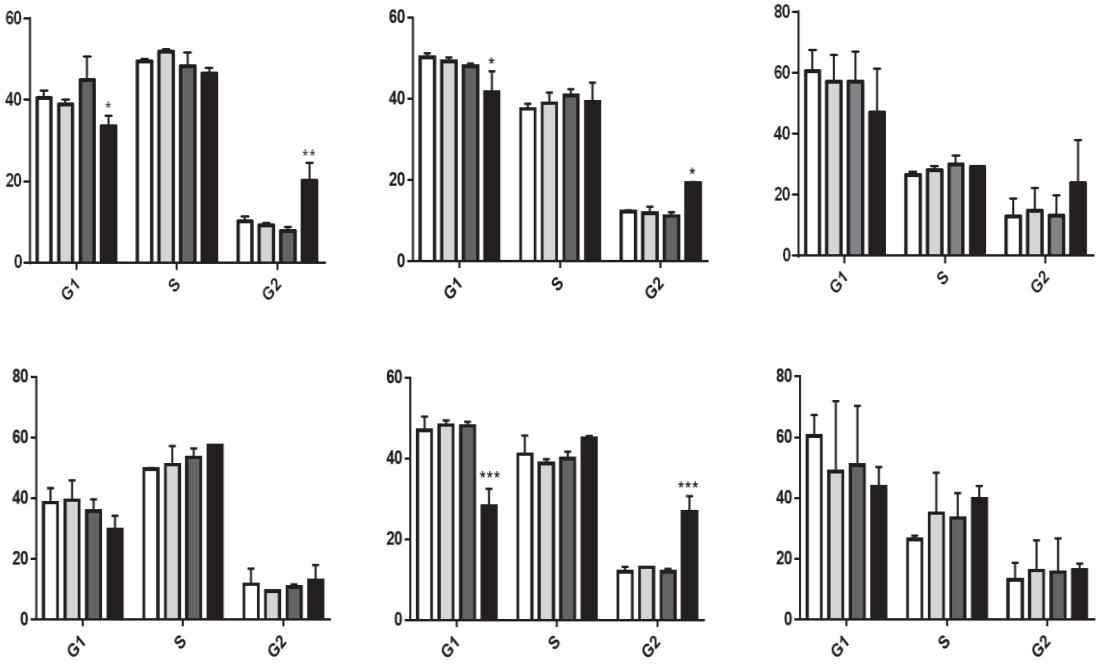

Figure 3.11. Cell cycle graphs for HuH-7 cells

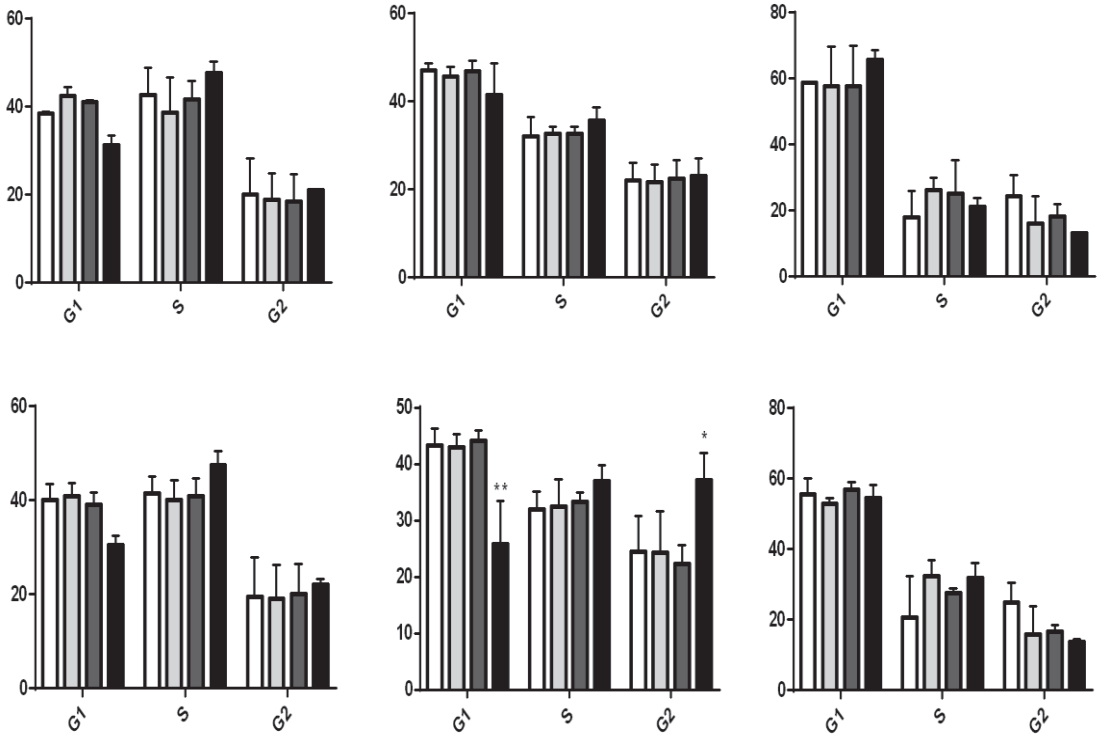

Figure 3.12. Cell cycle graphs for SK-HEP-1 cells

The cell cycle graphs for the cells after 24 (left), 48 (middle) and 72-hour (right) treatment at the above for 10SiNP and at below for 100SiNP were represented.

3.6.3. Genotoxicity Test

The genotoxic potential of 10SiNPs and 100SiNPs was investigated by the cytokinesis blocked micronucleus assay. The cells were treated with SiNPs for 72 hours. Cytochalasin-B was added at the 44 hour of the incubation for the cytokinesis block. Mitomycin was used to assess the performance of micronucleus assay on lymhocytes as it is recommended in the literature.

Up to the concentration of 20 μg/mL, both SiNPs did not induce any significant formation of micronuclei in lymphocytes *in vitro*. In fact, the frequency of micronucleated lymphocytes for 1000 cells corresponded to 9, 11, and 10 for 0.2, 2 and 20 μg/ml respectively for 10SiNPs and 10, 5, 7 for 100SiNPs after 72 h exposure. Therefore, compared to the untreated control (5 micronucleus) SiNPs did not trigger the formation of micronuclei, suggesting that neither the size nor the physicochemical properties of SiNPs induces genotoxicity. 5 micronucleus frequency reached to 46 in positive control group treated with Mitomycin C. Giemsa stained lymphocytes could be monitored as mononucleated (a), binucleated (b), trinucleated (c) and multinucleated (d) cells. The number of mononucleated, binucleated, trinucleated and multinucleated cells were counted and graphed in Figure 3.13 and 3.14. Nuclear bridge (NPB) and bund (NBUD) formation could be observed in e and f in Figure 3.13. The frequencies of micronuclei, nucleoplasmic bridges and nuclear bunds provide a measure of genomic damage and chromosomal instability.

Micronucleus frequency was summarized in Table 3.2 (I) and statistical data were given in Table 3.2 (II). NDI frequency was calculated approxiamately 2 and nearly constant after SiNP treatment of lymphocytes. The results demonstrated the cells were divided at least once and no abnomalities after cytokinesis-block. Micronucleus number per 1000 binucleated cells and cell number per 1000 binucleated cells were not statistically changed. The number distribution for nuclear buds and nucleoplasmic bridges were nearly similar compared to control group. MMC treated cells contained more NBUD and NPB number as it was expected (****$p<0.0001$).

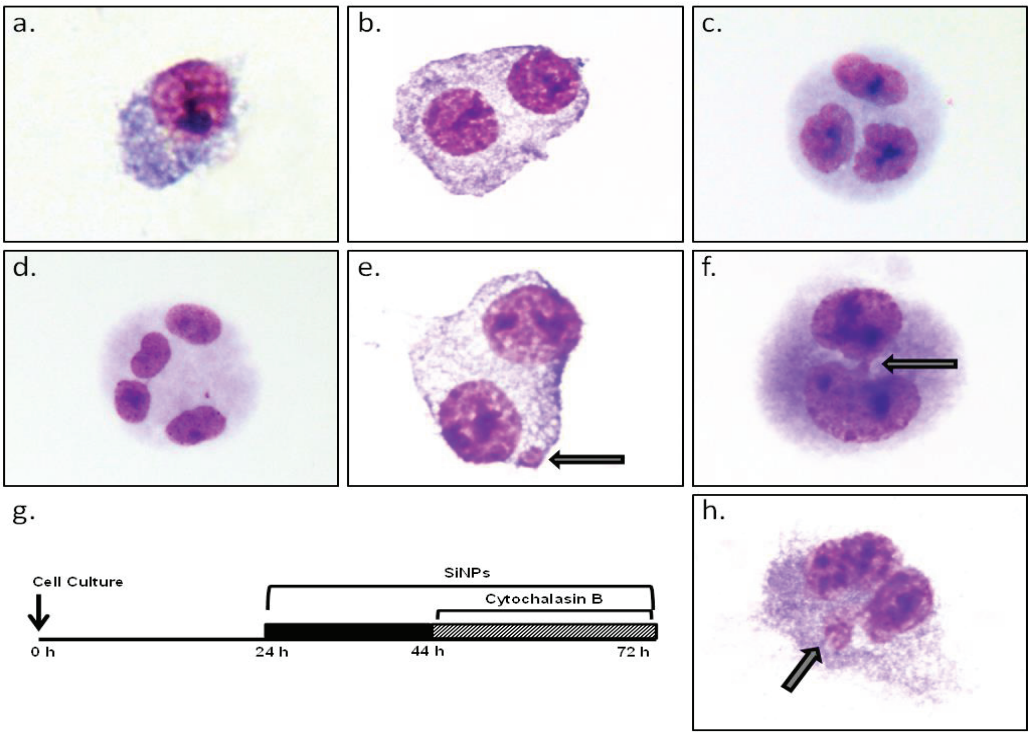

Figure 3.13. Photomicrographs of the lymphocytes scored in micronucleus assay.

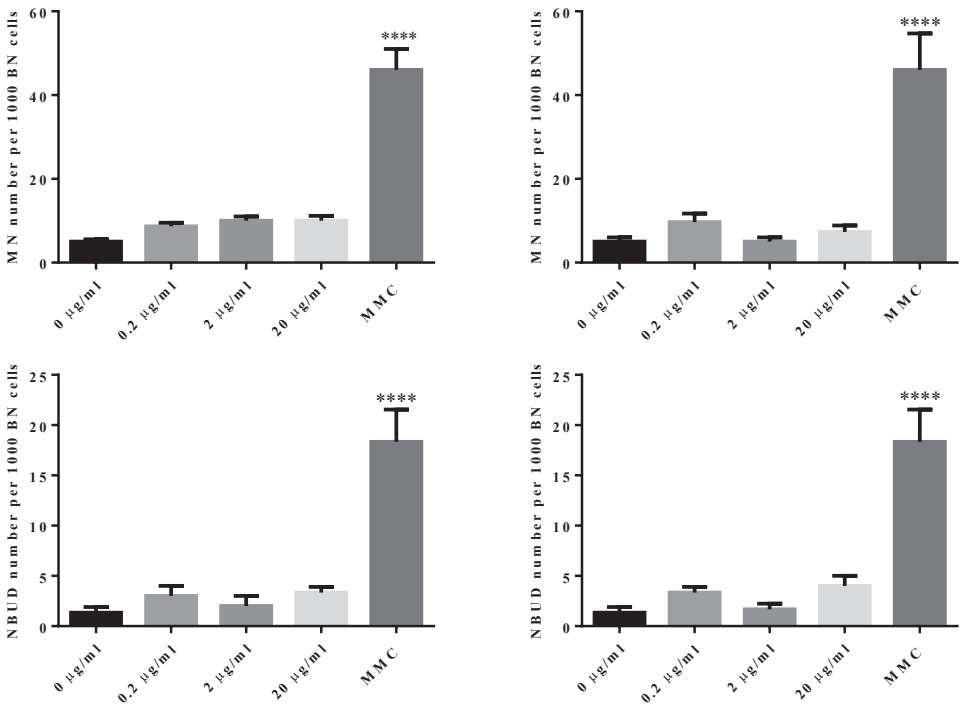

Figure 3.14. Micronuclei and nuclear bund distributions after 10SiNPs and 100SiNPs treatment for lymphocytes

Table 3.2. Mononucleated, binucleated, trinucleated and multinucleated cell number distributions (I) and statistics (II) for 10SiNP and 100SiNPs

I)	10SiNP				100SiNP			
	Concentration (µg/ml)							
	CTRL	0.2	2.0	20	CTRL	0.2	2.0	20
Mononucleotide cells /500 cells	144	123	115	132	144	144	148	160
Binucleotide cells /500 cells	294	313	316	299	294	294	292	272
Trinukleotide cells/ 500 cells	19	10	16	21	19	11	28	25
Multi-nucleotide cells/500 cells	43	69	73	52	43	49	42	45
NDI	1.92	1.97	1.97	1.97	1.92	1.93	1.94	1.90

II)	10SiNP					100SiNP				
	Concentration (µg/ml)									
	CTRL	0.2	2.0	20.0	MMC*	CTRL	0.2	2.0	20.0	MMC*
MN/1000 BN cells	5±1	9±2	11±2	10±2	46±9	5±1	10±2	5±1	7±2	46±9
p value		0.8124	0.5994	0.5994	< 0.0001		0.6474	> 0.9999	0.9532	< 0.0001
# Cells have MN /1000 BN cells	5±1	8±1	8±1	9±1	37±7	5±1	8±1	5±1	7±2	37±7
p value		0.7227	0.7888	0.5124	< 0,0001		0.804	> 0.9999	0.9072	< 0.0001
NBUD/ 1000 BN cells	1±1	3±1	2±1	3±1	18±3	1±1	3±1	2±1	4±1	18±3
p value		0.7161	0.9848	0.5738	< 0.0001		0.5512	0.9988	0.2991	< 0.0001
NPB/1000 BN cells	1±1	1±1	2±1	1±1	10±2	1±1	1±1	2±1	1±1	10±2
p value		> 0.9999	0.994	> 0.9999	< 0.0001		> 0.9999	0.9405	> 0.9999	< 0.0001

3.7. Conclusion

In summary, the 10SiNP and 100SiNP nanoparticles were detected as non-toxic for hepatocellular carcinoma cell lines up to 200 µg/ml for 120 hours. Genotoxic effects of SiNPs were measured on blood lymphocytes. The results indicated that 10SiNPs and 100SiNPs were not genotoxic up to 20 µg/ml concentration. Cell cycle of the hepatocarcinoma cells seemed to be not affected from 10SiNP and 100SiNP exposure for 3 days.

CHAPTER 4

CONFOCAL IMAGING OF SILICA NANOPARTICLE TREATED CELLS

Nanoparticles at the cellular membrane of the cell interact with all components of the cellular membrane or extracellular matrix of the cell. It has been reviewed in the literature that nanoparticle size, shape, surface functionality, surface charge, hydrophobicity effect the nanoparticle uptake into the cells (Behzadi et al. 2017). Generally accepted, most of the nanoparticles are found to enter the cells via endocytosis process during incubation. Normally the endocytosed nanoparticles are found in membrane bound organelles in the cytoplasm. On the other hand bare nanoparticles are found to be in the cytoplasm or other organelles such as nucleus and mitochondria Figure 4.1.

The electrostatic attraction between the nanoparticle surface and the organelle membranes may resulted in organelle rupture. The results of the confocal microscopy studies taken from lysotracker labeled samples suggested that very few of the nanoparticles were released to the cytoplasm due to organelle rupture (Chu et al. 2011). The studies performed on H1299 cells (human lung carcinoma cell) and NE083 (human esophageal epithelial cell) cell lines indicated that the SiNPs were uptaken by non-specific endocytosis independent from size or SiNPs and found in lysosomes (Chu et al. 2011). In an another study, it has been proposed that SiNPs migrated to the perinuclear region of the HMVEC cells by microtubulles independent from size, charge or shape of the nanoparticles (Ferrati et al. 2010)

Study in the literature seemed to achieve a concensus that final destinations of SiNP nanoparticles were lysosomes (Table 4.1.). Also it has been discussed that the particles larger than 100 nm can easily enter the cells even if the uptake efficiency is low (Shapero et al. 2011).

Besides qualitative microscopy imaging analysis, quantitative microscopy analysis were performed in order to assess possible effects of nanoparticles on physiology of the cells. In 2013 precise nanoparticle quantification studies were performed by confocal laser scanning microscopy of which internalized nanoparticles can be obtained

by a mathematically integrated technique (Gottstein et al. 2013) Effects of silica nanoparticles was also studied on the mitochondrial potential especially for neuronal cells. Mitochondrial dynamics, trafficking and biogenesis as well as changes in mitochondrial potential play key roles in regulation of cellular homeostasis (Kretowski et al. 2017)

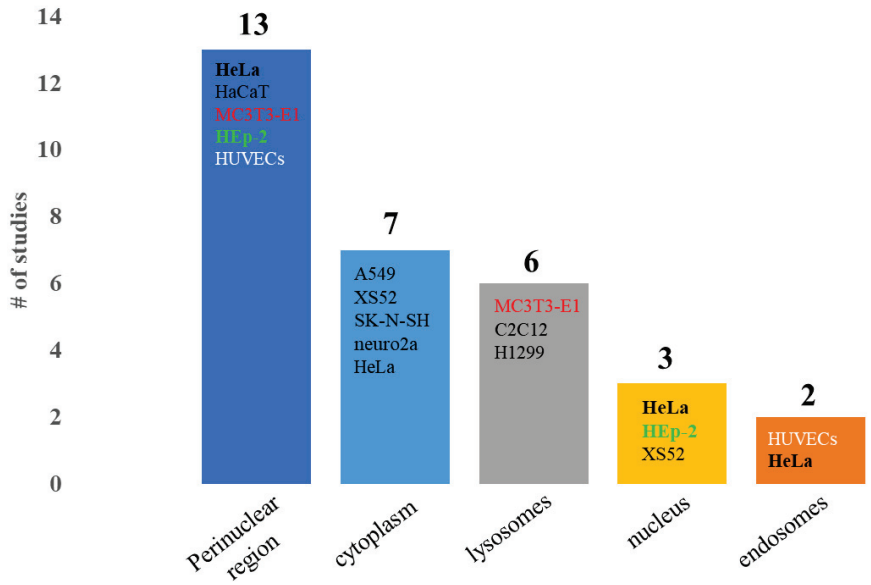

Figure 4.1. The graph for literature of nanoparticle distribution.

The oxidative stress of HepG2 cells induced by the particles that were treated with 43 nm non-modified amorphous silica nanoparticles which dispersed in serum-free DMEM at concentrations of 0, 25, 50, 100 and 200 μg/mL for 3 and 24 h. Additionally the mitochondrial potentials of the cells were visualized by JC-1 dye. Green and red intensity ratios were compared with non-treated groups. It was found that SiNPs could play an important role of the mitochondrial membrane damage and the cell apoptosis (Sun et al. 2011).

Same methodology was applied for HUVECs that the green/red fluorescence intensity ratio was elevated with the increasing of silica nanoparticles exposure concentrations indicating the MMP changes were concentration dependent for 24 hours (Duan et al. 2013).

There are limited knowledge about mitochondrial change after the nanoparticle treatment expecially for silica nanoparticles at single cell level. Mostly the analyses performed based on confocal microscopy and flow cytometry techniques. In our study we

scanned two different hepatocarcinoma cell lines which were HuH-7 well differentiated, epithelial like, low motile and less invasive and SK-HEP-1 poorly differentiated, mesenchymal like, highly motile and highly invasive cell lines (Yuzugullu et al. 2009b). The cellular responses of the cells were assessed in terms of mitochondrial physiology by quantitative confocal scanning microscopy with mitochondrial dye Mitored and DCF-DA as an oxidative stress sensor. The cellular uptake studies were performed as time-dependent experiments. Colocalization of the fluorescent silica nanoparticles were determined by lysosome (Lysotracker DND-99) and mitochondria staining. Quantitative colocalization experiments and mitochondrial potential changes were analyzed by Image J platform.

Table 4.1. Summary of literature for SiNP localization into the cells.

	Cell line	NP Size (nm)	Organelle/Data	References
1	H1299	50	lysosomes	(Chu et al. 2011)
2	MC3T3-E1	55	perinuclear region	(Gan et al. 2012)
3	MC3T3-E1	100	perinuclear region	
4	MC3T3-E1	200	perinuclear region	
5	MC3T3-E1	440	perinuclear region	
6	MC3T3-E1	55	lysosomes	
7	MC3T3-E1	100	lysosomes	
8	MC3T3-E1	200	lysosomes	
9	MC3T3-E1	440	lysosomes	
10	C2C12	50	lysosomes	(Poussard et al. 2015)
11	HEp-2 cells	46	perinuclear region	(Hemmerich and von Mikecz 2013)
12	HEp-2 cells	46	nucleus	
13	A549	14	cytoplasm	(Mu, Hondow, Krzemiński, et al. 2012)
14	HUVECs	310	endosomes	(Torrano and Brauchle 2014)
15	HUVECs	310	perinuclear region	
16	HeLa	310	endosomes	
17	HeLa	310	perinuclear region	
18	HeLa	56	cytoplasm	(Zhu et al. 2013)
19	HeLa	56	nucleus	
20	XS52	70	cytoplasm	(Nabeshi et al. 2010)
21	XS52	70	nucleus	
22	XS52	300	cytoplasm	
23	XS52	1000	cytoplasm	
24	HaCaT	42	perinuclear region	(Rancan et al. 2012)
25	HaCaT	76	perinuclear region	
26	HaCaT	191	perinuclear region	
27	HaCaT	292	perinuclear region	
28	HUVECs	310	perinuclear region	(Julia et al. 2013)
29	HeLa	304	perinuclear region	
30	SK-N-SH	15	cytoplasm	(Yang et al. 2014)
31	neuro2a	15	cytoplasm	

4.1. Confocal Imaging

HuH-7 and SK-HEP-1 cells were plated on glass bottom petri dishes (Ibidi® plates) for live cell imaging of mitochondria by spinning disc confocal microscope, Andor Revolution system equipped with Olympus IX71 and Okolab stage incubator system. Mitochondria of the HuH-7 and SK-HEP-1 cells were stained by 200 nM of Mitored (Sigma Aldrich) to visualize active mitochondria (having high potentials) in the presence and absence of silica particles. Lysosomal parts were stained by 1μM Lysotracker DND-99 (Thermo Fisher Scientific) dye in order to determine SiNP colocalization with lysosomes. Cells were treated with fluorescein isothiocyanate (FITC) -conjugated 100SiNP nanoparticles (20 and 200 μg/ml) to determine the localization of nanoparticles in the cytoplasm of the cells. Coherent Innova diode lasers ® operating at 488 nm and 532 nm were utilized to obtain emissions of FITC-conjugated nanoparticles and Mitored stained mitochondria, respectively. Emission filters of 530/50 nm and 560/30 nm were used to collect emission originating from FITC-conjugated silica nanoparticles and stained mitochondria.

The imaging of the cells and nanoparticles were studied in IZTECH-Chemistry Department by Olympus IX-71 Microscopy equipped with Andor Revolution System. Live cell imaging system was purchased from OkoLab Bold Line Stage Incubator System.

Our confocal microscopy set-up is composed of the following equipments; (Figure 4.2.)

- Inverted microscope (Olympus IX-71)
- Andor Revolution Imaging System.
- Stage incubator system (Okolab).
- The optical working table for vibration (Newport)
- The CCD camera works in 15-200 fps (Andor)
- Piezoelectronical set-up (Physik Instrumente) (100 nm resolution in Z direction)
- AOTF photon regulator (Andor) (Acousto-Optical Tunable Filter)
- 4 lasers in 405, 488, 532, 640 nm wavelength.

The spectra of emission filters for 488 and 532 nm excitation with Mitored and FITC dyes were sketched in Figure 4.3. and Figure 4.4. The graphs were plotted by using Origin Sofware.

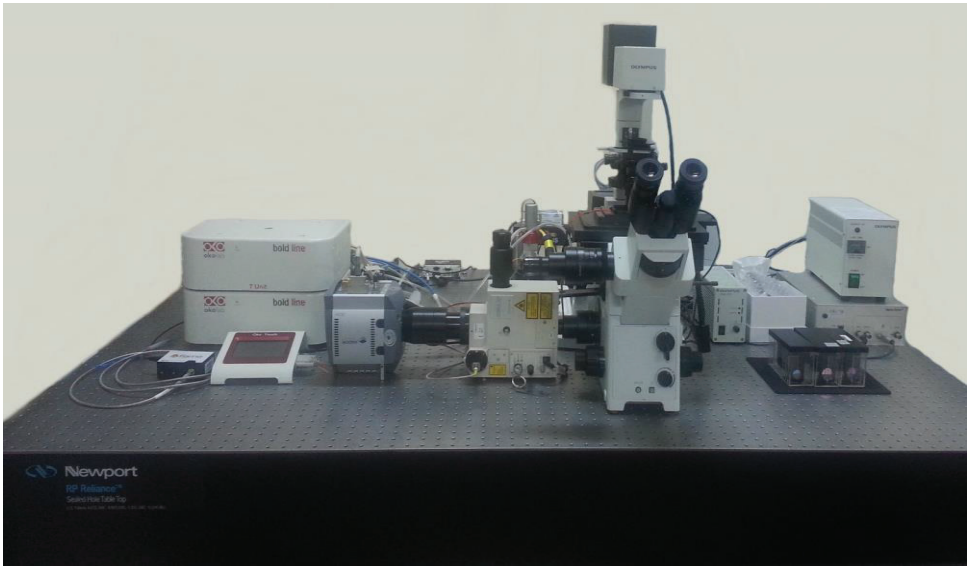

Figure 4.2. Our laser scanning confocal microscopy imaging set-up

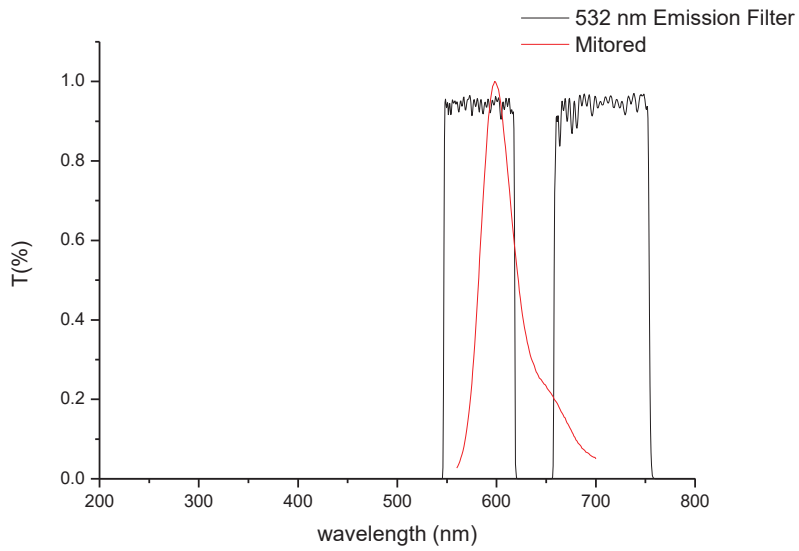

Figure 4.3. The spectra of emission filter for 532 nm excitation and Mitored

The LysoTracker® probes are consisted of a fluorophore linked to a weak base that is only partially protonated at neutral pH. They are freely permeant to cell membranes and typically concentrate in spherical organelles. Lysotracker DND-99 dye (Molecular Probes) was used for determination of nanoparticle compartmentalization with lysosomes by co-localization experiments. The emission spectra of the dye was sketched in Figure 4.4)

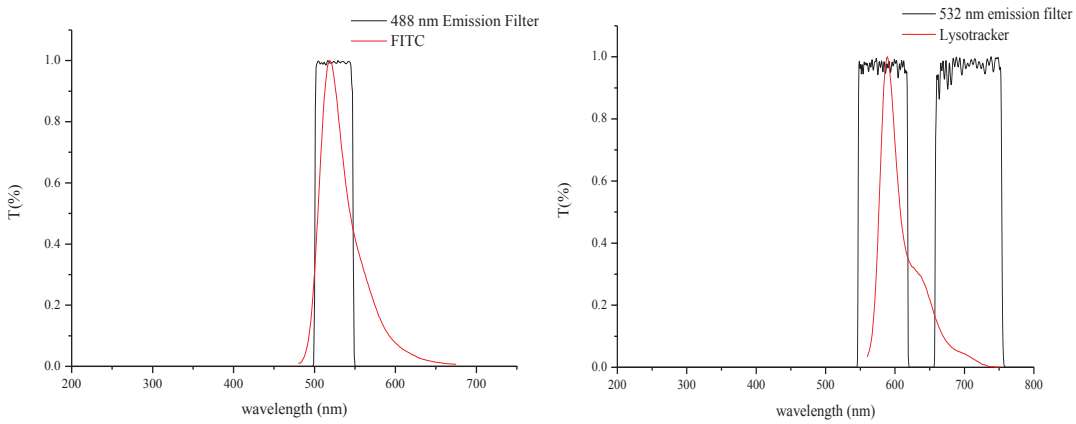

Figure 4.4. The spectra of the emission filter for 488 and 532 nm excitation and FITC-conjugated SiNPs and Lysotracker-Red.

Cells were treated after inoculation in μ-dishes or 8-well imaging chambers. The imaging studies performed by using chambers and dishes purchased by ibidi ®

Imaging studies were performed by either stage incubator for live-cell imaging or paraformaldehyde (PFA) fixed cells. Paraformaldehyde fixation (3.7%) was performed for uptake studies. The cells were washed with PBS at the end of the incubation with SiNPs. Paraformaldehyde solution was added on to the cells for 20 minutes. The cells washed with PBS for three times after fixation. Samples were dehydrated by ethanol solution series in order to harden the membrane of the cell populations (Thavarajah et al. 2012).

4.1.1. Mitochondrial Imaging

Mitochondrial imaging was performed in order to assess the potential effects on metabolic capacity of the cells. Additionally it was expected that the viability experiments must be correlated with the imaging data which indicate the mitochondrial response after nanoparticle treatment. Mitored stained cells were plated on glass bottom dishes (ibidi ®).

The nanoparticle concentration was optimized for the imaging studies were determined. HuH-7 and SK-HEP-1 cells (150.000 cells/ibidi plate) were plated on glass bottom petri dishes (Ibidi® plates) for live cell imaging of mitochondria by spinning disc confocal microscope, Andor Revolution system equipped with Olympus IX71 and

Okolab stage incubator system. Mitochondria of the HuH-7 and SK-HEP-1 cells were stained by 200 nM of Mito Red (Sigma Aldrich) to visualize mitochondria having high potentials in the presence/absence of silica particles for 30 minutes. Cells were treated with fluorescein isothiocyanate (FITC)-conjugated 100SiNP nanoparticles (20 and 200 μg/ml) to determine the localization of nanoparticles in the cytoplasm of the cells. The cells were treated with 2mM of hydrogen peroxide as a negative control.

4.1.2. Cellular Uptake of SiNPs and Lysosome Staining

10SiNPs and 100SiNPs FITC-conjugated silica nanoparticles were used in order to determine the localization of the nanoparticles in the cytoplasm of hepatocellular carcinoma cell lines. 100SiNPs were synthesized and following purified by centrifugation. The resulting pellet was re-dispersed in cell culture media. 10SiNPs were synthesized and available in our laboratory from earlier graduate students. 10SiNP powders were prepared for imaging studies in similar methodology. Cells were plated at 100.000 cells/dish density and incubated with SiNPs for 24 hours. The samples were washed with warm 1X PBS solution at least three times. The cells were then stained with Lysotracker (1μM) for 30 minutes and washed with PBS at the end of the incubation. Imaging was perfomed for paraformaldehyde fixed cells for this part of the imaging studies. The incubation times were 0 minute, 30 minutes, 1 hour, 2 hours, 3 hours, 6 hours, 12 and 24 hours.

4.1.3. Reactive Oxygen Species Imaging

The generation of the ROS may be resulted in oxidative stress which may lead permanent cell damage. Mitochondrial activity and nanoparticle toxicity can be assayed by measuring the reactive oxygen species level of the cell if the endocytosed nanoparticles trigger the oxidative stress mechanisms. A cell permeant reagent 2',7' – dichlorofluorescin diacetate (DCFDA, also known as H2DCFDA) was used to measure hydroxyl, peroxyl and other reactive oxygen species (ROS) activity within the cell. DCFDA / H2DCFDA is deacetylated by cellular esterases to a non-fluorescent compound

thereafter it is oxidized in the presence of ROS into 2', 7' dichlorofluorescein (DCF). The fluorescent DCF excitation and emission spectra were 495 nm and 529 nm respectively (Figure 4.5). The cells were cultured in 8-well ibidi chambers before silica nanoparticle treatment. Non-fluorescent 10SiNP and 100SiNP nanoparticles were used instead of FITC-conjugated SiNPS in order to prevent spectral overlap with DCF-DA dye. The cells were incubated with 200 µg/ml of SiNPs up to 24 hours and stained with 1 µg/ml DCF-DA for 30 minutes. The cells were imaged immediately after incubation to visualize the presence of ROS in the cells. Non-treated cells were used as negative control group and hydrogen peroxide treated cells were used as positive control group.

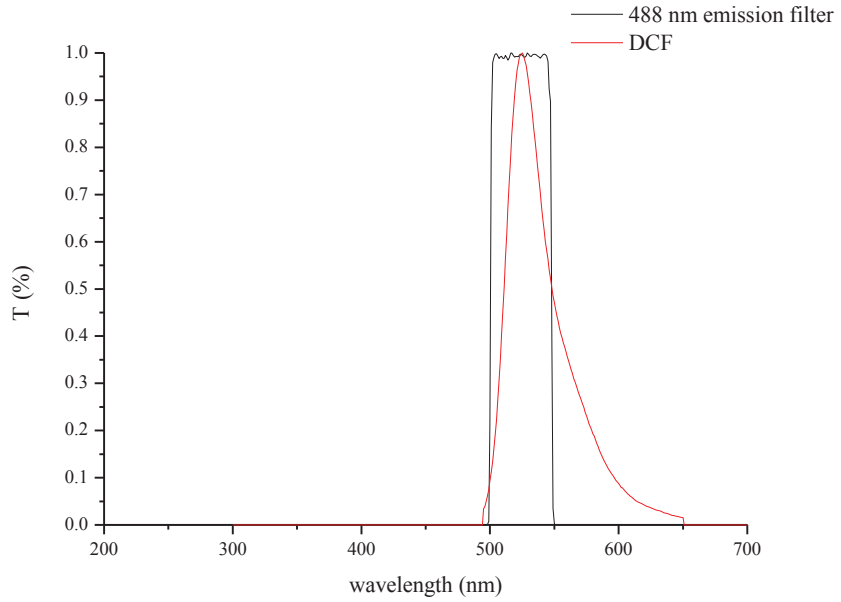

Figure 4.5. The spectra of emission filter for 488 nm excitation and DCF

4.1.4. Differential Interference Contrast Imaging

The optical path difference is resulted from product of the refractive index difference between samples and their medium. Nomarski Lens was used for DIC microscopy in our laboratory. The photography of the Nomarski prism was given in Figure 4.6. Differential interference contrast microscopy (Nomarski DIC) is a phase contrast technique that allows structure in transparent to be visualized by utilizing changes in refractive index.

Figure 4.6. Nomarski Prism structure and aperture (Source: Olympus Microscopy Web Site)

4.2. Image Analysis

4.2.1. Mitochondrial Intensity Analysis

The images were analyzed by using Image J program developed by NIH (National Institute of Health). The area of the cells and all mitochondrial counts gained by Mitored staining were obtained in order to determine mitochondrial potential change due to SiNP treatment.

The boundary of the each cells were sketched by polygon tool as region of interest (ROI). All ROIs were sketched and saved manually (Figure 4.7). Area of the each ROI were calculated in ROI Manager Menu under Analysis. The area measurement records were collected after setting scale for 40X magnification. The histogram data for all ROIs were transferred into Excel (Microsoft). The counts were calculated by multiplying the bins and count/bin values for each ROI. Total count were calculated by sum of counts from all ROIs for one image. The data were collected at least 70 cells/for each condition. Overall calculations were used for concluding the effects of nanoparticles by comparing control group data for Mitored total intensity ratio with experimental groups. The control, peroxide treated, fluorescent 100-nm SiNPs treated cells were visualized by live cell imaging. A decrease in the fluorescence of mitochondria for peroxide treated cell was

expected. On the other hand, no or slight change was expected after nanoparticle treatment.

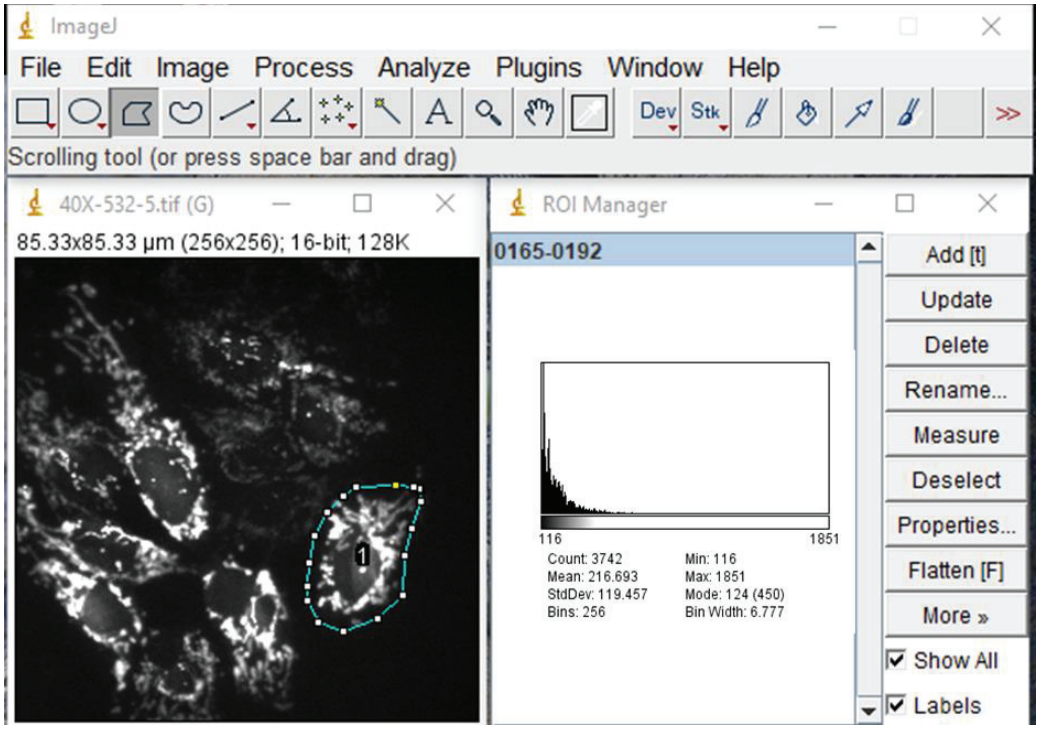

Figure 4.7. The screenshot image for Image J histogram command.

4.2.2. Colocalization Analysis

Colocalization of SiNPs with lysosomes and mitochondrial areas were analysed by determination of colocalization amount of fluorescently labelled two channels. Pearson correlation coefficients values were collected by Fiji platform (Image J) under Coloc plug-in (Figure 4.8). The green channel which was assigned to fluorescent SiNPs needed to be shifted to 5 pixels on X-coordinate. The shift action was calibrated by commercially available fluorescent polystyrene spheres. The images that captured in green channel were opened in Mathlab program. An algorithm which was developed for the pixel correction was launched before saving in shifted form. The cellular areas were sketched by as described in mitochondrial intensity analysis part. Coloc plug-in was used to determine the each Pearson correlation coefficients for SiNPs with mitochondria and

SiNPs with lysosomal parts in the cellular ROIs. The values were recorded for Mitored and Lysotracker stained cells after SiNP treatment.

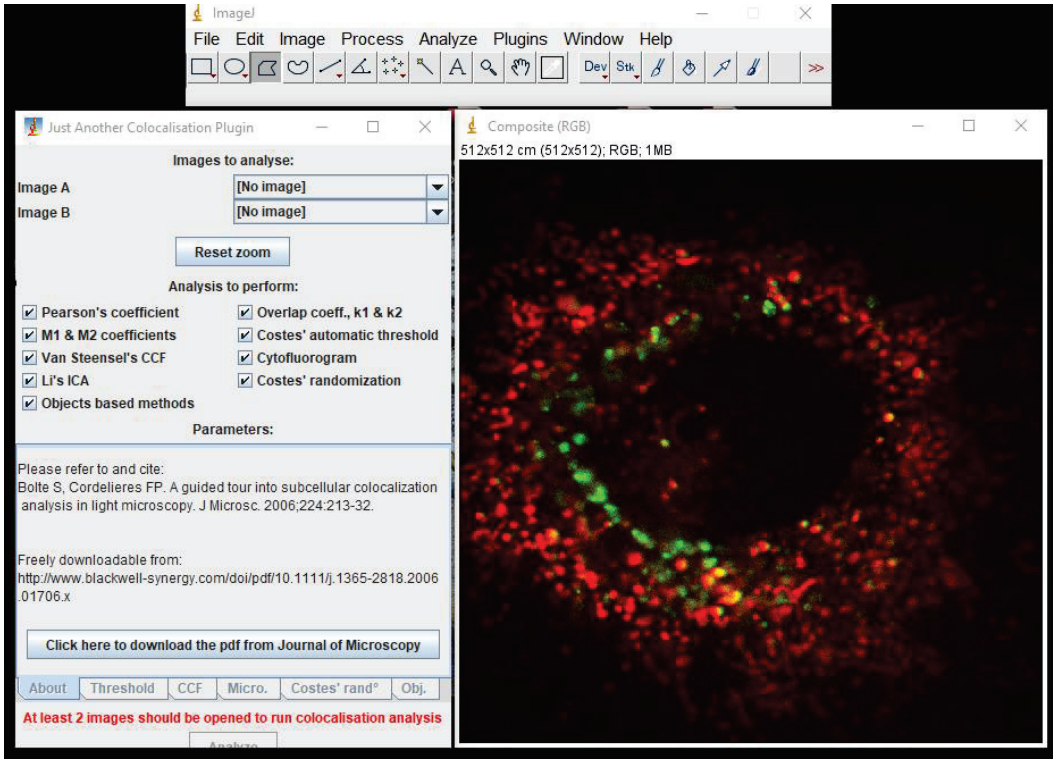

Figure 4.8. Screenshot of colocalization plug-in on Image J.

4.3. Results and Discussion

4.3.1. Confocal Imaging

The morphology of the non-treated HuH-7 and SK-HEP-1 cells were observed in bright field illumination and Differential Interference Contrast microscopy (Figure 4.9). The physical morphology of the cells were observed after nanoparticle treatments by comparing the images of the non-treated groups.

The DIC images were captured after and before paraformaldehyde fixation of the cells throughout the study. The images in Figure 4.9 were captured without fixation. The magnification was 400X. HuH-7 cells were observed as having more area than SK-HEP-1 cells.

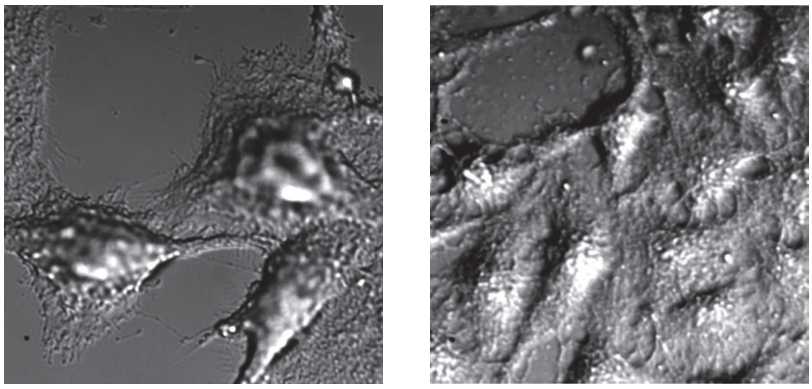

Figure 4.9. DIC images of HuH-7 (left) and SK-HEP-1 (right) cells

Fluorescent nanoparticle concentration for the images studies were optimized for SK-HEP-1 cells. It was decided that it was very hard to observe nanoparticles at low concentrations. The nanoparticles can be visualized after 20 µg/ml concentration into the cells (Figure 4.10). The images were processed by using Image J platform. Brighfield images were captured sequentially before/after 488 nm excitation for FITC-conjugated 100SiNPs.

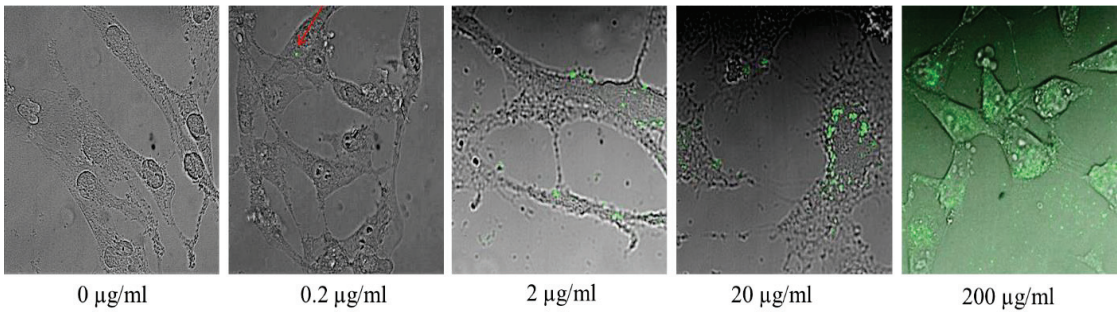

Figure 4.10. SK-HEP-1 cells treated by 0.2-200 µg/ml 100SiNPs for the optimization of imaging concentration.

4.3.1.1. Mitochondrial Intensity Analysis

HuH-7 and SK-HEP-1 cells were incubated with 200 µg/ml of FITC-conjugated 100SiNPs for 24 hours. The mitochondria were stained with Mitored (Sigma) at the end of the particle treatment. The images were captured in live cell conditions by using Andor

Revolution system with a CCD camera (Andor iXon EMCCD). The images were coloured with merge function by using Fiji (Image J) platform. Mitochondrial activity of the cells was visualized by Mitored emission (red coloured) in each pixel. Nanoparticle intensity was collected from FITC-conjugated particles distributed into the cell (green coloured) (Figure 4.11).

The coloured image of FITC-conjugated SiNP treated HuH-7 cells was given as an example. Mitored intensity were collected by 532 nm laser excitation and silica nanoparticles were illuminated by 488 nm laser excitation. The images were collected and re-opened in Image J. The image of the Mitored stained cells was labelled in red channel and the images of 100SiNPs treated cells were labelled in green channel. Merge channels option under Image→Colour menu was launched for getting one image from 2 images obtained from separated optical channels.

Figure 4.11. The image of HuH-7 cells after mitochondrial staining at the end of nanoparticle incubation

Merged images of silica nanoparticle treated and Mitored stained HuH-7 and SK-HEP-1 cells were represented as panels in Figure 4.12. The mitochondrial intensity was not decreased up to 200 μg/ml of 100SiNP, meaning that mitochondrial activity of the cells was not affected in the presence of the silica particles. On the other hand, the cells treated hydrogen peroxide showed decreased Mitored intensity comparing with the control and FITC-SiNP treated cells. The decrease in Mitored intensity proved that peroxide treatment resulted in lowered membrane potential of the mitochondria in the HuH-7 and SK-HEP-1 cell lines. Similarly mitochondrial intensity was not affected in the presence of 10SiNPs (Figure 4.13).

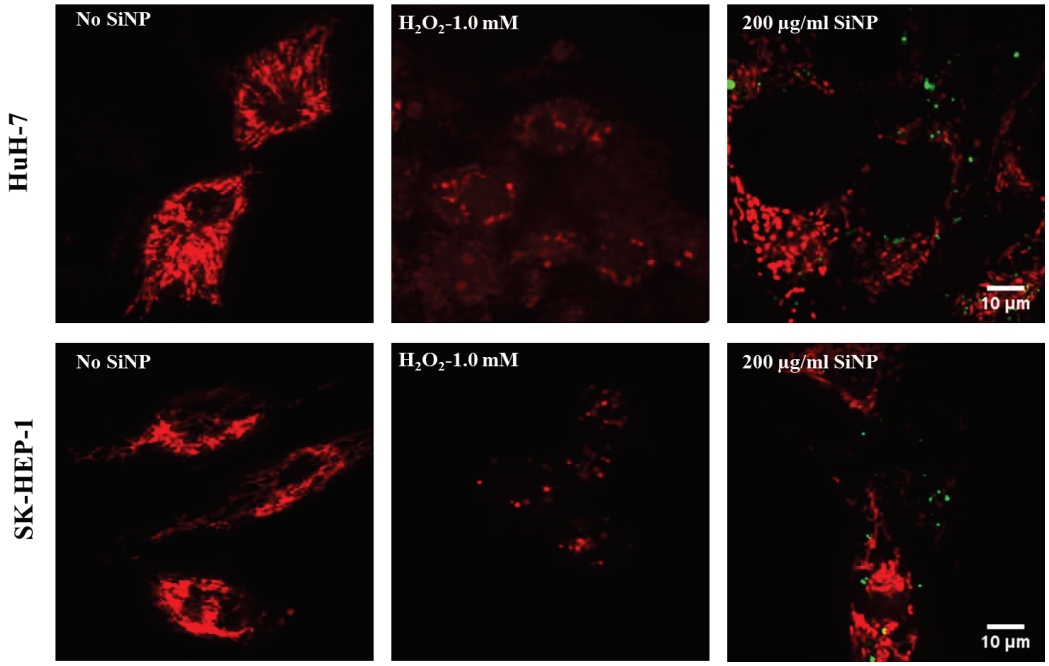

Figure 4.12. The confocal images of Mitored stained HuH-7 and SK-HEP-1 cells after 100SiNP silica nanoparticle treatment.

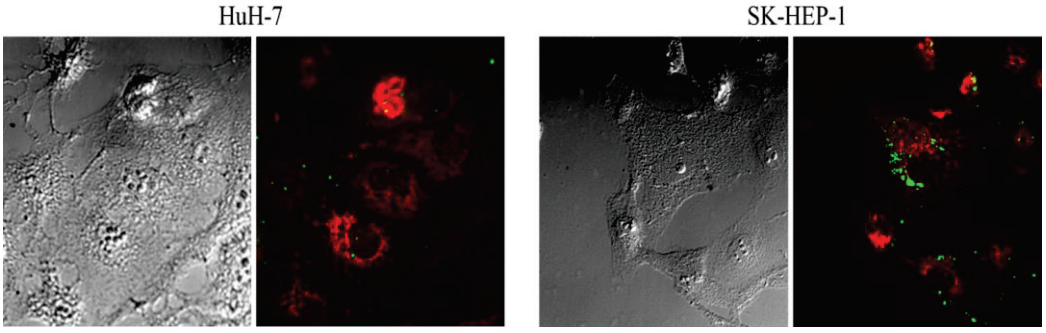

Figure 4.13. The confocal images of Mitored stained HuH-7 and SK-HEP-1 cells after 10SiNP silica nanoparticle treatment.

The images were analysed by comparing intensity changes regarding to ROI (intensity/selected area) that each referred one cell. The results were graphed to point out intensity difference by area. Green, blue and red colours indicated the mitochondria intensity of control, SiNP and peroxide treated cells (Figure 4.14 and 4.15).

Mitochondria potential analysis results indicated that the intensity values were decreased after peroxide treatment. Similary area of the cells was decreased after peroxide treatment for both cells. The intensity per area of the HuH-7 cells after 10SiNP treatment

seemed to be greater than 100SiNP treated cells. However, the intensity and the area of the cells were not significantly changed after SiNP treatment compared to control group mitochondria. The scatter graph pointed that area of the SK-HEP-1 cells slightly reduced comparing to HuH-7 cells after hydrogen peroxide treatment. Intensity/area distribution of the cells remained in similar range after either 10SiNPs or 100SiNPs treatment.

This result validated that FITC-conjugated silica nanoparticles do not interfere with the chemical processes in the mitochondria, confirming the results of MTT assays.

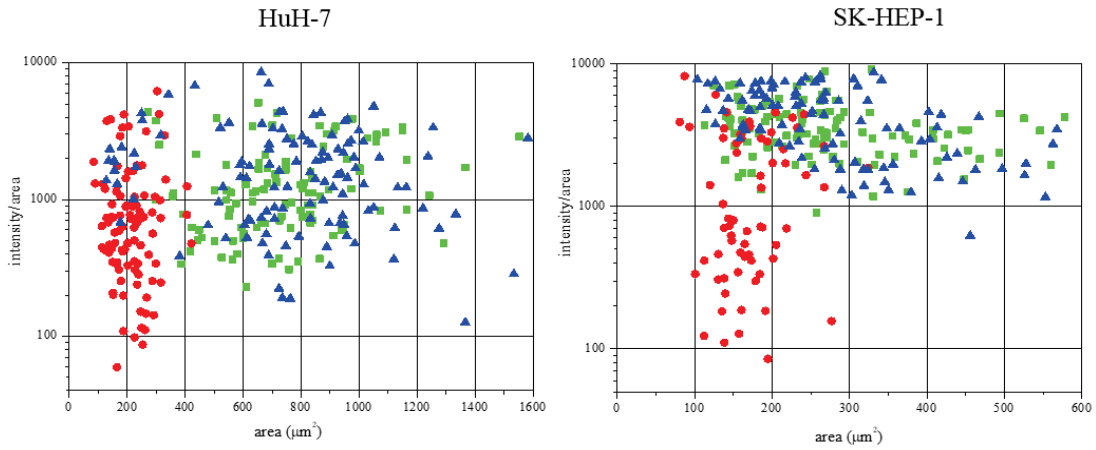

Figure 4.14. Scatterplots obtained from intensity analysis for both cell lines after 10SiNP treatment.

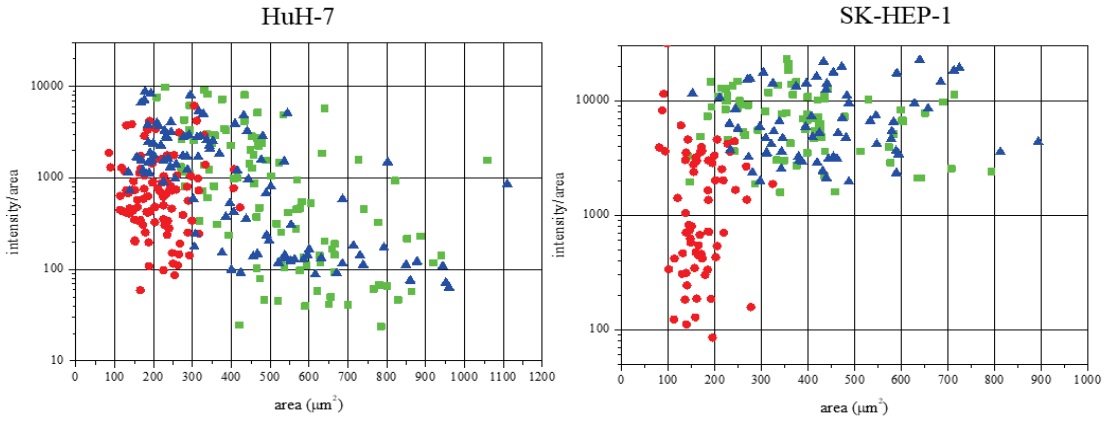

Figure 4.15. Scatterplots obtained from intensity analysis for both cell lines after 100SiNP treatment.

The graphs indicated the intensity distribution per cell area analysed by Image J software. Green squares, red spheres and blue triangles indicated the data for control,

peroxide treated, 10SiNP (A) and 100SiNP (B) treated cells respectively. Each symbol represents total number of counts in one cell area drawn by polygon tool determining region of interest (ROI) for HuH-7 cells (left panel) and SK-HEP-1 cells (right panel).

4.3.1.2. ROS Imaging

The ROS formation in the cells were analysed by imaging of the fluorescence of DCF. Despite of the fact that the ROS formation is a dynamic process the cells should be imaged immediately after the end of nanoparticle incubation. DCF intensity was green coloured which was indicating the presence of the oxidative stress in the cell (Figure 4.16). The DCF intensity was very low in non-treated cells but highly detectable in peroxide treated cells as expected for both HuH-7 and SK-HEP-1 cells. SiNPs treated cells show similar behaviour as non-treated cells for HuH-7 cell line. The DCF fluorescence in non-treated HuH-7 cells higher than non-treated SK-HEP-1 cells. It is seemed that ROS level a little higher in HuH-7 cells than SK-HEP-1 cells at basal cellular activity. The fluorescent DCF was detected at very low in SiNPs treated SK-HEP-1 cells. Non-fluorescent 10SiNP and 100SiNPs were used because of spectral overlapping with FITC and DCF. Green coloured cells indicated fluorescense of DCF depending on presence of ROS in the cells. Peroxide treated cells have much more ROS than non-treated and SiNP treated cells. The DCF intensity for peroxide treated cells were increased but very similar to control group after SiNP treatment. The DCF intensity was notably increased for SK-HEP-1 cells after peroxide treatment. However the ROS level remained nearly same after 100SiNP treatment. 10SiNPs have minimal effect on ROS production for both cell lines. The cell numbers were counted for control, peroxide treated, 10SiNP and 100SiNP treated cells as 117, 93, 108 and 112 respectively (HuH-7 cells). 182, 150, 251 and 213 cells were counted for SK-HEP-1 cells. Intensity analysis was performed by same methodology as in Mitored intensity analysis part (Figure 4.17). The image analysis of DCF-stained cells by using Image J program. The images were opened in Image J and rounded cells were labeled as dead cells with “multi point tool”. The dots were recorded in ROI manager later on using for counting dead and alive cells. Besides counting cells on brightfield images, the intensity measurements were recorded for each ROI. The counted cells were graphed in Figure 4.18. The panels were illustrated as panels showing DCF signals for control groups and peroxide treated, 10SiNP and 100SiNP treated cells.

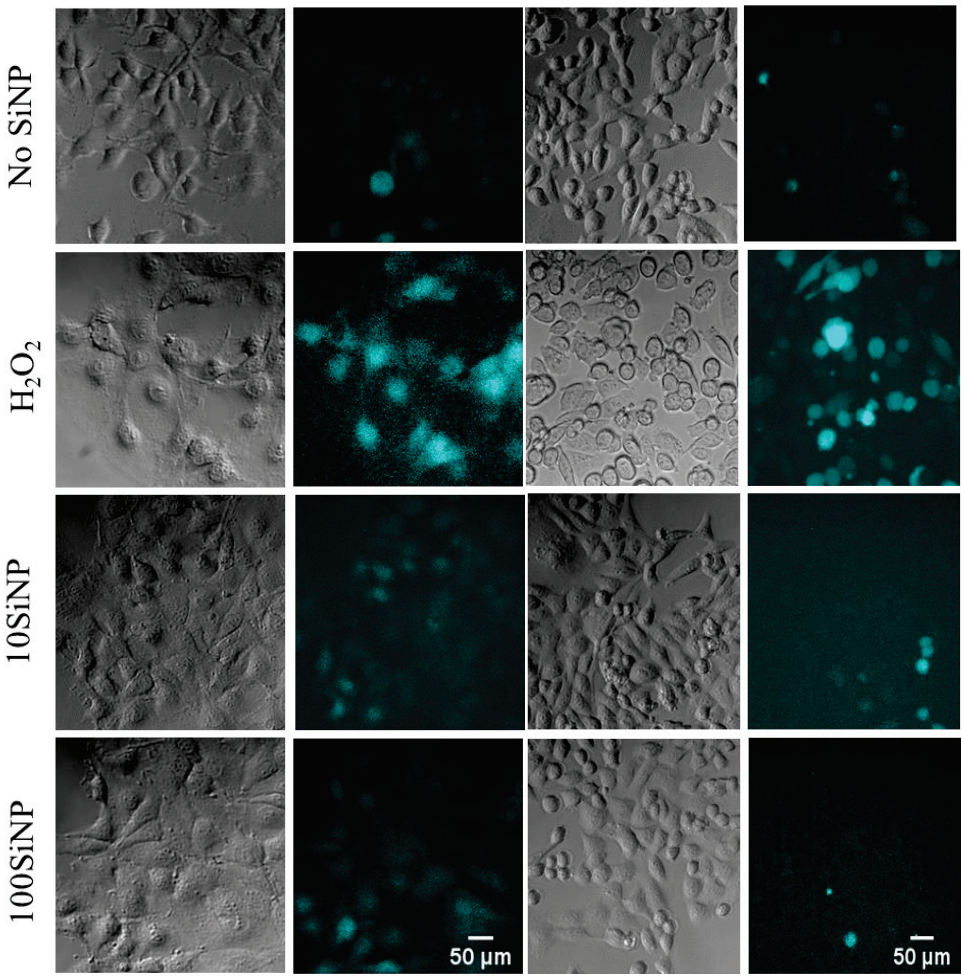

Figure 4.16. DCF-DA stained HuH-7 and SK-HEP-1 cells

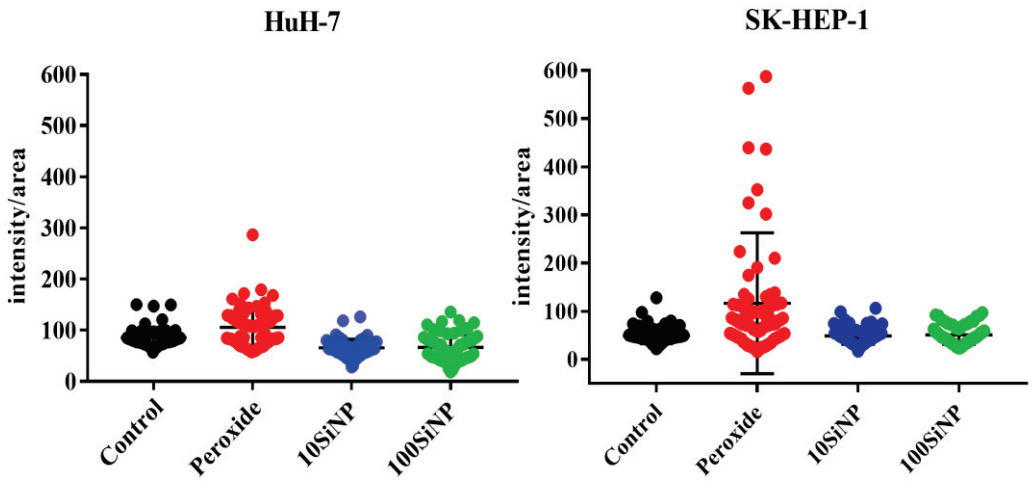

Figure 4.17. DCF intensity analysis for HuH-7 and SK-HEP-1 cells.

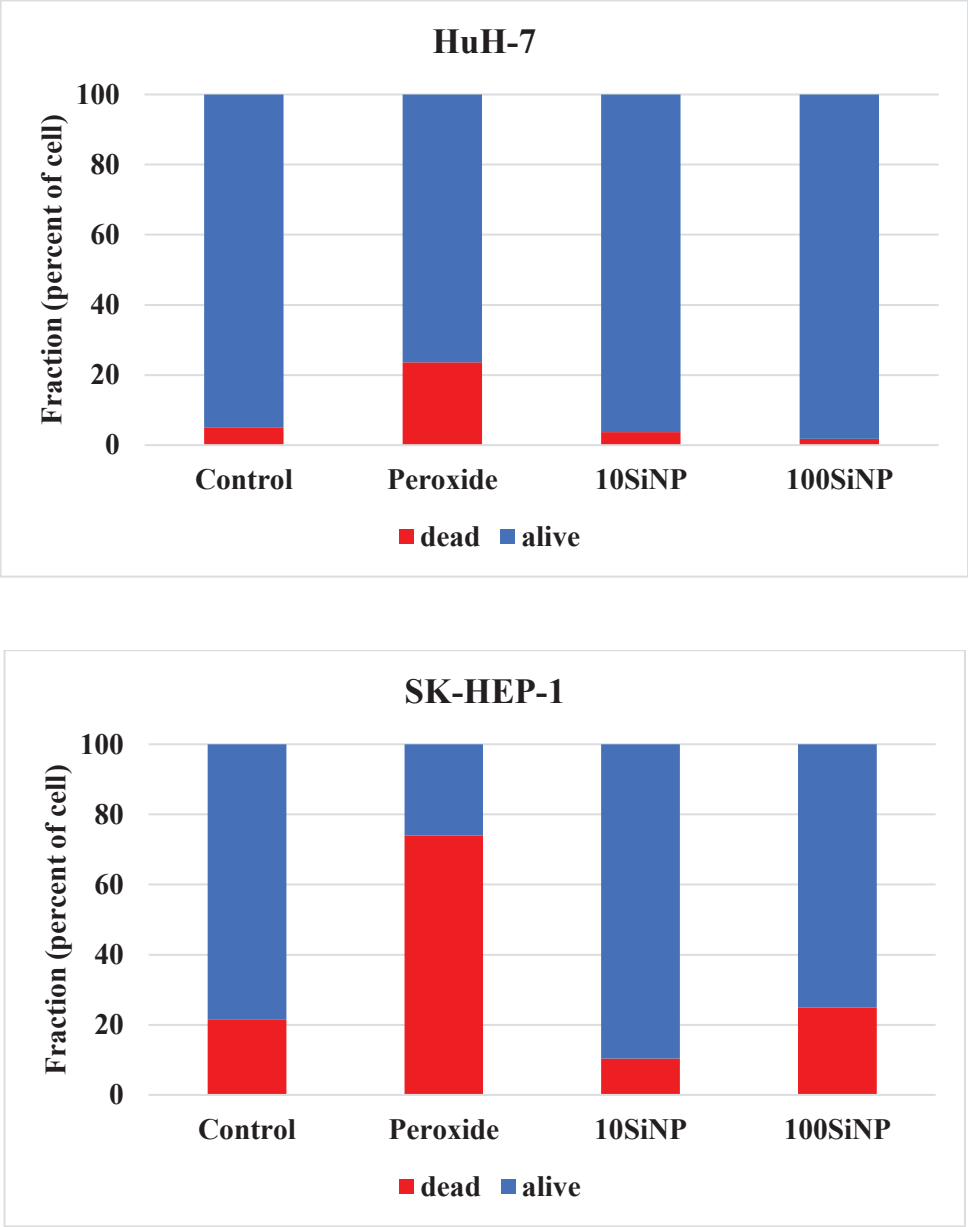

Figure 4.18. DCF intensity changes for control, peroxide and SiNP treated HuH-7 and SK-HEP-1 cells.

ROS intensity levels were graphed based on histogram data for each cell. It was obvious that ROS amount was higher in peroxide treated cells than control group or silica nanoparticle treated cells. It seemed that peroxide treatment resulted in production of ROS products in HuH-7 cells comparing to SK-HEP-1 cells.

The area of the HuH-7 cells remained nearly similar after peroxide treatment. However the area of the SK-HEP-1 cells were decreased after peroxide treatment. Intensity/area ratio increased showing the percentages of the dead cells were increased.

4.3.1.3. Colocalization Analysis

Fluorescence colocalization analysis is used to determine whether two molecules associate with the same structures. For example, to determine whether a particular protein associates with endosomes, mitochondria or two proteins associate with the same subcellular structures or with the same plasma membrane domains. The images that were captured for colocalization of SiNPs with mitochondria or lysosomes were analysed by Image J Coloc-2 plug-in.

It was determined that SiNPs were co-localized in lysosomes rather than mitochondria independent from cell type that were treated. It can be clearly pointed out that fluorescent SiNPs had a tendency to accumulate in lysosomes. The pearson coefficients were recorded and colocalization of SiNPs were displayed as box-plots in Figure 4.19.

Coloc plug in output can be collected as pearson coefficients, overlap coefficients (k_1 and k_2) and M_I, M_2 coefficients in order to determine the colocolalization level. k_1 and k_2 coefficients describe the differences in intensities of red and green. k_1 is sensitive to differences in intensity for green on the other hand k_2 is sensitive to differences in intensity for red. M_1 is used to measure the contribution of green to the colocalized area while M_2 is used to measure the contribution of red. Adler and Parmryd suggested that the pearson correlation coefficient is superior to the Mander's overlap coefficient in terms of sensitivity (Jeremy and Ingela 2010).

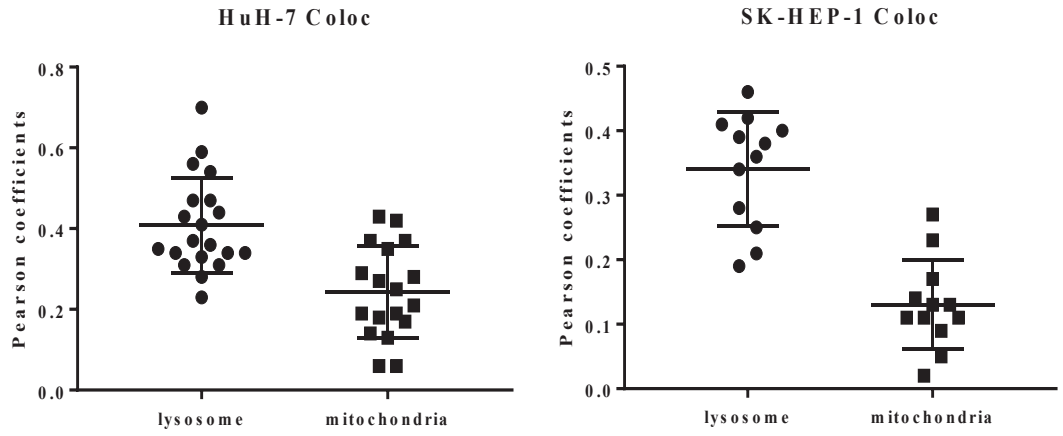

Figure 4.19. Distribution of the pearson coefficients for HuH-7 and SK-HEP-1 cells.

4.3.1.4. Cellular Uptake of SiNPs and Lysosome Staining

Hepatocellular carcinoma cell lines were treated with 10SiNP and 100SiNP suspensions and fixed with PFA at the end of the incubations. The nanoparticle uptake by HuH-7 and SK-HEP-1 cells were recorded up to 24 hours. The nuclei parts of the cells stained just before fixation by DAPI (4',6-diamidino-2-phenylindole). Lysosomes of the cells were stained by Lysotracker in order to determine nanoparticle localization in to the cytoplasm and capture the nanoparticle entrance by time.

Blue, green and red coloured parts represented nuclei, SiNP and lysosome localization in the cells respectively. The data were given for HuH-7 and SK-HEP-1 cells after 10SiNPs treatment for between 30 minutes-24 hours incubation (Figure 4.20 and 4.21). The results of the colocalization studies indicated that the cellular uptake of nanoparticles occurred 30 minutes after addition nanoparticles in to the cellular media.

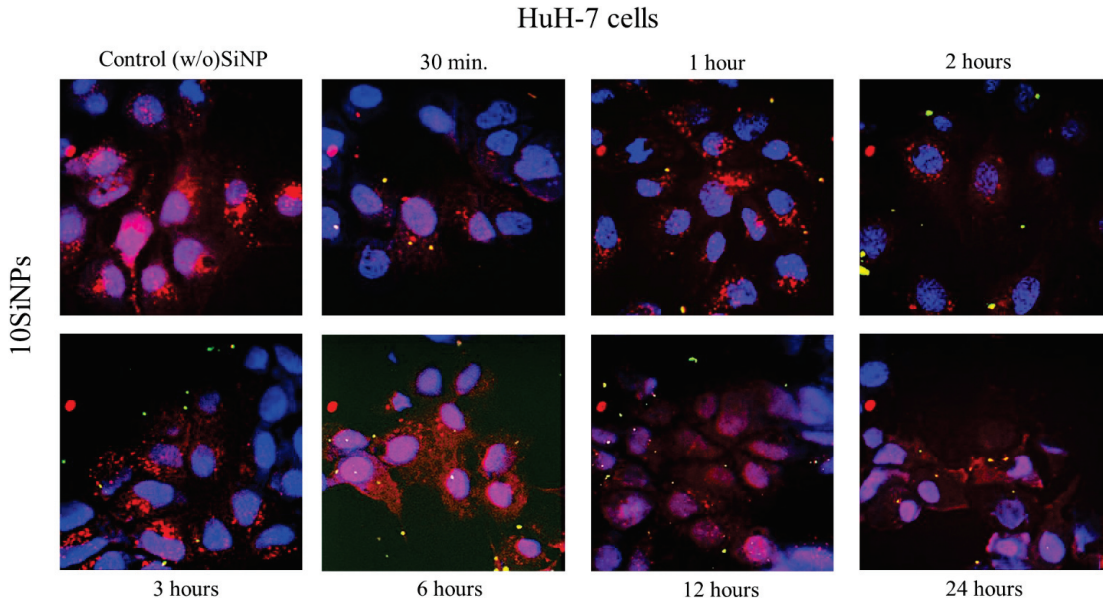

Figure 4.20. Cellular uptake of 10SiNPs (HuH-7)

Nuclei was stained by DAPI (blue), and lysosomal parts were stained by Lysotracker (red).

The experiment was also performed for 100SiNPs uptake of the both cell line. Similarly, the nanoparticles were observed after 30 minutes incubation. Green dots

represented FITC-conjugated SiNP localization in the cytoplasm. The nuclei were stained by DAPI and brighfield images were captured by DIC miscroscopy (Figure 4.22).

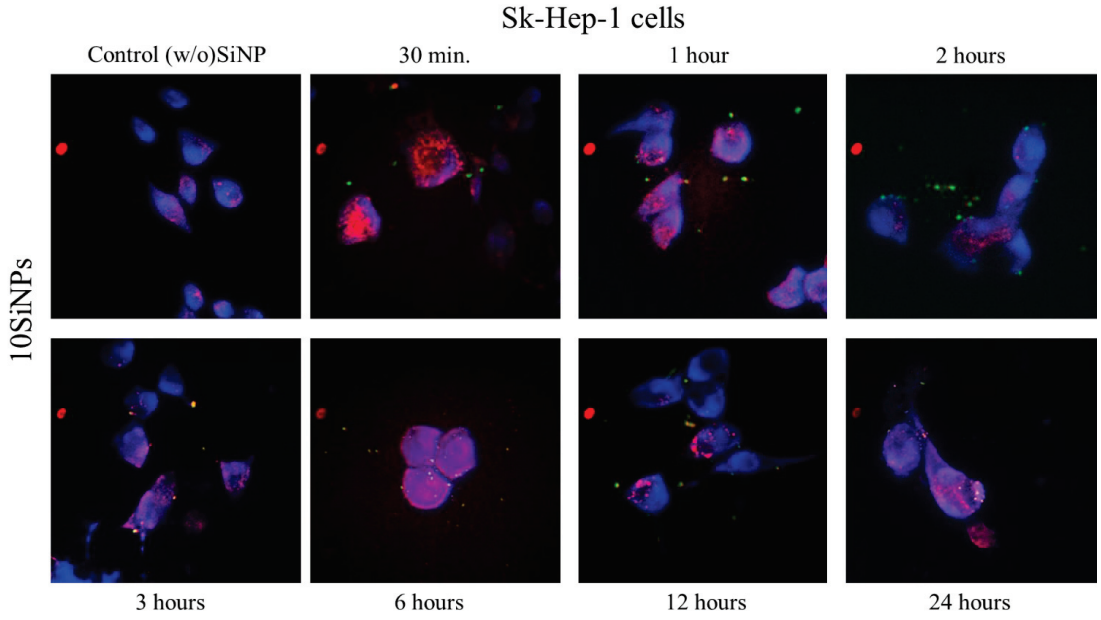

Figure 4.21. Cellular uptake of 10SiNPs (SK-HEP-1).

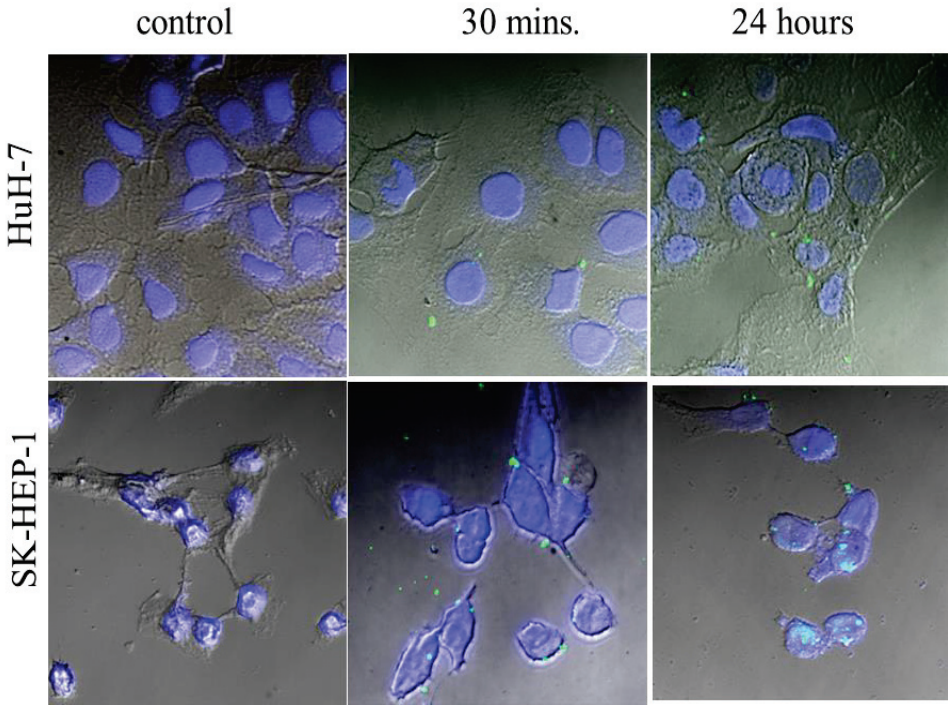

Figure 4.22. HuH-7 and SK-HEP-1 uptake of 100SiNPs

4.4. Conclusion

Qualitative and quantitative microscopy analysis results indicated that mitochondrial function of the cells were not affected by silica nanoparticles. Mitochondria potential were not changed after SiNP exposure.

SiNPs were started to internalized at 30 minutes.

It can be deduced from DCF staining results that the cells did not produce ROS after SiNP treatment. A quantitative method was followed for calculation of the mitochondrial potential in the absence/presence of SiNPs.

SiNPs were mostly colocalized in lysosomes.

Quantitative microscopic method was developed for mitochondria potential analysis.

CHAPTER 5

DETERMINATION OF TRAJECTRORIES OF SILICA NANOPARTICLES BY LIVE CELL IMAGING

Single Particle Tracking (SPT) are becoming requisite in cell biology. The quantitative analysis of the resulting trajectories provides important information about working mechanisms and structures in living cells (Sbalzarini and Koumoutsakos 2005). It can be possible to classify the motions of nanoparticles in live cells and determine diffusion coefficients of single molecules (Goulian and Simon 2000). SPT allow someone to follow the motion of single proteins within cells in order to probe the dynamics of intracellular macromolecules. In 2000, the researchers used R-phycoerythrin which is a 240-kDa autofluorescent protein and 11-nm size were tracked in TC7 cells. The intracellular dynamics of this protein were determined in both cytoplasm and nucleoplasm (Goulian and Simon 2000). The diffusion coefficient has been measured from the trajectory of an individual particle in the cell membrane and is examined by Monte Carlo calculations (Saxton 1997).

The diffusion coefficient of silica nanoparticles in nucleus of the HEp-2 cells determined by FCS (fluorescence correlation spectroscopy) as 1.2 $\mu m^2 s^-$ (Hemmerich and von Mikecz 2013). The diffusion coefficient of the silica nanoparticles were determined as 12.4 $\mu m^2 s^-$. In same study the diffusion of the silica nanoparticles were recorded as approxiamately 6 $\mu m^2 s^-$ in DMEM. They have indicated that larger the size resulted in decrease in diffusion coefficient of SiNPs. The trajectories of the particles were analyzed for their type of motional behavior. The most common analysis starts with calculation of the so called mean-square displacement (MSD). The type of diffusional behavior of the particles can be determined by time dependence of the mean square displacement. The MSD (<r2>) is defined as average of the squared distances between a particle's start and end position for all time-lags (Ruthardt, Lamb, and Brauchle 2011) (Figure 5.1).

In the literature it was investigated that the single quantum dot-labeled GM1 ganglioside complexes have confined lateral diffusion with a diffusion coefficient of $\sim 7.87 \times 10^{-2}$ $\mu m^2/s$ in living RN46A neuronal cells (Chang and Rosenthal 2012).

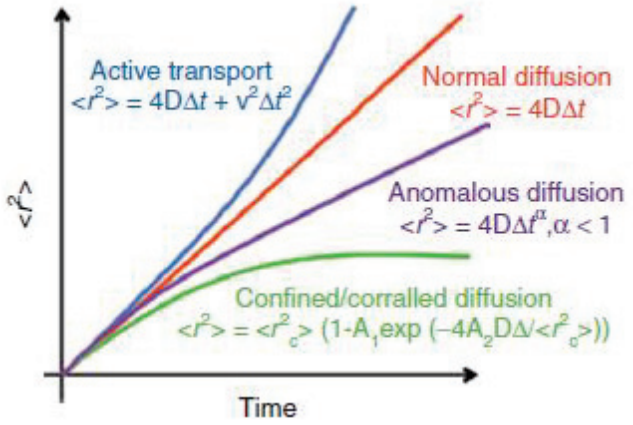

Figure 5.1. The MSD versus time graph for types of motion (Source: Ruthardt, Lamb, and Brauchle 2011)

We have captured the images of nanoparticles in the cells and determined the diffusion coefficients of SiNPs by quantitative microscopy. The data were collected by Image J after image acquisition. Algorithms were run in Matlab software.

5.1. Live cell imaging

The cells (HuH-7) were cultured on glass bottomed petri dishes. 100SiNPs were added in 200 μg/ml concentration for nanoparticle tracking experiments. Nanoparticles were observed by using live cell confocal imaging set-up. The cells were incubated with fluorescent 100SiNPs for 30 minutes. The surface of the imaging dish was washed with PBS. Remained nanoparticles were observed after washing of the cells immediately. The images were captured by Andor CCD camera at 500 ms exposure time after adding the particles 30 minutes and 1 hour time scale. 100 frames were scanned and recorded for each condition.

5.1.1. Image Analysis

The movie images were processed by Particle Tracker 2D plug-in on Image J (Figure 5.2). The ROI of moving particles were detected by plug-in. The outputs were

recorded as tracjectories and x and y coordinates of tracking particles. The parameters were radius, cut-off, percentile, link range, displacement and dynamics.

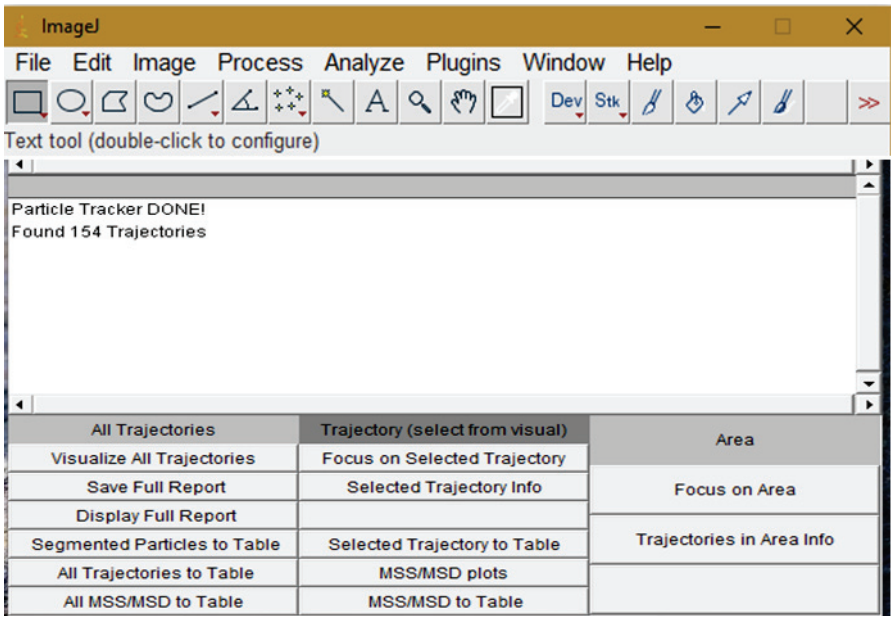

Figure 5.2. The screenshot of Particle tracker plug-in on Image J.

Radius is termed as approximate radius of the particles in the images in units of pixels. The *cut-off* score is used for the non-particle discrimination. *Percentile* determines which bright pixels are accepted as particles. *Displacement* was described as the maximum number of pixels a particle is allowed to move between two frames. The number of subsequent frames that is taken into account to determine the optimal correspondence matching was considered as *link range*. Particles displacements were explained and calculated based on Brownian motion dynamics (Sbalzarini and Koumoutsakos 2005).

5.1.2. Determination of Diffusion Coefficients

An algorithm was developed by Dr. Bilge Karacali (IZTECH/IZMIR) that was run for all trajectories in order to obtain diffusion coefficient distributions. The algorithm was given in Appendix. Diffusion coefficients and graphs were calculated by using following formulas on Matlab.

$\mathbf{t_{lag}}$ is the time between image frames;

$\mathbf{MSD_m}$ is the mean squared displacements for each individiual trajectory.

N; number of frames

n; image frame number

The MSD was calculated by; (Clausen and Lagerholm 2013)

$$\mathrm{MSD}_m(nt_{\mathrm{lag}}) = \frac{1}{N-n}\sum_{N-n}^{i=1}[(x_m((i+n)t_{\mathrm{lag}}) - x_m(it_{\mathrm{lag}}))^2 + (y_m((i+n)t_{\mathrm{lag}}) - y_m(it_{\mathrm{lag}}))^2] \quad (5.1)$$

It was presumed that the movement of silica nanoparticles can be modeled based on Brownian motion. Brownian motion is a physical phenomenon which a small particle is immersed in a liquid. In the two-dimensional Brownian motion the MSD over time is linear.

$$m = \frac{\sum_{N-n}^{i=1}(+lag\ dispdata)^2}{\sum_{N-n}^{i=1}(+lag\ disp\ data^*)+(lag\ disp\ data)} \quad (5.2)$$

Diffusion coefficient (D) is calculated from a linear fit of MSD over time.

MSD is given by MSD(t)= 4DΔt, where Δt is the time resolution.

5.2. Results and Discussion

5.2.1. Image Analysis

5.2.1.1. Determination of Diffusion Coefficients

Image J program output were obtained as tracjectory movie that displacements of bright spots were recorded in seperated .csv files. All trajectories were obtained by Particle tracker plug-in. The trajectories and displacements were recorded by the Particle tracker command window (Figure 5.3). The drawn nanoparticle trajectories after 1-hour

incubation was given in Figure 5.4. Lysotracker stained HuH-7 cells were imaged by real time confocal microscopy. Individual 154 trajectories were found to be analyzed by Particle Tracker plug-in.

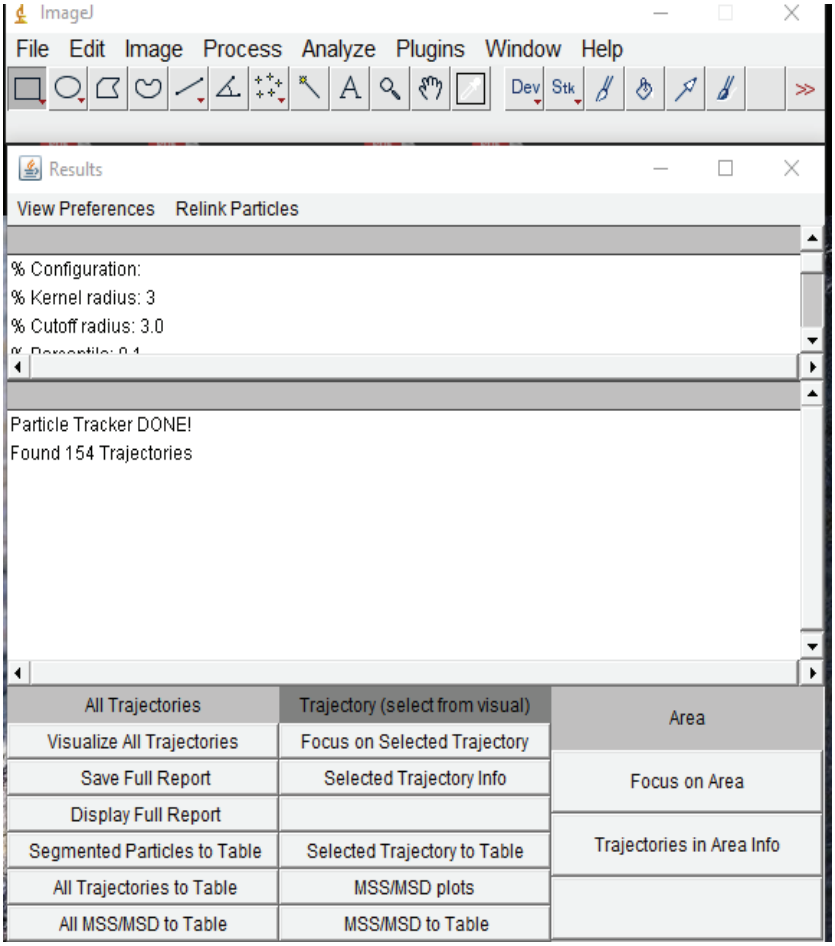

Figure 5.3. Particle tracker command window after run.

All trajectories were collected as .csv files and saved in Documents in Matlab file. Matlab was launched and the files including coordinates were recorded by related trajectory name. Each trajectory file was run on Matlab. Output files were four graphs representing; (Figure 5.5, 5.6 and 5.7)

- x vs y,
- time vs instantaneous velocity,
- instantaneous velocity vs point count,
- time lag vs average time lag displacement,
- time vs total displacements.

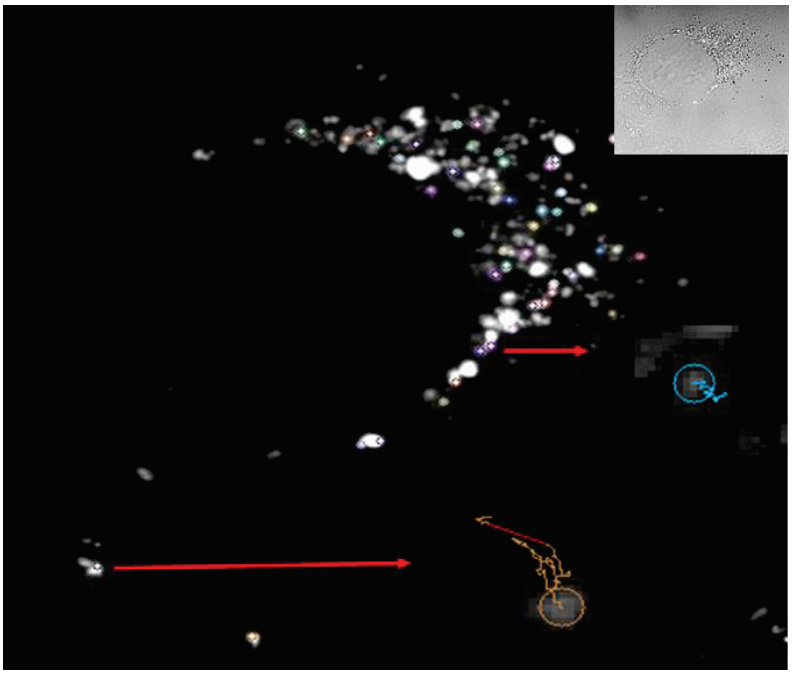

Figure 5.4. Two of the 154 trajectories were selected as examples of particle movements in the cell

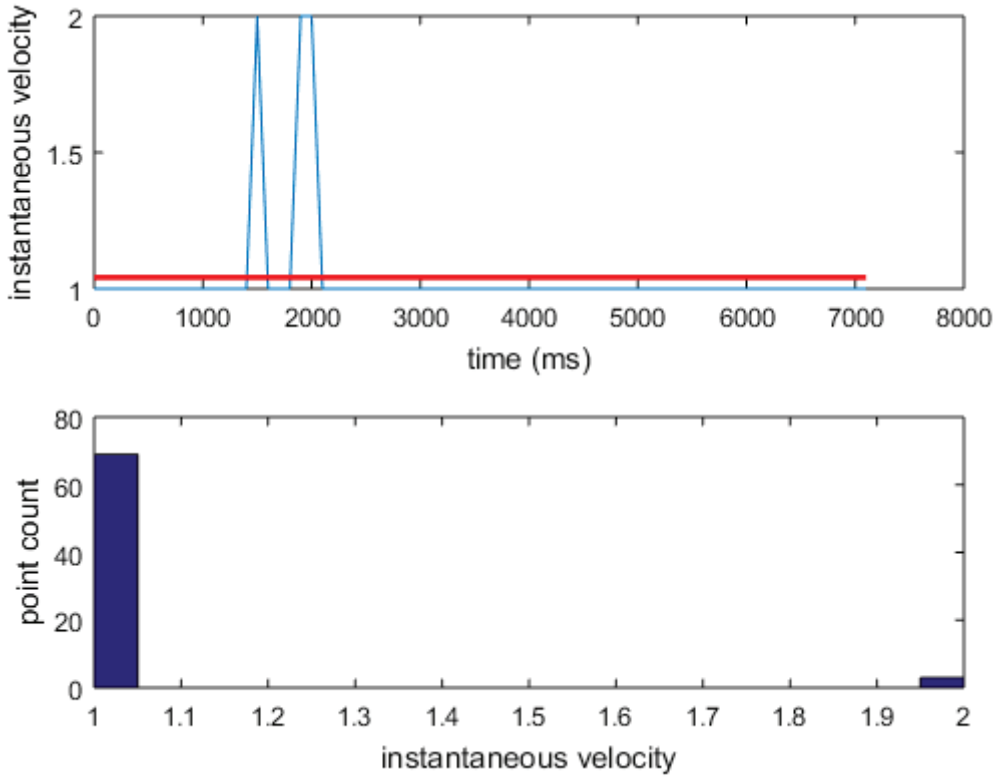

Figure 5.5. The displacements of particles x vs y was given as an example of one spot.

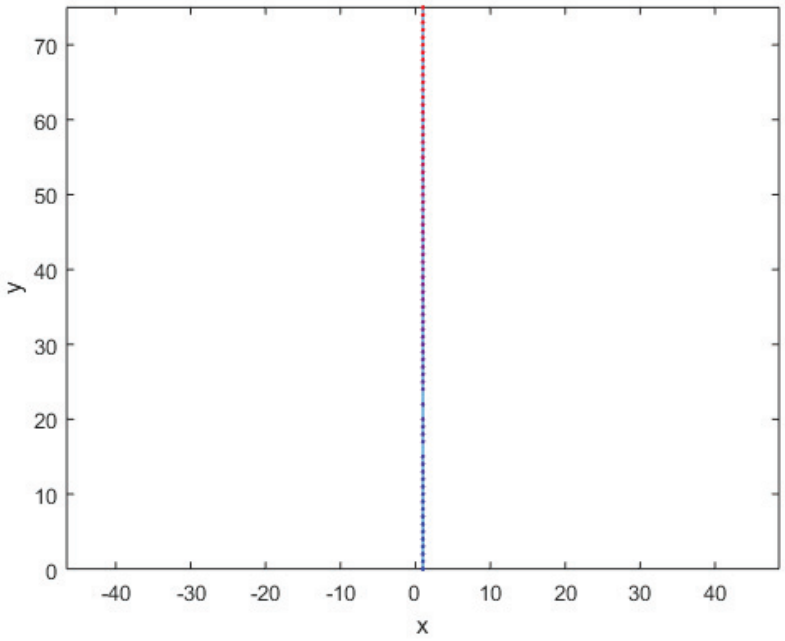

Figure 5.6. The graphs for velocity by time and velocity by count (intensity)

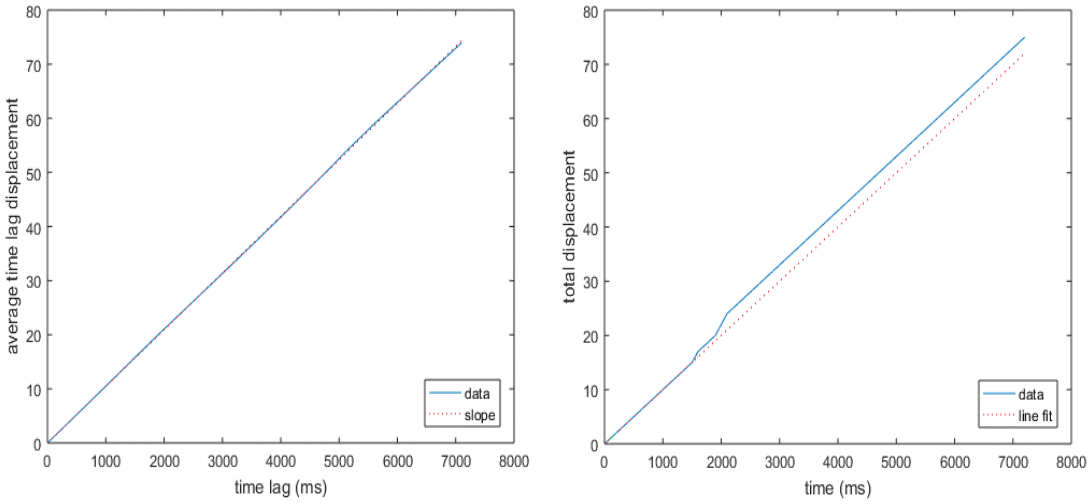

Figure 5.7. Average time lag displacement and total displacements by time obtained by Matlab algorithm.

100 bright spots were detected as particles by Particle tracker. Resultingly MSD graphs and diffusion coefficients were collected for each particle after 30 minutes and 24 hour incubations. The collected coefficients were plotted as histograms (Figure 5.8). One-tail t-test was applied to determine the change in nanoparticle movement between

up on treatment (after 30 minutes) and 24-hours treatment. The p value was 1.82 x 10^{-5} meaning that the difference is sratistically important.

The mean of the diffusion coefficient frequency of the 100SiNPs was 2.92x10^{-3} and 2.70x10^{-3} for after 30 minutes and 24 hours incubations of HuH-7 cells. It can be deduced from the histograms that the particle movement lower than after 24 hours incubation. It was thought that the reason for the decrease in diffusion was resulted from particle interaction in the cytoplasm with organelles and biological molecules. The diffusions of the particles seemed to be supported the colocalization data that the cells make nanoparticle aggregates in cytoplasm specifically in lysosomal parts.

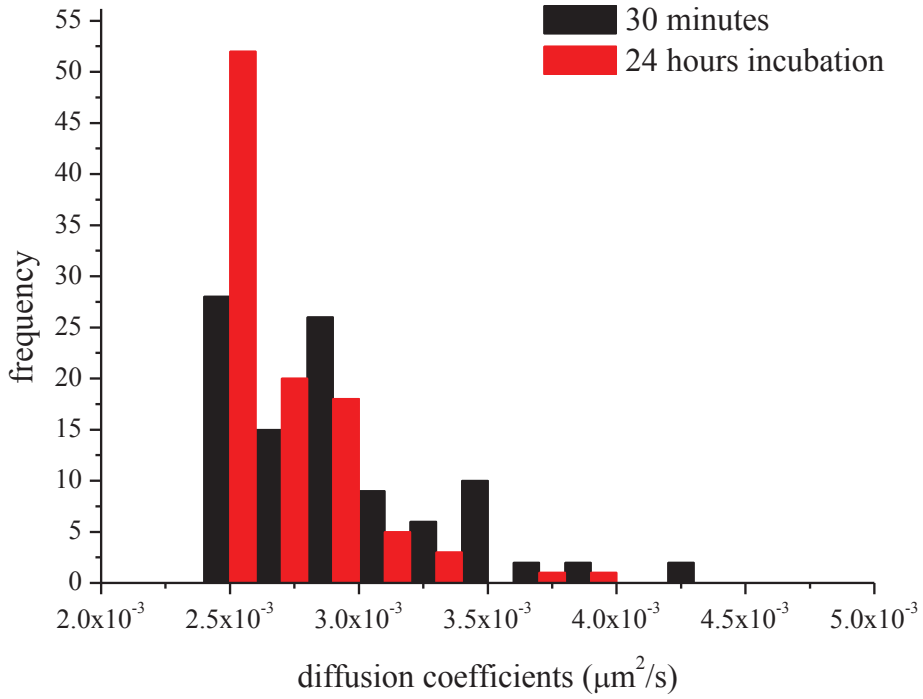

Figure 5.8. Diffusion coefficient distributions of the 100SiNPs into the cytoplasm of HuH-7 cells.

DLS measures Brownian motion of the particles suspended in a liquid. Then the measurement combined with the size of the particles. The sizes of the nanoparticles were calculated from diffusion coefficients by using Stokes-Einstein equation.

Stokes-Einstein equation;

$$d(H)=\frac{kT}{3\pi\eta D} \qquad (5.3)$$

The D is translational diffusion coefficient, k is the Boltzmann's constant, T is absolute temperature and η is viscosity in the equation.

Diffusion coefficients of the particles were also determined by DLS as in indicated in materials and method part in Chapter 1. The measured sample was prepared in DMEM and diluted into distilled water. The concentration was same as used in imaging studies (200 μg/ml). Size of the nanoparticles were determined as 91 ± 25 nm. Diffusion coefficients were determined by plug-in in Malvern Instruments Software as 0.58 $\mu m^2/s$ in measurement cuvette. Diffusion coefficients graph obtained from Malvern Instruments Software was shown in Figure 5.9).

The coefficents obtained from Zetasizer and image analysis tools were not comparable because of the nature of the measurement environment.

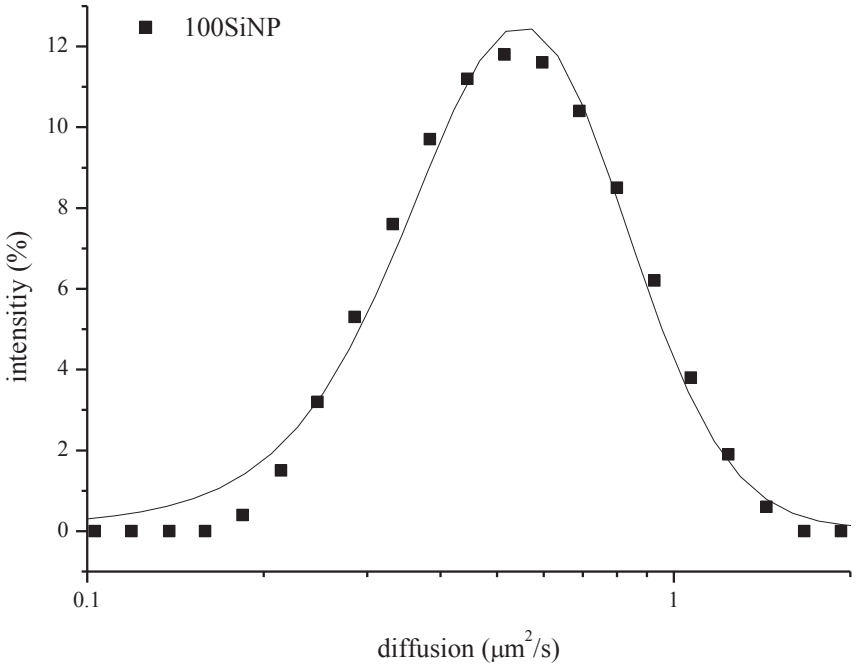

Figure 5.9. The diffusion graph of fluorescent 100SiNPs.

CHAPTER 6

CONCLUSION

The well characterized 10 and 100 nm sized Stöber SiNPs were detected as non-toxic for the hepatocarcinoma cell lines. SiNPs can be used as a cargo for drugs or biological molecules for the safe delivery. It has been calculated that there are 1.36×10^{15} SiNPs in 1.0 g powder.

10SiNPs and 100SiNPs were non-cytotoxic for HuH-7 and SK-HEP-1 regardless of the amount, size and time.

Alternatively the toxicity of the SiNPs were experimented by determining the mitochondrial potential analysis by confocal microscopy. Quantitative microscopic method was developed for mitochondria potential analysis. The area and intensity analysis can be used to elucidate the toxicity of a nanoparticle or drug.

10SiNPs and 100SiNPs were non-genotoxic for lymphocytes. Additionally SiNPs do not induce ROS production.

No arrest at the cell cycle of HuH-7 and SK-HEP-1 regardless of the amount, size and time.

The possible nanoparticle localization was observed in lysosomes and cytosol by co-localization parameters. SiNPs were started to internalized at 30 minutes.

Live-cell imaging results showed that mean diffusion coefficient of the 100SiNP was nearly 2.4×10^{-3} $\mu m^2/s$ in the cell and 0.58 $\mu m^2/s$ in DLS measurement cuvette. The microscopic data may provide feedback for improvements of nanoparticles.

It is reviewed in the literature that once liposomes are engulfed by Kupffer cells, they accumulate in a phagosome and then fuse with a lysosome to be digested by lysosomal enzymes. This knowledge gives rise a thought that when SiNPs are injected *in vivo* the nanoparticle removal can be managed by hepatobiliary clearance.

REFERENCES

Alexander, Leroy, and H. P. Klug. 1948. "Basic Aspects of X-Ray Absorption in Quantitative Diffraction Analysis of Powder Mixtures." *Analytical Chemistry* 20 (10):886-889. doi: 10.1021/ac60022a002.

Asweto, C. O., J. Wu, H. Hu, L. Feng, X. Yang, J. Duan, and Z. Sun. 2017. "Combined Effect of Silica Nanoparticles and Benzo[a]pyrene on Cell Cycle Arrest Induction and Apoptosis in Human Umbilical Vein Endothelial Cells." *Int J Environ Res Public Health* 14 (3). doi: 10.3390/ijerph14030289.

Athinarayanan, J., V. S. Periasamy, M. A. Alsaif, A. A. Al-Warthan, and A. A. Alshatwi. 2014. "Presence of nanosilica (E551) in commercial food products: TNF-mediated oxidative stress and altered cell cycle progression in human lung fibroblast cells." *Cell Biol Toxicol* 30 (2):89-100. doi: 10.1007/s10565-014-9271-8.

Behzadi, S., V. Serpooshan, W. Tao, M. A. Hamaly, M. Y. Alkawareek, E. C. Dreaden, D. Brown, A. M. Alkilany, O. C. Farokhzad, and M. Mahmoudi. 2017. "Cellular uptake of nanoparticles: journey inside the cell." *Chem Soc Rev* 46 (14):4218-4244. doi: 10.1039/c6cs00636a.

Chang, J. C., and S. J. Rosenthal. 2012. "Visualization of lipid raft membrane compartmentalization in living RN46A neuronal cells using single quantum dot tracking." *ACS Chem Neurosci* 3 (10):737-43. doi: 10.1021/cn3000845.

Chang, J. S., H. P. Kuo, K. L. Chang, and Z. L. Kong. 2015. "Apoptosis of Hepatocellular Carcinoma Cells Induced by Nanoencapsulated Polysaccharides Extracted from Antrodia Camphorata." *PLoS One* 10 (9):e0136782. doi: 10.1371/journal.pone.0136782.

Chang, Jenq-Sheng, Ke Liang B. Chang, Deng-Fwu Hwang, and Zwe-Ling Kong. 2007. "In Vitro Cytotoxicitiy of Silica Nanoparticles at High Concentrations Strongly Depends on the Metabolic Activity Type of the Cell Line." *Environmental Science & Technology* 41 (6):2064-2068. doi: 10.1021/es062347t.

Chen, Z., P. Zhu, Y. Zhang, Y. Liu, Y. He, L. Zhang, and Y. Gao. 2016. "Enhanced Sensitivity of Cancer Stem Cells to Chemotherapy Using Functionalized Mesoporous Silica Nanoparticles." *Mol Pharm* 13 (8):2749-59. doi: 10.1021/acs.molpharmaceut.6b00352.

Chu, Z., Y. Huang, Q. Tao, and Q. Li. 2011. "Cellular uptake, evolution, and excretion of silica nanoparticles in human cells." *Nanoscale* 3 (8):3291-9. doi: 10.1039/c1nr10499c.

Clausen, M. P., and B. C. Lagerholm. 2013. "Visualization of plasma membrane compartmentalization by high-speed quantum dot tracking."*Nano Lett* 13 (6):2332-7. doi: 10.1021/nl303151f.

Corvi, Raffaella, and Federica Madia. 2017. "In vitro genotoxicity testing–Can the performance be enhanced?" *Food and Chemical Toxicology* 106:600-608. doi: https://doi.org/10.1016/j.fct.2016.08.024.

David, Eastmond, and Tucker James. 1989. "Identification of aneuploidy-inducing agents using cytokinesis-blocked human lymphocytes and an antikinetochore antibody." *Environmental and Molecular Mutagenesis* 13 (1):34-43. doi: doi:10.1002/em.2850130104.

Duan, Junchao, Yongbo Yu, Yang Li, Yang Yu, Yanbo Li, Xianqing Zhou, Peili Huang, and Zhiwei Sun. 2013. "Toxic Effect of Silica Nanoparticles on Endothelial Cells through DNA Damage Response via Chk1-Dependent G2/M Checkpoint." *PLOS ONE* 8 (4):e62087. doi: 10.1371/journal.pone.0062087.

Durgun, Gulay, Kasim Ocakoglu, and Serdar Ozcelik. 2011. "Systematic Tuning the Hydrodynamic Diameter of Uniformed Fluorescent Silica Nanoparticles." *The Journal of Physical Chemistry C* 115 (33):16322-16332. doi: 10.1021/jp204323d.

Eun, Jong Ryeol, Yong Jin Jung, Yanling Zhang, Yanhong Zhang, Benjamin Tschudy-Seney, Rajen Ramsamooj, Yu-Jui Yvonne Wan, Neil D. Theise, Mark A. Zern, and Yuyou Duan. 2014. "Hepatoma SK Hep-1 Cells Exhibit Characteristics of Oncogenic Mesenchymal Stem Cells with Highly Metastatic Capacity." *PLOS ONE* 9 (10):e110744. doi: 10.1371/journal.pone.0110744.

Faix, O. 1992. "Fourier Transform Infrared Spectroscopy." In *Methods in Lignin Chemistry*, edited by Stephen Y. Lin and Carlton W. Dence, 233-241. Berlin, Heidelberg: Springer Berlin Heidelberg.

Fenech, Michael. 2007. "Cytokinesis-block micronucleus cytome assay." *Nature Protocols* 2:1084. doi: 10.1038/nprot.2007.77.

Ferrati, Silvia, Aaron Mack, Ciro Chiappini, Xuewu Liu, Andrew J. Bean, Mauro Ferrari, and Rita E. Serda. 2010. "Intracellular trafficking of silicon particles and logic-embedded vectors." *Nanoscale* 2 (8):1512-1520. doi: 10.1039/C0NR00227E.

Gan, Q., D. Dai, Y. Yuan, J. Qian, S. Sha, J. Shi, and C. Liu. 2012. "Effect of size on the cellular endocytosis and controlled release of mesoporous silica nanoparticles for intracellular delivery." *Biomed Microdevices* 14 (2):259-70. doi: 10.1007/ s10544-011-9604-9.

Gonzalez, L., M. Lukamowicz-Rajska, L. C. Thomassen, C. E. Kirschhock, L. Leyns, D. Lison, J. A. Martens, A. Elhajouji, and M. Kirsch-Volders. 2014. "Co-assessment of cell cycle and micronucleus frequencies demonstrates the influence of serum on the in vitro genotoxic response to amorphous monodisperse silica nanoparticles of varying sizes." *Nanotoxicology* 8(8): 876-84. doi: 10.3109/17435390.2013.842266.

Gottstein, Claudia, Guohui Wu, Benjamin J. Wong, and Joseph Anthony Zasadzinski. 2013. "Precise Quantification of Nanoparticle Internalization." *ACS Nano* 7 (6):4933-4945. doi: 10.1021/nn400243d.

Goulian, M., and S. M. Simon. 2000. "Tracking single proteins within cells." *Biophys J* 79 (4):2188-98. doi: 10.1016/s0006-3495(00)76467-8.

Guarnieri, Daniela, Maria Ada Malvindi, Valentina Belli, Pier Paolo Pompa, and Paolo Netti. 2014. "Effect of silica nanoparticles with variable size and surface functionalization on human endothelial cell viability and angiogenic activity." *Journal of Nanoparticle Research* 16 (2):2229. doi: 10.1007/s11051-013-2229-6.

Heather Herd, Nicole Daum, Arwyn T. Jones, Hanno Huwer, Hamidreza Ghandehari, and Claus-Michael Lehr. 2013. "Nanoparticle Geometry and Surface Orientation Influence Mode of Cellular Uptake." *ACS NANO* 7 (3):1961-1973.

Hemmerich, Peter H., and Anna H. von Mikecz. 2013. "Defining the Subcellular Interface of Nanoparticles by Live-Cell Imaging." *PLOS ONE* 8 (4):e62018. doi: 10.1371/journal.pone.0062018.

Herd, Heather, Nicole Daum, Arwyn T. Jones, Hanno Huwer, Hamidreza Ghandehari, and Claus-Michael Lehr. 2013. "Nanoparticle Geometry and Surface Orientation Influence Mode of Cellular Uptake." *ACS Nano* 7 (3):1961-1973. doi: 10.1021/nn304439f.

Huang, X., J. Zhuang, X. Teng, L. Li, D. Chen, X. Yan, and F. Tang. 2010. "The promotion of human malignant melanoma growth by mesoporous silica nanoparticles through decreased reactive oxygen species." *Biomaterials* 31 (24):6142-53. doi: 10.1016/j.biomaterials.2010.04.055.

ISO/TC 229, Nanotechnologies. 2017. "Nanotechnologies — Plain language explanation of selected terms from the ISO/IEC 80004 series." *ISO TR 18401, Technical Report*.

Jeremy, Adler, and Parmryd Ingela. 2010. "Quantifying colocalization by correlation: The Pearson correlation coefficient is superior to the Mander's overlap coefficient." *Cytometry Part A* 77A (8):733-742. doi: doi:10.1002/cyto.a.20896.

Jin, Yuhui, Shibichakravarthy Kannan, Min Wu, and Julia Xiaojun Zhao. 2007. "Toxicity of Luminescent Silica Nanoparticles to Living Cells." *Chemical Research in Toxicology* 20 (8):1126-1133. doi: 10.1021/tx7001959.

Julia, Blechinger, Bauer Alexander T., Torrano Adriano A., Gorzelanny Christian, Bräuchle Christoph, and Schneider Stefan W. 2013. "Uptake Kinetics and Nanotoxicity of Silica Nanoparticles Are Cell Type Dependent." *Small* 9 (23):3970-3980. doi: doi:10.1002/smll.201301004.

Kretowski, R., M. Kusaczuk, M. Naumowicz, J. Kotynska, B. Szynaka, and M. Cechowska-Pasko. 2017. "The Effects of Silica Nanoparticles on Apoptosis and Autophagy of Glioblastoma Cell Lines." *Nanomaterials (Basel)* 7 (8). doi: 10.3390/nano7080230.

Landgraf, L., D. Nordmeyer, P. Schmiel, Q. Gao, S. Ritz, S. Gebauer J, S. Grass, S. Diabate, L. Treuel, C. Graf, E. Ruhl, K. Landfester, V. Mailander, C. Weiss, R.

Zellner, and I. Hilger. 2017. "Validation of weak biological effects by round robin experiments: cytotoxicity/biocompatibility of SiO2 and polymer nanoparticles in HepG2 cells." *Sci Rep* 7 (1):4341. doi: 10.1038/s41598-017-02958-9.

Lin, W., Y. W. Huang, X. D. Zhou, and Y. Ma. 2006. "In vitro toxicity of silica nanoparticles in human lung cancer cells." *Toxicol Appl Pharmacol* 217 (3):252-9. doi: 10.1016/j.taap.2006.10.004.

Lunova, M., A. Prokhorov, M. Jirsa, M. Hof, A. Olzynska, P. Jurkiewicz, S. Kubinova, O. Lunov, and A. Dejneka. 2017. "Nanoparticle core stability and surface functionalization drive the mTOR signaling pathway in hepatocellular cell lines." *Sci Rep* 7 (1):16049. doi: 10.1038/s41598-017-16447-6.

Mahmoudi, M., K. Azadmanesh, M. A. Shokrgozar, W. S. Journeay, and S. Laurent. 2011. "Effect of nanoparticles on the cell life cycle." *Chem Rev* 111 (5):3407-32. doi: 10.1021/cr1003166.

Merly, L., and S. L. Smith. 2017. "Murine RAW 264.7 cell line as an immune target: are we missing something?" *Immunopharmacol Immunotoxicol* 39 (2):55-58. doi: 10.1080/08923973.2017.1282511.

Mu, Q., N. S. Hondow, L. Krzeminski, A. P. Brown, L. J. Jeuken, and M. N. Routledge. 2012. "Mechanism of cellular uptake of genotoxic silica nanoparticles." *Part Fibre Toxicol* 9:29. doi: 10.1186/1743-8977-9-29.

Mu, Qingshan, Nicole S. Hondow, Łukasz Krzemiński, Andy P. Brown, Lars JC Jeuken, and Michael N. Routledge. 2012. "Mechanism of cellular uptake of genotoxic silica nanoparticles." *Particle and Fibre Toxicology* 9 (1):29. doi: 10.1186/1743-8977-9-29.

Nabeshi, H., H. Nabeshi, T. Yoshikawa, T. Yoshikawa, K. Matsuyama, K. Matsuyama, Y. Nakazato, Y. Nakazato, A. Arimori, A. Arimori, M. Isobe, M. Isobe, S. Tochigi, S. Tochigi, S. Kondoh, S. Kondoh, T. Hirai, T. Hirai, T. Akase, T. Akase, T. Yamashita, T. Yamashita, K. Yamashita, K. Yamashita, T. Yoshida, T. Yoshida, K. Nagano, Y. Abe, Y. Yoshioka, Y. Yoshioka, H. Kamada, H. Kamada, T. Imazawa, N. Itoh, S. Tsunoda, S. Tsunoda, S. Tsunoda, Y. Tsutsumi, Y. Tsutsumi, and Y. Tsutsumi. 2010. "Size-dependent cytotoxic effects of amorphous silica nanoparticles on Langerhans cells." *Die Pharmazie - An International Journal of Pharmaceutical Sciences* 65 (3):199-201. doi: 10.1691/ph.2010.9268.

Napierska, D., L. C. Thomassen, D. Lison, J. A. Martens, and P. H. Hoet. 2010. "The nanosilica hazard: another variable entity." *Part Fibre Toxicol* 7 (1):39. doi: 10.1186/1743-8977-7-39.

Napierska, D., L. C. Thomassen, V. Rabolli, D. Lison, L. Gonzalez, M. Kirsch-Volders, J. A. Martens, and P. H. Hoet. 2009. "Size-dependent cytotoxicity of monodisperse silica nanoparticles in human endothelial cells." *Small* 5 (7):846-53. doi: 10.1002/smll.200800461.

Nel, Andre, Tian Xia, Lutz Mädler, and Ning Li. 2006. "Toxic Potential of Materials at the Nanolevel." *Science* 311 (5761):622-627. doi: 10.1126/science.1114397.

Orellana, Esteban A., and Andrea L. Kasinski. 2016. "Sulforhodamine B (SRB) Assay in Cell Culture to Investigate Cell Proliferation." *Bio-protocol* 6 (21):e1984. doi: 10.21769/BioProtoc.1984.

Panariti, Alice, Giuseppe Miserocchi, and Ilaria Rivolta. 2012. "The effect of nanoparticle uptake on cellular behavior: disrupting or enabling functions?" *Nanotechnology, Science and Applications* 5:87-100. doi: 10.2147/NSA.S25515.

Park, J. H., H. Jeong, J. Hong, M. Chang, M. Kim, R. S. Chuck, J. K. Lee, and C. Y. Park. 2016. "The Effect of Silica Nanoparticles on Human Corneal Epithelial Cells." *Sci Rep* 6:37762. doi: 10.1038/srep37762.

Park, M. V., H. W. Verharen, E. Zwart, L. G. Hernandez, J. van Benthem, A. Elsaesser, C. Barnes, G. McKerr, C. V. Howard, A. Salvati, I. Lynch, K. A. Dawson, and W. H. de Jong. 2011. "Genotoxicity evaluation of amorphous silica nanoparticles of different sizes using the micronucleus and the plasmid lacZ gene mutation assay." *Nanotoxicology* 5 (2):168-81. doi: 10.3109/17435390.2010.506016.

Patravale, Vandana, Prajakta Dandekar, and Ratnesh Jain. 2012. "3 - Characterization techniques for nanoparticulate carriers." In *Nanoparticulate Drug Delivery*, 87-121. Woodhead Publishing.

Periasamy, V. S., J. Athinarayanan, M. A. Akbarsha, and A. A. Alshatwi. 2015. "Silica nanoparticles induced metabolic stress through EGR1, CCND, and E2F1 genes in human mesenchymal stem cells." *Appl Biochem Biotechnol* 175 (2):1181-92. doi: 10.1007/s12010-014-1342-z.

Piotr Pozarowski , and Zbigniew Darzynkiewicz. 2014. "Analysis of Cell Cycle by Flow Cytometry." *Methods in Molecular Biology* 281.

Poussard, S., M. Decossas, O. Le Bihan, S. Mornet, G. Naudin, and O. Lambert. 2015. "Internalization and fate of silica nanoparticles in C2C12 skeletal muscle cells: evidence of a beneficial effect on myoblast fusion." *Int J Nanomedicine* 10:1479-92. doi: 10.2147/IJN.S74158.

Rancan, Fiorenza, Qi Gao, Christina Graf, Stefan Troppens, Sabrina Hadam, Steffen Hackbarth, Cynthia Kembuan, Ulrike Blume-Peytavi, Eckart Rühl, Jürgen Lademann, and Annika Vogt. 2012. "Skin Penetration and Cellular Uptake of Amorphous Silica Nanoparticles with Variable Size, Surface Functionalization, and Colloidal Stability." *ACS Nano* 6 (8):6829-6842. doi: 10.1021/nn301622h.

Ruthardt, N., D. C. Lamb, and C. Brauchle. 2011. "Single-particle tracking as a quantitative microscopy-based approach to unravel cell entry mechanisms of viruses and pharmaceutical nanoparticles." *Mol Ther* 19 (7):1199-211. doi: 10.1038/mt.2011.102.

Saxton, M. J. 1997. "Single-particle tracking: the distribution of diffusion coefficients." *Biophys J* 72 (4):1744-53. doi: 10.1016/s0006-3495(97)78820-9.

Sbalzarini, I. F., and P. Koumoutsakos. 2005. "Feature point tracking and trajectory analysis for video imaging in cell biology." *J Struct Biol* 151 (2):182-95. doi: 10.1016/j.jsb.2005.06.002.

Science, Olympus-Life. "DIC Microscope Configuration and Alignment." https://www.olympus-lifescience.com/en/microscope/dic/dicconfiguration

Shackelford, J.F., and R.H. Doremus. 2008. *Ceramic and Glass Materials: Structure, Properties and Processing*: Springer US.

Shapero, Kayle, Federico Fenaroli, Iseult Lynch, David C. Cottell, Anna Salvati, and Kenneth A. Dawson. 2011. "Time and space resolved uptake study of silica nanoparticles by human cells." *Molecular BioSystems* 7 (2):371-378. doi: 10.1039/C0MB00109K.

Shindo, Daisuke, and Tetsuo Oikawa. 2002. "Energy Dispersive X-ray Spectroscopy." In *Analytical Electron Microscopy for Materials Science*, 81-102. Tokyo: Springer Japan.

Stöber, Werner, Arthur Fink, and Ernst Bohn. 1968. "Controlled growth of monodisperse silica spheres in the micron size range." *Journal of Colloid and Interface Science* 26 (1):62-69. doi: https://doi.org/10.1016/0021-9797(68)90272-5.

Sun, Lei, Yang Li, Xiaomei Liu, Minghua Jin, Long Zhang, Zhongjun Du, Caixia Guo, Peili Huang, and Zhiwei Sun. 2011. "Cytotoxicity and mitochondrial damage caused by silica nanoparticles." *Toxicology in Vitro* 25 (8):1619-1629. doi: https://doi.org/10.1016/j.tiv.2011.06.012.

Terry L Riss, Richard A Moravec, Andrew L Niles, Sarah Duellman, Hélène A Benink, Tracy J Worzella, and Lisa Minor. 2004. "Cell Viability Assays." *Eli Lilly & Company and the National Center for Advancing Translational Sciences*.

Thavarajah, Rooban, Vidya Kazhiyur Mudimbaimannar, Joshua Elizabeth, Umadevi Krishnamohan Rao, and Kannan Ranganathan. 2012. "Chemical and physical basics of routine formaldehyde fixation." *Journal of Oral and Maxillofacial Pathology : JOMFP* 16 (3):400-405. doi: 10.4103/0973-029X.102496.

Torrano, A. A., and C. Brauchle. 2014. "Precise quantification of silica and ceria nanoparticle uptake revealed by 3D fluorescence microscopy." *Beilstein J Nanotechnol* 5:1616-24. doi: 10.3762/bjnano.5.173.

Uboldi, C., G. Giudetti, F. Broggi, D. Gilliland, J. Ponti, and F. Rossi. 2012. "Amorphous silica nanoparticles do not induce cytotoxicity, cell transformation or genotoxicity in Balb/3T3 mouse fibroblasts." *Mutat Res* 745 (1-2):11-20. doi: 10.1016 /j.mrgentox. 2011.10.010.

van Blaaderen, A., and A. Vrij. 1993. "Synthesis and Characterization of Monodisperse Colloidal Organo-silica Spheres." *Journal of Colloid and Interface Science* 156 (1):1-18. doi: https://doi.org/10.1006/jcis.1993.1073.

W., Boyle, and Chow A. 1969. "Isolation of Human Lymphocytes by a Ficoll Barrier Method." *Transfusion* 9 (3):151-155. doi:10.1111/j.1537-2995.1969.tb05534.x.

Wang, F., F. Gao, M. Lan, H. Yuan, Y. Huang, and J. Liu. 2009. "Oxidative stress contributes to silica nanoparticle-induced cytotoxicity in human embryonic kidney cells." *Toxicol In Vitro* 23 (5):808-15. doi: 10.1016/j.tiv.2009.04.009.

Wang, Y., Q. Zhao, N. Han, L. Bai, J. Li, J. Liu, E. Che, L. Hu, Q. Zhang, T. Jiang, and S. Wang. 2015. "Mesoporous silica nanoparticles in drug delivery and biomedical applications." *Nanomedicine* 11 (2):313-27. doi: 10.1016/j.nano.2014.09.014.

Waters, K. M., L. M. Masiello, R. C. Zangar, B. J. Tarasevich, N. J. Karin, R. D. Quesenberry, S. Bandyopadhyay, J. G. Teeguarden, J. G. Pounds, and B. D. Thrall. 2009. "Macrophage responses to silica nanoparticles are highly conserved across particle sizes." *Toxicol Sci* 107 (2):553-69. doi: 10.1093/toxsci/kfn250.

Wu, L., M. Wu, Y. Zeng, D. Zhang, A. Zheng, X. Liu, and J. Liu. 2015. "Multifunctional PEG modified DOX loaded mesoporous silica nanoparticle@CuS nanohybrids as photo-thermal agent and thermal-triggered drug release vehicle for hepatocellular carcinoma treatment." *Nanotechnology* 26 (2):025102. doi: 10.1088/0957-4484/26/2/025102.

Xie, M., Y. Xu, H. Shen, S. Shen, Y. Ge, and J. Xie. 2014. "Negative-charge-functionalized mesoporous silica nanoparticles as drug vehicles targeting hepatocellular carcinoma." *Int J Pharm* 474 (1-2):223-31. doi: 10.1016/j.ijpharm.2014.08.027.

Xu, Xiaowei, Kai Zhang, Liang Zhao, Dandan Wang, Wenhuan Bu, Changyu Zheng, and Hongchen Sun. 2014. "Characteristics of three sizes of silica nanoparticles in the osteoblastic cell line, MC3T3-E1." *RSC Advances* 4 (87):46481-46487. doi: 10.1039/C4RA06863G.

Yanez, Josefa, Vicente Vicente, Miguel Alcaraz, Julian Castillo, Obdulio Benavente-Garcia, Manuel Canteras, and Jose A. Lozano Teruel. 2004. "Cytotoxicity and Antiproliferative Activities of Several Phenolic Compounds Against Three Melanocytes Cell Lines: Relationship Between Structure and Activity." *Nutrition and Cancer* 49 (2):191-199. doi: 10.1207/s15327914nc4902_11.

Yang, H., Q. Y. Wu, C. S. Lao, M. Y. Li, Y. Gao, Y. Zheng, and B. Shi. 2016. "Cytotoxicity and DNA damage in mouse macrophages exposed to silica nanoparticles." *Genet Mol Res* 15 (3). doi: 10.4238/gmr.15039005.

Yang, X., C. He, J. Li, H. Chen, Q. Ma, X. Sui, S. Tian, M. Ying, Q. Zhang, Y. Luo, Z. Zhuang, and J. Liu. 2014. "Uptake of silica nanoparticles: neurotoxicity and Alzheimer-like pathology in human SK-N-SH and mouse neuro2a neuroblastoma cells." *Toxicol Lett* 229 (1):240-9. doi: 10.1016/j.toxlet.2014.05.009.

Yu, C., L. Qian, M. Uttamchandani, L. Li, and S. Q. Yao. 2015. "Single-Vehicular Delivery of Antagomir and Small Molecules to Inhibit miR-122 Function in Hepatocellular Carcinoma Cells by using "Smart" Mesoporous Silica Nanoparticles." *Angew Chem Int Ed Engl* 54 (36):10574-8. doi: 10.1002/anie.201504913.

Yu, Tian, Alexander Malugin, and Hamidreza Ghandehari. 2011. "Impact of Silica Nanoparticle Design on Cellular Toxicity and Hemolytic Activity." *ACS Nano* 5 (7):5717-5728. doi: 10.1021/nn2013904.

Yu, Y., J. Duan, W. Geng, Q. Li, L. Jiang, Y. Li, Y. Yu, and Z. Sun. 2015. "Aberrant cytokinesis and cell fusion result in multinucleation in HepG2 cells exposed to silica nanoparticles." *Chem Res Toxicol* 28 (3):490-500. doi: 10.1021/tx500473h.

Yuzugullu, Haluk, Khemais Benhaj, Nuri Ozturk, Serif Senturk, Emine Celik, Asli Toylu, Nilgun Tasdemir, Mustafa Yilmaz, Esra Erdal, Kamil Akcali, Nese Atabey, and Mehmet Ozturk. 2009a. "Canonical Wnt signaling is antagonized by noncanonical Wnt5a in hepatocellular carcinoma cells." *Molecular Cancer* 8 (1). doi: 10.1186/1476-4598-8-90.

Zhang, Jin, Lihua Ren, Yang Zou, Lianshuang Zhang, Jialiu Wei, Yanbo Li, Ji Wang, Zhiwei Sun, and Xianqing Zhou. 2016. "Silica nanoparticles induce start inhibition of meiosis and cell cycle arrest via down-regulating meiotic relevant factors." *Toxicology Research* 5 (5):1453-1464. doi: 10.1039/c6tx00236f.

Zhang, X., X. Chen, F. Li, S. Guo, J. Li, and Y. Gan. 2015. "Smart lipid capped mesoporous silica nanoparticles with tumor extracellular pH activated charge-conversion property for deep hepatocellular carcinoma penetration." *J Control Release* 213:e121-2. doi: 10.1016/j.jconrel.2015.05.204.

Zhang, Y. N., W. Poon, A. J. Tavares, I. D. McGilvray, and W. C. W. Chan. 2016. "Nanoparticle-liver interactions: Cellular uptake and hepatobiliary elimination." *J Control Release* 240:332-348. doi: 10.1016/j.jconrel.2016.01.020.

Zhu, J., L. Liao, L. Zhu, P. Zhang, K. Guo, J. Kong, C. Ji, and B. Liu. 2013. "Size-dependent cellular uptake efficiency, mechanism, and cytotoxicity of silica nanoparticles toward HeLa cells." *Talanta* 107:408-15. doi: 10.1016/j.talanta.2013.01.037.

VITA

PERSONAL INFORMATION

Surname, Name: TÜNCEL ÇERİK, Özge
Nationality: Turkish (T.C.)
Date and Place of Birth: 08.09.1983, Edirne
Marital Status: Married
Phone: (+90) 53 7348-9198
E-mail: ozge.tuncel@gmail.com

EDUCATION

Degree	Institution	Year
PhD	İzmir Institute of Technology	2018
MSc	İzmir Institute of Technology	2009
BSc	Trakya University	2005

CONFERENCES

1. Yaşam Bilimleri Konferansı–, February 2016, Abdullah Gül Üniversitesi, Kayseri, TÜRKİYE (Poster presentation)
2. The 11th National Conference On Nanoscience And Nanotechnology – NanoTR11, June 2015, Middle East Technical University METU, Ankara, TÜRKİYE (Poster presentation)
3. Yaşam Bilimleri ve Sağlık Proje Yarışması–September 2015, IBG İzmir, İzmir, TÜRKİYE (Poster presentation)
4. International Symposium on Cancer Nanomedicine–November 2013, Ege University İzmir, TÜRKİYE (Poster presentation)
5. Advanced Materials World Congress, September 2013, İzmir TURKEY. (Poster Presentation)
6. The 8th National Conference On Nanoscience And Nanotechnology – NanoTR8, June 2012, Ankara, TÜRKİYE (Oral Presentation)